

Robust Principal Components by Casewise and Cellwise Weighting

Fabio Centofanti^{1,2}, Mia Hubert², and Peter J. Rousseeuw²

¹*Department of Industrial Engineering, University of Naples Federico II, Naples, Italy*

²*Section of Statistics and Data Science, Department of Mathematics, KU Leuven, Belgium*

October 31, 2025

Abstract

Principal component analysis (PCA) is a fundamental tool for analyzing multivariate data. Here the focus is on dimension reduction to the principal subspace, characterized by its projection matrix. The classical principal subspace can be strongly affected by the presence of outliers. Traditional robust approaches consider casewise outliers, that is, cases generated by an unspecified outlier distribution that differs from that of the clean cases. But there may also be cellwise outliers, which are suspicious entries that can occur anywhere in the data matrix. Another common issue is that some cells may be missing. This paper proposes a new robust PCA method, called cellPCA, that can simultaneously deal with casewise outliers, cellwise outliers, and missing cells. Its single objective function combines two robust loss functions, that together mitigate the effect of casewise and cellwise outliers. The objective function is minimized by an iteratively reweighted least squares (IRLS) algorithm. Residual cellmaps and enhanced outlier maps are proposed for outlier detection. The casewise and cellwise influence functions of the principal subspace are derived, and its asymptotic distribution is obtained. Extensive simulations and two real data examples illustrate the performance of cellPCA.

Keywords: Casewise outliers; Cellwise outliers; Iteratively reweighted least squares; Missing values; Principal subspace.

1 Introduction

The prevalence of ever larger datasets poses substantial challenges for statistical analysis. A common issue is the presence of outliers and missing data, caused by a variety of factors such as measurement errors and rare and unexpected events. Multivariate data are typically represented by a rectangular matrix in which the n rows are the cases (objects) and the p columns are the variables (measurements). Outliers or anomalies are pieces of data that behave differently from the overall pattern. Depending on the situation, outliers may be undesirable errors, or valuable nuggets of unexpected information. Either way, first we want our statistical analysis to summarize the information contained in the regular values and don't want it to be adversely affected by the outliers. Afterward we want to detect the outliers.

Diagnostic approaches first apply a classical fitting method to the data, next they detect the anomalies using diagnostic tools (such as standardized residuals), and finally they run a standard estimation procedure on the outlier-free data set. However, classical methods can be affected by outliers so strongly that the resulting fitted model may not allow to detect the outliers. This is called the masking effect. Additionally, some regular values might even appear to be outlying, which is known as swamping. A real-data example of how diagnostic approaches can be affected by masking and swamping is provided in Section A of the Supplementary Material. To avoid these effects, robust approaches aim to find an estimate that is close to the one we would have found without the outliers (Huber, 1981; Hampel et al., 1986; Rousseeuw and Leroy, 1987; Maronna et al., 2019). They construct a fit that is affected little by outliers without the need for searching and explicitly removing them. Outlier detection is then performed by looking at large deviations from the robustly estimated model.

For a long time, the term “outlier” meant an outlying case. These *casewise outliers* are assumed not to be generated by the same mechanism as the majority of the cases. Consider for example the TopGear dataset from the R package `robustHD` (Alfons, 2021). It contains technical information of 297 cars such as their height, weight, acceleration, fuel consumption, horsepower, miles per gallon (MPG), etc. Most cars in this dataset have an internal combustion engine that runs on petrol or diesel. Only a few are hybrid or

electric cars with different technical properties. In a sense they do not belong to the same population, and as such can be considered as casewise outliers.

Formally, the *casewise contamination model* assumes that the observed $n \times p$ data matrix \mathbf{X} is a random sample from a p -variate random variable X_ε distributed as $(1 - \varepsilon^{\text{case}})H_0 + \varepsilon^{\text{case}}H_Z$, where $0 \leq \varepsilon^{\text{case}} < 0.5$, H_0 is the distribution generating the clean cases, and H_Z is an unspecified outlier-generating distribution. No conditions regarding support or symmetry are imposed on H_Z . The variable X_ε can equivalently be written as

$$X_\varepsilon = A^{\text{case}} \odot X + (\mathbf{1}_p - A^{\text{case}}) \odot Z \quad (1)$$

where the Hadamard product \odot multiplies vectors (and matrices) entry by entry. Here $X \sim H_0$, $Z \sim H_Z$, and $\mathbf{1}_p$ is a column vector with all p components equal to 1. The p -variate variable A^{case} has Bernoulli distributed marginals A_j^{case} for $j = 1, \dots, p$ with success parameter $1 - \varepsilon^{\text{case}}$, and jointly they are fully dependent in the sense that $P(A_1^{\text{case}} = \dots = A_p^{\text{case}}) = 1$. When X , A^{case} and Z are independent from each other, model (1) corresponds to the classical ε -contamination model of Huber (1981), also called the *fully dependent contamination model* (FDCM) by Alqallaf et al. (2009). It implies that on average, $(1 - \varepsilon^{\text{case}})100\%$ of the cases are clean. The left panel of Figure 1 visualizes this setting for a toy data set with 15 cases and 10 variables. Here 3 out of the 15 cases (20%) are casewise outliers.

Casewise robust methods require that fewer than half of the cases are contaminated. This assumption is often realistic in low-dimensional datasets, but it becomes harder in high dimensions because then there are many variables in which something can go wrong. Moreover casewise robust methods work by downweighting or deleting all variables of the outlying cases, whereas their outlying behavior might occur in only a few measurements. This has motivated the study of *cellwise outliers* in recent years. These are deviating measurements (cells) that can occur anywhere in the data matrix. For example, in the TopGear data the weight of the Peugeot 207 was reported as only 210 kg, which is clearly wrong. That outlying cell was easy to spot, as other cars are much heavier. But not all cellwise outliers deviate marginally. The MPG of the Suzuki Jimny is 39, which is not an uncommon value by itself, but it is very low given its other characteristics such as its small size. The *cellwise contamination model* assumes that the data are generated according to

$$X_\varepsilon = A^{\text{cell}} \odot X + (\mathbf{1}_p - A^{\text{cell}}) \odot Z \quad (2)$$

with X and Z as in (1). The p -variate variable A^{cell} has Bernoulli components A_j^{cell} with success probability $1 - \varepsilon_j^{\text{cell}}$. If the components of A^{cell} are independent, we obtain the *fully independent contamination model* (FICM) of Alqallaf et al. (2009). Then on average each variable has $(1 - \varepsilon_j^{\text{cell}})100\%$ clean values, but even a relatively small proportion of outlying cells can contaminate over half the cases, which may cause casewise robust methods to fail. The middle panel of Figure 1 illustrates how a dataset with $22/150 \approx 15\%$ of outlying cells yields only $4/15 \approx 27\%$ entirely uncontaminated cases. It also illustrates that a case can have zero, one, a few, or many outlying cells. In general, when $\varepsilon_j^{\text{cell}} = \varepsilon$ the probability that a case contains at least one outlying cell is $1 - (1 - \varepsilon)^p$ which grows quickly with the dimension p . For example, when $\varepsilon = 0.05$ and $p = 14$ this probability is 51%. It increases to 97% when $p = 70$, thus impacting the vast majority of cases.

To cope with data from model (2) one needs cellwise robust methods. They can differ markedly from casewise robust methods. For instance, cellwise robust fits cannot be equivariant under orthogonal transformations, because rotating data destroys its cells. In the last decade cellwise robust estimators have been constructed for multivariate location and covariance matrices (Agostinelli et al., 2015; Raymaekers and Rousseeuw, 2024b; Puchhammer et al., 2025), for compositional data (Rieser et al., 2023), regression (Öllerer et al., 2016) and clustering of low-dimensional data (Zaccaria et al., 2025). For a recent review of the properties and challenges of cellwise methods see Raymaekers and Rousseeuw (2025).

In real data both types of outliers often occur simultaneously, and some measurements might be missing. We define the *mixed contaminated and partially observed contamination model* (MCPO) as

$$X_\varepsilon = A \odot X + (\mathbf{1}_p - A) \odot Z \quad (3)$$

where $A = A^{\text{case}} \odot A^{\text{cell}} \odot A^{\text{obs}}$, the variable A^{case} is defined as in (1), and A^{cell} as in (2). The entries A_j^{obs} in A^{obs} are binary variables with possible outcomes 1 and NA and $P(A_j^{\text{obs}} = 1) = 1 - \varepsilon_j^{\text{obs}}$. The right panel of Figure 1 shows a toy example. Different assumptions on the dependence structure of X , Z , A^{case} , A^{cell} and A^{obs} lead to different contamination models. For instance, when A^{obs} is independent of the other variables, the values in the dataset are missing completely at random.

In this paper we focus on Principal Component Analysis (PCA), a popular dimension reduction method. Cellwise outliers cause problems in this setting as PCA projects cases

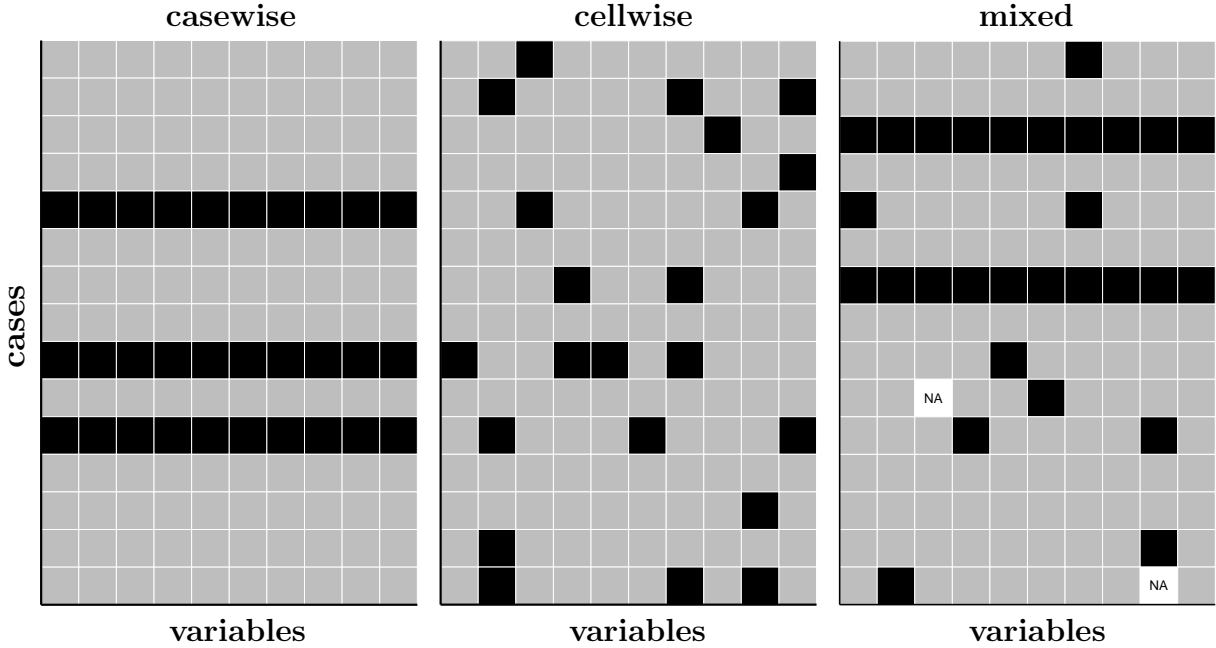


Figure 1: Illustration of the casewise, cellwise, and mixed contamination models.

orthogonally on a lower dimensional subspace, so outlying cells can propagate to all cells. Therefore, whenever a projection is made, outlying cells should be handled. Classical PCA is strongly affected by both casewise and cellwise outliers because it is a least squares method. Also the PCA method of Kiers (1997) that can handle incomplete data is not robust to outliers. Several casewise robust PCA methods have been proposed, such as Locantore et al. (1999), Hubert et al. (2005), and She et al. (2016). Some were designed for structured data matrices (Engelen and Hubert, 2011; De Klerk, 2015), and some for sparsity (Hubert et al., 2016). Serneels and Verdonck (2008) constructed a casewise robust method that can also cope with missing values. None of these approaches was designed to handle cellwise outliers. On the other hand, the cellwise robust PCA approaches developed in (De La Torre and Black, 2003; Maronna and Yohai, 2008; Candès et al., 2011) are not robust to casewise outliers, as will be illustrated in our simulations.

The more recent MacroPCA method (Hubert et al., 2019) was the first to address the three issues of casewise outliers, cellwise outliers, and missing values simultaneously. However, it is a combination of elements from earlier methods and lacks a unifying underlying principle, so it was not possible to derive statistical properties.

In this paper we propose the cellPCA method that also handles data generated from

the MCPO model (3) and offers several major improvements over MacroPCA:

1. It is the first cellwise and casewise robust PCA method that minimizes a single objective function. It combines two robust losses that effectively mitigate the effect of casewise and cellwise outliers.
2. It uses the hyperbolic tangent loss function, which yields cellwise and casewise weights between 0 and 1, reflecting the degree of outlyingness of each entry and each case. Regular cases and cells are not downweighted. This makes cellPCA more efficient than MacroPCA.
3. The optimization of the objective function is performed by an iteratively reweighted least squares algorithm, that is proved to converge.
4. We derive the casewise and cellwise influence functions of cellPCA. So far only casewise influence functions were obtained for robust PCA methods.
5. We prove asymptotic normality of the estimated principal subspace.
6. We construct imputed cases by modifying suspicious and missing cells, in such a way that their projection on the principal subspace corresponds to the fitted values.
7. Predictions are constructed for new cases, even when they are themselves incomplete and/or contain cellwise outliers.
8. Enhanced graphical displays are introduced that combine information about the cellwise and casewise outlyingness in the data.

Section 2 presents the cellPCA objective and its iteratively reweighted least squares (IRLS) algorithm. Section 3 provides the casewise and cellwise influence functions of the estimator, as well as its asymptotic distribution. Section 4 contains some practical extensions such as imputations and predictions, and Section 5 illustrates our enhanced graphical displays of outliers. The performance of cellPCA is assessed by Monte Carlo in Section 6, and Section 7 illustrates it on real data. Section 8 concludes.

2 Methodology

This section contains the core of the proposed methodology, starting with the principal subspace model and continuing with the objective function and the algorithm.

2.1 The principal subspace model

The p coordinates of the n cases are stored in an $n \times p$ data matrix \mathbf{X} . In the absence of outliers and missing values, the goal is to represent the data in a lower dimensional space:

$$\mathbf{X} = \mathbf{X}^0 + \mathbf{1}_n \boldsymbol{\mu}^T + \mathbf{E} \quad (4)$$

where \mathbf{X}^0 is an $n \times p$ matrix of rank $k < p$, $\mathbf{1}_n$ is a column vector with all n components equal to 1, the center $\boldsymbol{\mu} = (\mu_1, \dots, \mu_p)^T$ is a column vector of size p , and \mathbf{E} is the error term. We can also write this as

$$\mathbf{X} = \mathbf{X}^0 \mathbf{P} + \mathbf{1}_n \boldsymbol{\mu}^T + \mathbf{E} \quad (5)$$

where \mathbf{P} is a $p \times p$ orthogonal projection matrix of rank k , that is, $\mathbf{P}^T = \mathbf{P}$, $\mathbf{P}^2 = \mathbf{P}$ and $\text{rank}(\mathbf{P}) = k$, which projects \mathbf{X}^0 on itself, i.e. $\mathbf{X}^0 \mathbf{P} = \mathbf{X}^0$. We denote the rows of \mathbf{X}^0 as \mathbf{x}_i^0 . The image of \mathbf{P} is a k -dimensional linear subspace Π_0 through the origin. The predicted datapoints $\widehat{\mathbf{x}}_i = \mathbf{x}_i^0 + \boldsymbol{\mu}$ lie on the affine subspace $\Pi = \Pi_0 + \boldsymbol{\mu}$, which is called the *principal subspace*. Note that any k -dimensional linear subspace Π_0 determines a unique \mathbf{P} satisfying the constraints $\text{rank}(\mathbf{P}) = k$, $\mathbf{P}^T = \mathbf{P}$ and $\mathbf{P}^2 = \mathbf{P}$, and that any such \mathbf{P} determines a unique subspace Π_0 of dimension k .

In actual computations it may be unwieldy to work with the matrix \mathbf{P} because it might not fit in memory. For instance, the example in Section 7 has $p = 40,000$ so \mathbf{P} has 1.6 billion entries. Therefore we parametrize \mathbf{P} more economically. We take an orthonormal basis of Π_0 and form a $p \times k$ matrix $\mathbf{V} = \{v_{j\ell}\} = [\mathbf{v}^1, \dots, \mathbf{v}^k] = [\mathbf{v}_1, \dots, \mathbf{v}_p]^T$ whose columns are the basis vectors. Therefore \mathbf{V} is orthonormal too, that is, $\mathbf{V}^T \mathbf{V} = \mathbf{I}_k$. We can then write $\mathbf{P} = \mathbf{V} \mathbf{V}^T$. We call \mathbf{V} a loadings matrix, and define the corresponding scores matrix as $\mathbf{U} := \mathbf{X}^0 \mathbf{V} = \{u_{i\ell}\} = [\mathbf{u}^1, \dots, \mathbf{u}^k] = [\mathbf{u}_1, \dots, \mathbf{u}_n]^T$ which is $n \times k$. This way we can carry out the computations with the smaller matrices \mathbf{V} and \mathbf{U} instead of \mathbf{P} and \mathbf{X}^0 . For more on this reformulation see Section B of the Supplementary Material.

2.2 The objective function

Classical PCA approximates \mathbf{X} by $\widehat{\mathbf{X}} = \mathbf{X}^0 \mathbf{P} + \mathbf{1}_n \boldsymbol{\mu}^T$ which minimizes

$$\|\mathbf{X} - \mathbf{X}^0 \mathbf{P} - \mathbf{1}_n \boldsymbol{\mu}^T\|_F^2 \quad (6)$$

under the same constraints on \mathbf{X}^0 and \mathbf{P} , where $\|\cdot\|_F$ is the Frobenius norm. Note that (6) estimates the principal subspace $\mathbf{\Pi}$ determined by \mathbf{P} and $\boldsymbol{\mu}$, and not (yet) any principal directions inside $\mathbf{\Pi}$. Minimizing (6) is equivalent to minimizing

$$\sum_{i=1}^n \sum_{j=1}^p (x_{ij} - \hat{x}_{ij})^2 = \sum_{i=1}^n \sum_{j=1}^p r_{ij}^2 \quad (7)$$

with $\hat{x}_{ij} := \mathbf{p}_j^T \mathbf{x}_i^0 + \mu_j$, where $\mathbf{p}_1, \dots, \mathbf{p}_p$ are the columns of \mathbf{P} , and $r_{ij} := x_{ij} - \hat{x}_{ij}$. The solution is easily obtained. First carry out a singular value decomposition (SVD) of rank k as $\mathbf{X} - \mathbf{1}_n \bar{\mathbf{x}}^T \approx \mathbf{U}_k \mathbf{D}_k \mathbf{V}_k^T$ where $\bar{\mathbf{x}}$ is the sample mean, the $k \times k$ diagonal matrix \mathbf{D}_k contains the k leading singular values, and the columns of \mathbf{V}_k are the right singular vectors. Then the solution is $\mathbf{P} = \mathbf{V}_k \mathbf{V}_k^T$, $\mathbf{X}^0 = \mathbf{U}_k \mathbf{D}_k \mathbf{V}_k^T$, and $\boldsymbol{\mu} = \bar{\mathbf{x}} - \mathbf{P} \bar{\mathbf{x}}$. But the quadratic loss function in (7) makes this a least squares fit, which is very sensitive to casewise as well as cellwise outliers. Moreover, some x_{ij} may be missing.

To deal with data generated according to the MCPO model (3), we propose the cellPCA method which approximates \mathbf{X} by $\widehat{\mathbf{X}} = \mathbf{X}^0 + \mathbf{1}_n \boldsymbol{\mu}^T$ obtained by minimizing

$$L_{\rho_1, \rho_2}(\mathbf{X}, \mathbf{P}, \mathbf{X}^0, \boldsymbol{\mu}) := \frac{\widehat{\sigma}_2^2}{m} \sum_{i=1}^n m_i \rho_2 \left(\frac{1}{\widehat{\sigma}_2} \sqrt{\frac{1}{m_i} \sum_{j=1}^p m_{ij} \widehat{\sigma}_{1,j}^2 \rho_1 \left(\frac{x_{ij} - \hat{x}_{ij}}{\widehat{\sigma}_{1,j}} \right)} \right) \quad (8)$$

with respect to $(\mathbf{P}, \mathbf{X}^0, \boldsymbol{\mu})$, under the same constraints $\mathbf{P}^T = \mathbf{P}$, $\mathbf{P}^2 = \mathbf{P}$, $\text{rank}(\mathbf{P}) = k$, and $\mathbf{X}^0 \mathbf{P} = \mathbf{X}^0$. Here m_{ij} is 0 if x_{ij} is missing and 1 otherwise, $m_i = \sum_{j=1}^p m_{ij}$, and $m = \sum_{i=1}^n m_i$. The objective (8) can be interpreted as follows. The *cellwise residuals* of variable j are given by

$$r_{ij} := x_{ij} - \hat{x}_{ij} \quad (9)$$

and divided by a scale estimate $\widehat{\sigma}_{1,j}$. The *casewise total deviation* of case i is defined as

$$t_i := \sqrt{\frac{1}{m_i} \sum_{j=1}^p m_{ij} \widehat{\sigma}_{1,j}^2 \rho_1 \left(\frac{r_{ij}}{\widehat{\sigma}_{1,j}} \right)} \quad (10)$$

and standardized by $\widehat{\sigma}_2$. For $\rho_1(z) = \rho_2(z) = z^2$ the objective (8) would become the objective (7) of classical PCA. But we use bounded functions ρ_1 and ρ_2 instead. The combination of ρ_1 and ρ_2 in (8) makes cellPCA robust against both cellwise and casewise outliers. Indeed, a cellwise outlier in the cell (i, j) yields a cellwise residual r_{ij} with a large absolute value, but the boundedness of ρ_1 reduces its effect on the estimates. Similarly, a

casewise outlier results in a large casewise total deviation t_i but its effect is reduced by ρ_2 . Note that in the computation of t_i the effect of cellwise outliers is tempered by ρ_1 . This avoids that a single cellwise outlier would always give its case a large t_i .

The algorithm starts from an initial estimate, the MacroPCA fit (Hubert et al., 2019) which is robust against both cellwise and casewise outliers and can deal with NAs, but is less efficient. MacroPCA begins by imputing the NAs by the DDC algorithm (Rousseeuw and Van den Bossche, 2018). It yields an initial fit $\widehat{\mathbf{X}}_{(0)}$ from which we compute cellwise residuals $r_{ij}^{(0)}$ as in (9). For every coordinate $j = 1, \dots, p$ we then compute $\widehat{\sigma}_{1,j}$ as an M-scale of the cellwise residuals $r_{ij}^{(0)}$. An M-scale of a univariate sample (z_1, \dots, z_n) is the solution $\widehat{\sigma}$ of the equation

$$\frac{1}{n} \sum_{i=1}^n \rho\left(\frac{z_i}{\sigma}\right) = \delta \quad (11)$$

for some δ . The classical standard deviation corresponds to $\rho(z) = z^2$, but for robust methods it is important to use a bounded function ρ , otherwise the M-scale can become arbitrarily large due to even a single outlier. Also the choice of δ has an impact on the robustness properties of the scale estimator. For more on this topic see Section C of the Supplementary Material. We use an M-scale that can resist up to 50% of outlying values. We then construct casewise total deviations $t_i^{(0)}$ by (10). Next, we compute $\widehat{\sigma}_2$ as the M-scale of those $t_i^{(0)}$.

Since the DDC algorithm robustly estimates all pairwise correlations between the variables, every pair of variables should have at least 50% uncontaminated observations so that a casewise robust correlation estimator can be applied. This condition is satisfied if each variable contains at most 25% of spoiled cells. This assumption was also made by Raymaekers and Rousseeuw (2024a) for cellwise robust covariance estimation.

Translation equivariance means that if we shift the data set \mathbf{X} by a vector \mathbf{a} yielding $\mathbf{X} + \mathbf{1}_n \mathbf{a}^T$, then the fitted $\widehat{\mathbf{X}}$ is transformed in the same way to $\widehat{\mathbf{X}} + \mathbf{1}_n \mathbf{a}^T$. This is true for the initial estimator, and $\widehat{\sigma}_{1,j}$ and $\widehat{\sigma}_2$ do not change. Therefore also cellPCA is translation equivariant, as can be seen from its objective. On the other hand cellPCA is not orthogonally equivariant. Orthogonal equivariance would mean that when the data are rotated, the principal subspace and the fitted points in it would rotate in the same way. This property holds for classical PCA, but it cannot hold for cellwise robust methods.

Indeed, the cells of the data, that is, the coordinates of the data points, are tied with the coordinate system. If the data is rotated, or equivalently the coordinate system is rotated, the cells change. The effect of one outlying cell could be smeared out over all cells in its case. The loss of orthogonal equivariance is thus an unavoidable but necessary trade-off to attain robustness against cellwise contamination.

2.3 Description of the algorithm

We now address the minimization of our objective (8). The solution must satisfy the first-order necessary conditions for optimality which are derived in Section D of the Supplementary Material. For instance, the first one is obtained by setting the gradients of the objective function with respect to $\mathbf{v}_1, \dots, \mathbf{v}_p$ to zero. The second and third one use the gradients with respect to $\mathbf{u}_1, \dots, \mathbf{u}_n$ and to $\boldsymbol{\mu}$, yielding

$$(\mathbf{U}^T \mathbf{W}^j \mathbf{U}) \mathbf{v}_j = \mathbf{U}^T \mathbf{W}^j (\mathbf{x}^j - \mu_j \mathbf{1}_n), \quad j = 1, \dots, p \quad (12)$$

$$(\mathbf{V}^T \mathbf{W}_i \mathbf{V}) \mathbf{u}_i = \mathbf{V}^T \mathbf{W}_i (\mathbf{x}_i - \boldsymbol{\mu}), \quad i = 1, \dots, n \quad (13)$$

$$\sum_{i=1}^n \mathbf{W}_i \mathbf{V} \mathbf{u}_i = \sum_{i=1}^n \mathbf{W}_i (\mathbf{x}_i - \boldsymbol{\mu}) \quad (14)$$

where $\mathbf{x}_1^T, \dots, \mathbf{x}_n^T$ and $\mathbf{x}^1, \dots, \mathbf{x}^p$ are the rows and columns of \mathbf{X} . Here \mathbf{W}_i is a $p \times p$ diagonal matrix, whose diagonal entries are equal to the i th row of the $n \times p$ weight matrix

$$\mathbf{W} = \{w_{ij}\} = \mathbf{W}^{\text{case}} \odot \mathbf{W}^{\text{cell}} \odot \mathbf{M}. \quad (15)$$

Analogously, \mathbf{W}^j is an $n \times n$ diagonal matrix, whose diagonal entries are the j th column of the matrix \mathbf{W} . In expression (15) for \mathbf{W} , the $n \times p$ matrix $\mathbf{W}^{\text{cell}} = \{w_{ij}^{\text{cell}}\}$ contains the *cellwise weights*

$$w_{ij}^{\text{cell}} = \psi_1 \left(\frac{r_{ij}}{\widehat{\sigma}_{1,j}} \right) \Big/ \frac{r_{ij}}{\widehat{\sigma}_{1,j}}, \quad i = 1, \dots, n, \quad j = 1, \dots, p \quad (16)$$

where $\psi_1 = \rho'_1$ with the convention $w_{ij}^{\text{cell}}(0) = 1$. The $n \times p$ matrix \mathbf{W}^{case} has constant rows, where each entry of row i is the *casewise weight* w_i^{case} given by

$$w_i^{\text{case}} = \psi_2 \left(\frac{t_i}{\widehat{\sigma}_2} \right) \Big/ \frac{t_i}{\widehat{\sigma}_2}, \quad i = 1, \dots, n \quad (17)$$

with $\psi_2 = \rho'_2$, and the $n \times p$ matrix \mathbf{M} contains the missingness indicators m_{ij} . Note the similarity between the weight matrix \mathbf{W} in (15) and the variable $A = A^{\text{case}} \odot A^{\text{cell}} \odot A^{\text{obs}}$ in our model (3).

We now have to choose appropriate functions ρ_1 and ρ_2 . We take the hyperbolic tangent (\tanh) function $\rho_{b,c}$ introduced by Hampel et al. (1981), which is defined piecewise by

$$\rho_{b,c}(z) = \begin{cases} z^2/2 & \text{if } 0 \leq |z| \leq b \\ d - (q_1/q_2) \ln(\cosh(q_2(c - |z|))) & \text{if } b \leq |z| \leq c \\ d & \text{if } c \leq |z| \end{cases} \quad (18)$$

where $d = (b^2/2) + (q_1/q_2) \ln(\cosh(q_2(c - b)))$. Its first derivative $\psi_{b,c} = \rho'_{b,c}$ has been used as the *wrapping function* (Raymaekers and Rousseeuw, 2021a) and equals

$$\psi_{b,c}(z) = \begin{cases} z & \text{if } 0 \leq |z| \leq b \\ q_1 \tanh(q_2(c - |z|)) \text{ sign}(z) & \text{if } b \leq |z| \leq c \\ 0 & \text{if } c \leq |z|. \end{cases} \quad (19)$$

The function $\psi_{b,c}$ is continuous, which implies certain constraints on q_1 and q_2 . We use the default wrapping function shown in Figure 2, which has $b = 1.5$ and $c = 4$ with $q_1 = 1.54$ and $q_2 = 0.86$.

The bottom left panel of Figure 2 shows the weight function $w(z)$ used in (16) and (17). An advantage of the function $\psi_{b,c}$ is that it is linear in the central region $[-b, b]$, which yields a higher statistical efficiency than competing ψ functions as shown in Hampel et al. (1981). This linearity also makes the weight exactly 1 in that central region, so inlying cells will not be downweighted, which is an advantage over other ψ functions that could have been used. Moreover, far outliers get weight zero, which aids the robustness of cellPCA.

To address (12)–(14) we look at a different objective function, given by

$$\sum_{i=1}^n \sum_{j=1}^p w_{ij} (x_{ij} - \mu_j - (\mathbf{U}\mathbf{V}^T)_{ij})^2 \quad (20)$$

where $(\mathbf{U}\mathbf{V}^T)_{ij} = \mathbf{u}_i^T \mathbf{v}_j = \sum_{\ell=1}^k u_{i\ell} v_{j\ell}$ and the weight matrix \mathbf{W} is assumed fixed for now. What does this have to do with the objective (8) we are trying to minimize? Well, it is shown in Section D of the Supplementary Material that the first order conditions on the weighted PCA of (20) are exactly the same as the first order conditions (12)–(14) on the original objective (8).

The system of equations (12)–(14) is nonlinear because the weight matrices depend on the estimates, and the estimates depend on the weight matrices. The optimization

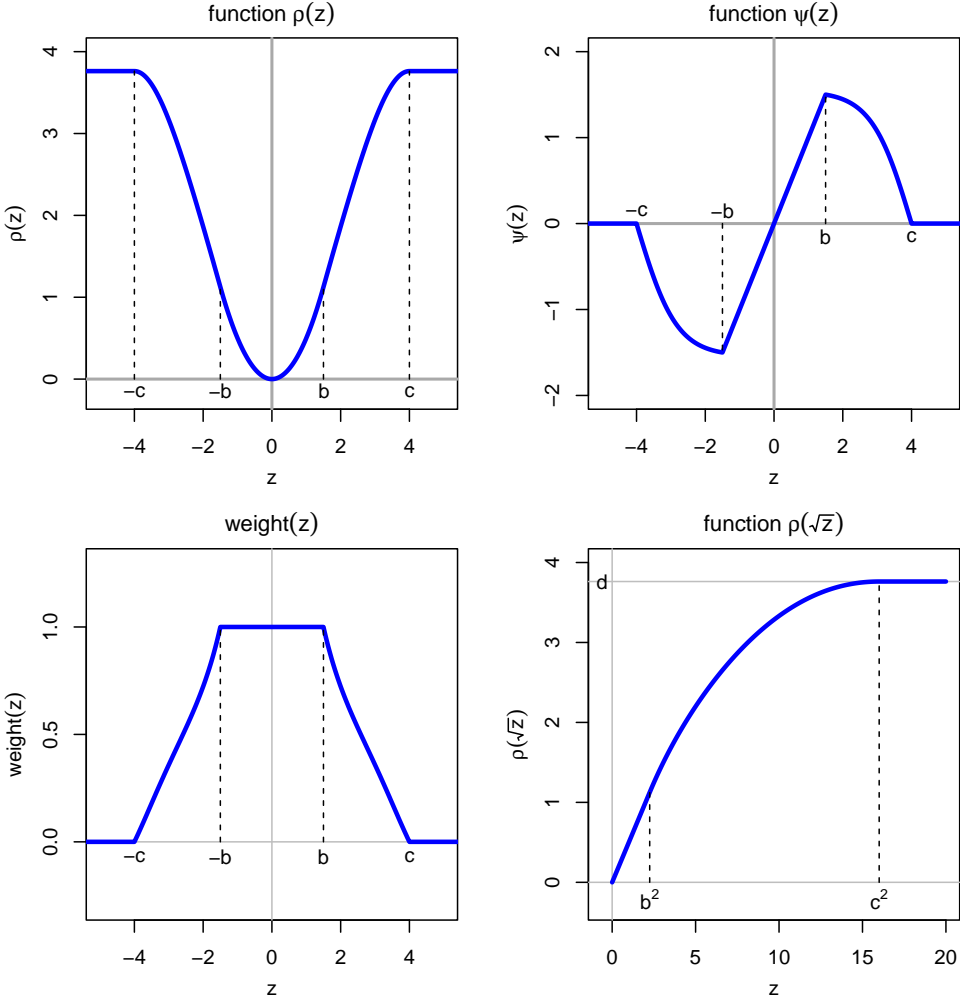


Figure 2: The function $\rho_{b,c}$ with $b = 1.5$ and $c = 4$ (top left), its derivative $\psi_{b,c}$ (top right), its weight function used in (16) and (17) (bottom left), and the function $\rho(\sqrt{z})$ (bottom right).

of (20) can be performed by alternating least squares (Gabriel, 1978). The IRLS algorithm starts from our initial estimate $(\mathbf{V}_{(0)}, \mathbf{U}_{(0)}, \boldsymbol{\mu}_{(0)})$ and the corresponding $\mathbf{W}_{(0)}$ obtained from (15), (16), and (17). Then, for each $q = 0, 1, 2, \dots$, we obtain $(\mathbf{V}_{(q+1)}, \mathbf{U}_{(q+1)}, \boldsymbol{\mu}_{(q+1)})$ from $(\mathbf{V}_{(q)}, \mathbf{U}_{(q)}, \boldsymbol{\mu}_{(q)})$ by the following four-step procedure, which is described in more detail in Section E of the Supplementary Material.

(a) Minimize (20) with respect to \mathbf{V} by applying (12) with $\mathbf{U}_{(q)}$, $\boldsymbol{\mu}_{(q)}$, and $\mathbf{W}_{(q)}$. This is done by computing

$$(\mathbf{v}_{(q+1)})_j = (\mathbf{U}_{(q)}^T \mathbf{W}_{(q)}^j \mathbf{U}_{(q)})^\dagger \mathbf{U}_{(q)}^T \mathbf{W}_{(q)}^j (\mathbf{x}^j - (\boldsymbol{\mu}_{(q)})_j \mathbf{1}_n) \quad j = 1, \dots, p \quad (21)$$

where † denotes the generalized inverse of a matrix. It is proved that starting from a different parametrization of the initial $\mathbf{P}_{(0)}$ by $\tilde{\mathbf{V}}_{(0)} = \mathbf{V}_{(0)} \mathbf{O}$ with corresponding

$\tilde{\mathbf{U}}_{(0)} = \mathbf{U}_{(0)} \mathbf{O}$ yields $\tilde{\mathbf{V}}_{(q+1)} = \mathbf{V}_{(q+1)} \mathbf{O}$ and hence the same $\mathbf{P}_{(q+1)}$.

(b) To obtain a new \mathbf{U} from the new $\mathbf{V}_{(q+1)}$ and the old $\boldsymbol{\mu}_{(q)}$ and $\mathbf{W}_{(q)}$ we apply

$$(\mathbf{V}^T \tilde{\mathbf{W}}_i \mathbf{V}) \mathbf{u}_i = \mathbf{V}^T \tilde{\mathbf{W}}_i (\mathbf{x}_i - \boldsymbol{\mu}), \quad i = 1, \dots, n \quad (22)$$

where $\tilde{\mathbf{W}}_i$ is a diagonal matrix whose diagonal is the i th row of $\mathbf{W}^{\text{cell}} \odot \mathbf{M}$. This implies (13) because each case i has a constant case weight w_i^{case} . We compute

$$(\mathbf{u}_{(q+1)})_i = (\mathbf{V}_{(q+1)}^T (\tilde{\mathbf{W}}_{(q)})_i \mathbf{V}_{(q+1)})^\dagger \mathbf{V}_{(q+1)}^T (\tilde{\mathbf{W}}_{(q)})_i (\mathbf{x}_i - \boldsymbol{\mu}_{(q)}) \quad i = 1, \dots, n. \quad (23)$$

It is proved that this minimizes (20), and that starting from the alternative parametrization yields $\tilde{\mathbf{U}}_{(q+1)} = \mathbf{U}_{(q+1)} \mathbf{O}$ and therefore the same $\mathbf{X}_{(q+1)}^0 = \mathbf{U}_{(q+1)} \mathbf{V}_{(q+1)}^T$.

(c) Minimize (20) with respect to $\boldsymbol{\mu}$ by applying (14) with the new $\mathbf{V}_{(q+1)}$ and $\mathbf{U}_{(q+1)}$ and the old $\mathbf{W}_{(q)}$ by setting

$$\boldsymbol{\mu}_{(q+1)} = \left(\sum_{i=1}^n (\mathbf{W}_{(q)})_i \right)^{-1} \sum_{i=1}^n (\mathbf{W}_{(q)})_i (\mathbf{x}_i - \mathbf{V}_{(q+1)} (\mathbf{u}_{(q+1)})_i). \quad (24)$$

(d) Update $\mathbf{W}_{(q)}$ according to (15), (16), and (17) with the new $\mathbf{V}_{(q+1)}$, $\mathbf{U}_{(q+1)}$ and $\boldsymbol{\mu}_{(q+1)}$.

The pseudocode of the algorithm is in Section I of the Supplementary Material.

Proposition 1. *Each iteration step of the algorithm decreases the objective function (8), that is, $L_{\rho_1, \rho_2}(\mathbf{X}, \mathbf{P}_{(q+1)}, \mathbf{X}_{(q+1)}^0, \boldsymbol{\mu}_{(q+1)}) \leq L_{\rho_1, \rho_2}(\mathbf{X}, \mathbf{P}_{(q)}, \mathbf{X}_{(q)}^0, \boldsymbol{\mu}_{(q)})$.*

This monotonicity result says that going from $(\mathbf{P}_{(q)}, \mathbf{X}_{(q)}^0, \boldsymbol{\mu}_{(q)})$ to $(\mathbf{P}_{(q+1)}, \mathbf{X}_{(q+1)}^0, \boldsymbol{\mu}_{(q+1)})$ reduces the variability around the PCA subspace. Therefore it is a *concentration step* in the terminology of Rousseeuw and Van Driessen (1999). The proof is given in Section F of the Supplementary Material, and uses the fact that for $z \geq 0$ the functions $z \rightarrow \rho_1(\sqrt{z})$ and $z \rightarrow \rho_2(\sqrt{z})$ are differentiable and concave, as we can see in Figure 2. Since the objective function is decreasing and it has a lower bound of zero, the algorithm must converge.

The complexity of the cellPCA algorithm is derived in Section J of the Supplementary Material. Its space complexity is $O(np)$, which equals that of the dataset. Its time complexity is that of the initial estimator MacroPCA, namely $O(np(\min(n, p) + \log(n) + \log(p)))$. This is not much higher than the complexity $O(np \min(n, p))$ of classical PCA.

3 Large-sample properties

In the following, the influence function and asymptotic normality of cellPCA are presented. All the proofs are provided in Section G of the Supplementary Material.

The influence function (IF) is a key robustness tool. It reveals how an estimating functional, i.e., a mapping from a space of probability measures to a parameter space, changes due to a small amount of contamination. Consider a p -variate random variable X with distribution H_0 . We then contaminate it as in (3) where $H_Z = \Delta_{\mathbf{z}}$ is the distribution that puts all of its mass in a fixed p -variate vector $\mathbf{z} = (z_1, \dots, z_p)^T$, yielding

$$X_\varepsilon = A \odot X + (\mathbf{1}_p - A) \odot \mathbf{z} \quad (25)$$

with $X \sim H_0$, $A \sim G_\varepsilon$ and $A = A^{\text{case}} \odot A^{\text{cell}}$.

The usual casewise IF of Hampel et al. (1986) is used for casewise contamination under the FDCM model (as defined in the introduction). It has $A = A^{\text{case}}$ with independent X and A^{case} . In that situation the distribution of X_ε simplifies to $(1 - \varepsilon^{\text{case}})H_0 + \varepsilon^{\text{case}}\Delta_{\mathbf{z}}$. We denote G_ε as G_ε^D and the distribution of X_ε as $H(G_\varepsilon^D, \mathbf{z})$. For a functional \mathbf{T} with values in \mathbb{R}^p , the casewise influence function is then defined as

$$\text{IF}_{\text{case}}(\mathbf{z}, \mathbf{T}, H_0) = \frac{\partial}{\partial \varepsilon} \mathbf{T}(H(G_\varepsilon^D, \mathbf{z})) \Big|_{\varepsilon=0} = \lim_{\varepsilon \downarrow 0} \frac{\mathbf{T}(H(G_\varepsilon^D, \mathbf{z})) - \mathbf{T}(H_0)}{\varepsilon}. \quad (26)$$

Alqallaf et al. (2009) proposed a cellwise version of the IF as well. It considers the contaminated variable (25) and the FICM model with $P(A_j^{\text{cell}} = 1) = 1 - \varepsilon^{\text{cell}}$ for all $j = 1, \dots, p$. We now denote G_ε as G_ε^I and the distribution of X_ε as $H(G_\varepsilon^I, \mathbf{z})$. The cellwise influence function $\text{IF}_{\text{cell}}(\mathbf{z}, \mathbf{T}, H_0)$ is then defined as

$$\text{IF}_{\text{cell}}(\mathbf{z}, \mathbf{T}, H_0) = \frac{\partial}{\partial \varepsilon} \mathbf{T}(H(G_\varepsilon^I, \mathbf{z})) \Big|_{\varepsilon=0} = \lim_{\varepsilon \downarrow 0} \frac{\mathbf{T}(H(G_\varepsilon^I, \mathbf{z})) - \mathbf{T}(H_0)}{\varepsilon} \quad (27)$$

So far influence functions of principal components have only been computed under the FDCM and for casewise robust PCA methods (Debruyne and Hubert, 2009; Croux et al., 2017). In the following, we derive the casewise and cellwise IF of cellPCA. We aim to study the robustness properties of $\mathbf{\Pi}$ characterized by \mathbf{P} . When there are no missing values we

can write the functional version $(\mathbf{P}(H), \boldsymbol{\mu}(H))$ of the minimizer of (8) as

$$(\mathbf{P}(H), \boldsymbol{\mu}(H)) = \underset{\mathbf{P}, \boldsymbol{\mu}}{\operatorname{argmin}} \mathbb{E}_H \left[\rho_2 \left(\frac{1}{\sigma_2(H)} \sqrt{\frac{1}{p} \sum_{j=1}^p \sigma_{1,j}^2(H) \rho_1 \left(\frac{x_j - \mu_j - \mathbf{p}_j^T \mathbf{x}^0}{\sigma_{1,j}(H)} \right)} \right) \right]$$

such that $\mathbf{x}^0 = \underset{\mathbf{x}^0}{\operatorname{argmin}} \rho_2 \left(\frac{1}{\sigma_2(H)} \sqrt{\frac{1}{p} \sum_{j=1}^p \sigma_{1,j}^2(H) \rho_1 \left(\frac{x_j - \mu_j - \mathbf{p}_j^T \mathbf{x}^0}{\sigma_{1,j}(H)} \right)} \right)$ (28)

where $\mathbf{x}^0 = (x_1^0, \dots, x_p^0)^T$ and \mathbf{P} satisfy the usual constraints and $\mathbf{x} = (x_1, \dots, x_p)^T \sim H$ with H a distribution on \mathbb{R}^p , \mathbf{p}_j and μ_j stay as before, and $\sigma_{1,j}(H)$ and $\sigma_2(H)$ are the initial scale estimators of $r_j := x_j - \mu_j - \mathbf{p}_j^T \mathbf{x}^0$ and $t := \sqrt{\frac{1}{p} \sum_{j=1}^p \sigma_{1,j}^2(H) \rho_1(r_j/\sigma_{1,j}(H))}$. If we parametrize \mathbf{P} by an orthonormal matrix \mathbf{V} with $\mathbf{V}\mathbf{V}^T = \mathbf{P}$ and set the corresponding $\mathbf{U} = \mathbf{X}^0 \mathbf{V}$, the functional versions of the first-order conditions (12)–(14) must hold:

$$\mathbb{E}_H [\mathbf{W}_x \mathbf{V} \mathbf{u}_x \mathbf{u}_x^T] = \mathbb{E}_H [\mathbf{W}_x (\mathbf{x} - \boldsymbol{\mu}) \mathbf{u}_x^T] \quad (29)$$

$$(\mathbf{V}^T \mathbf{W}_x \mathbf{V}) \mathbf{u}_x = \mathbf{V}^T \mathbf{W}_x (\mathbf{x} - \boldsymbol{\mu}) \quad (30)$$

$$\mathbb{E}_H [\mathbf{W}_x \mathbf{V} \mathbf{u}_x] = \mathbb{E}_H [\mathbf{W}_x (\mathbf{x} - \boldsymbol{\mu})]. \quad (31)$$

Here $\mathbf{W}_x = \operatorname{diag}(\mathbf{w}_x)$ for $\mathbf{w}_x = (w_1, \dots, w_p)^T$. The components of \mathbf{w}_x are $w_j = w_j^{\text{cell}} w^{\text{case}}$ with $w_j^{\text{cell}} = \psi_1 \left(\frac{r_j}{\sigma_{1,j}} \right) / \frac{r_j}{\sigma_{1,j}}$ and $w^{\text{case}} = \psi_2 \left(\frac{t}{\sigma_2} \right) / \frac{t}{\sigma_2}$. For simplicity we will assume that $\boldsymbol{\mu} = \mathbf{0}$.

Proposition 2. *The influence functions of \mathbf{P} under FDCM and FICM are*

$$\text{IF}_{\text{case}}(\mathbf{z}, \mathbf{P}, H_0) = -\mathbf{D} \left(\mathbf{S} \text{IF}_{\text{case}}(\mathbf{z}, \boldsymbol{\sigma}, H_0) + \mathbf{g}(\Delta_{\mathbf{z}}, \mathbf{V}_0, \boldsymbol{\sigma}_0) \right) \quad (32)$$

and

$$\text{IF}_{\text{cell}}(\mathbf{z}, \mathbf{P}, H_0) = -\mathbf{D} \left(\mathbf{S} \text{IF}_{\text{cell}}(\mathbf{z}, \boldsymbol{\sigma}, H_0) + p \sum_{j=1}^p \mathbf{g}(H(G_1^j, \mathbf{z}), \mathbf{V}_0, \boldsymbol{\sigma}_0) \right) \quad (33)$$

with $\boldsymbol{\sigma}(H) = (\sigma_{1,1}(H), \dots, \sigma_{1,p}(H), \sigma_2(H))^T$, $\mathbf{P}(H_0) = \mathbf{V}_0 \mathbf{V}_0^T$, $\boldsymbol{\sigma}_0 = \boldsymbol{\sigma}(H_0)$ and

$$\mathbf{g}(H, \mathbf{V}, \boldsymbol{\sigma}) = \operatorname{vec} (\mathbb{E}_H [\mathbf{W}_x (\mathbf{V} \mathbf{u}_x - \mathbf{x}) \mathbf{u}_x^T]) \quad (34)$$

where $\operatorname{vec}(\cdot)$ is the vectorization operator that converts a matrix to a vector by stacking its columns on top of each other. The matrices \mathbf{D} and \mathbf{S} are computed in Sections G and H of the Supplementary Material, and $\text{IF}_{\text{case}}(\mathbf{z}, \boldsymbol{\sigma})$ and $\text{IF}_{\text{cell}}(\mathbf{z}, \boldsymbol{\sigma})$ are the casewise and cellwise influence functions of $\boldsymbol{\sigma}$. The G_1^j in (33) puts all its mass in $(1, \dots, 0, \dots, 1)$ with the

single 0 in position j . Moreover, choosing a different parametrization \mathbf{V}_0 of $\mathbf{P}(H_0)$ yields the same $\text{IF}_{\text{case}}(\mathbf{z}, \mathbf{P})$ and $\text{IF}_{\text{cell}}(\mathbf{z}, \mathbf{P})$.

Note that (34) expresses one of the first order conditions, but the other first-order condition $(\mathbf{V}^T \mathbf{W}_x \mathbf{V}) \mathbf{u}_x = \mathbf{V}^T \mathbf{W}_x (\mathbf{x} - \boldsymbol{\mu})$ must hold as well, and acts as a constraint. Moreover, \mathbf{g} depends on $\boldsymbol{\sigma}$ through \mathbf{W}_x and \mathbf{u}_x . Also note that $H(G_1^j, \mathbf{z})$ in (33) is the distribution of $\mathbf{X} \sim H_0$ but with its j th component fixed at the constant z_j . It is thus a degenerate distribution concentrated on the hyperplane $X_j = z_j$.

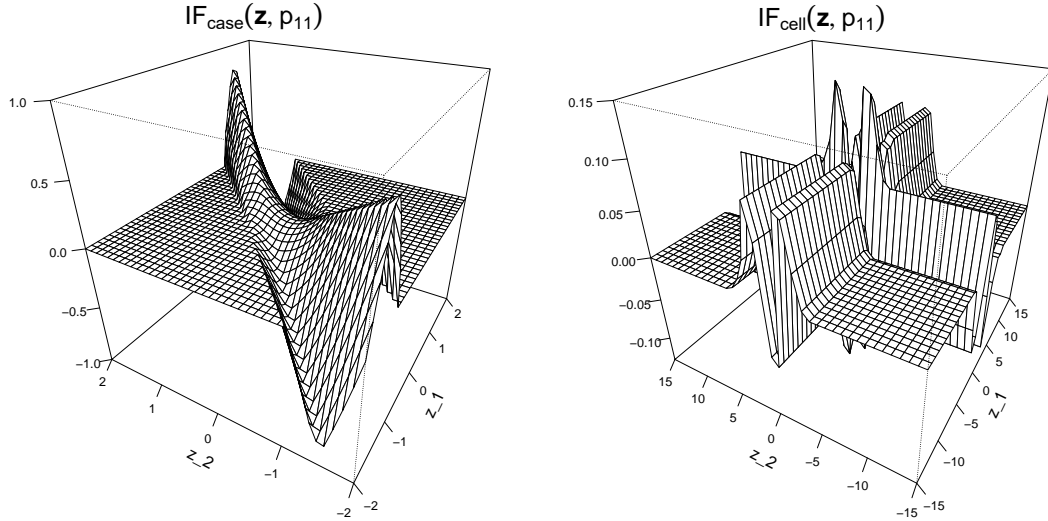


Figure 3: Casewise (left) and cellwise (right) $\text{IF}(\mathbf{z}, p_{11})$ for bivariate normal H_0 .

Let us look at a special case to get a feel for these results. For our model distribution we choose the bivariate normal $H_0 = N\left(\mathbf{0}, \begin{bmatrix} 1 & 0.9 \\ 0.9 & 1 \end{bmatrix}\right)$ and we want to fit a one-dimensional PCA subspace ($k = 1$). The PCA subspace of the population is thus the 45° line $x_2 = x_1$. The left panel of Figure 3 shows the casewise influence function of the entry p_{11} of the estimated projection matrix \mathbf{P} . If we look along the line $z_2 = -z_1$ we see the shape of the ψ -function in the right panel of Figure 2 which is bounded and redescending, from which we conclude that cellPCA is rather insensitive to outliers orthogonal to the fitted subspace. Along lines of the type $z_2 = z_1 + \text{constant}$ with small nonzero constant, the IF is unbounded. This is harmless because those (z_1, z_2) are so-called good leverage points, which are closely aligned with the fitted subspace. For the bad leverage points, i.e. with large constant, the IF is zero. Also note that \mathbf{P} itself is always bounded, since any rank- k projection matrix has Frobenius norm $\|\mathbf{P}\|_F = \sqrt{k}$.

The right panel of Figure 3 shows the cellwise IF in the same setting, which looks quite different. As a function of z_1 for a large fixed z_2 it again has the shape of the ψ -function, and for large $|z_1|$ the cellwise weight becomes zero. The situation is the same in the other direction. Also note that this IF is bounded. The exact same behavior was found by Alqallaf et al. (2009) for a redescending M-estimator of a bivariate location vector $[\mu_1 \mu_2]^T$.

It is harder to visualize the IF of the entire 2×2 matrix \mathbf{P} . Figure 4 shows the norm of the casewise and cellwise IF of \mathbf{P} , in the same setting as in Figure 3. The shape is similar to before, bearing in mind that the norm is nonnegative.

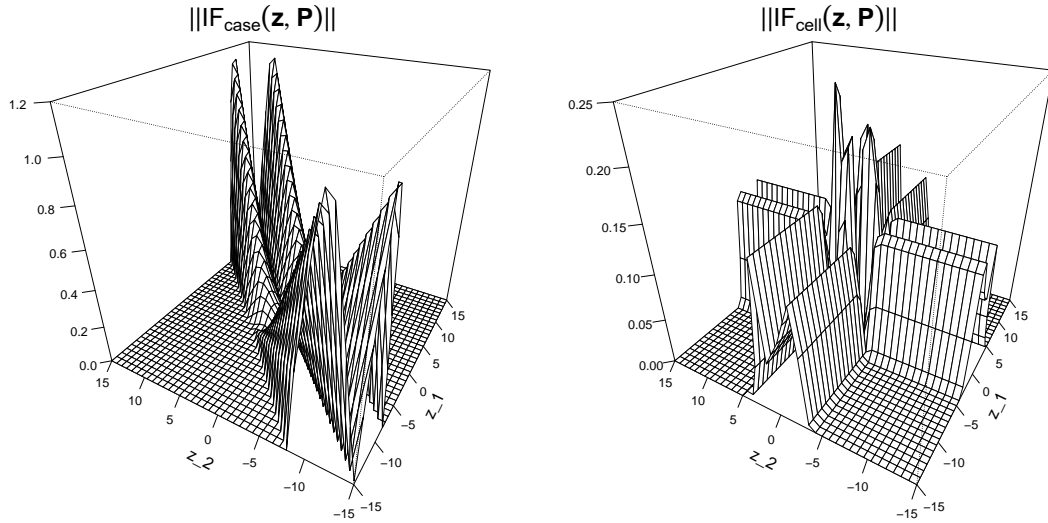


Figure 4: Norm of casewise (left) and cellwise (right) $\text{IF}(\mathbf{z}, \mathbf{P})$ for bivariate normal H_0 .

Let us now look at the asymptotic distribution of cellPCA. Suppose we obtain i.i.d. observations $\mathbf{x}_1, \mathbf{x}_2, \dots$ from H_0 . For simplicity we assume that $\boldsymbol{\mu} = \mathbf{0}$ and that $\widehat{\sigma}_{1,j}$ and $\widehat{\sigma}_2$ are fixed at $\sigma_{1,j}(H)$ and $\sigma_2(H)$. We use a fixed initial estimate $\mathbf{P}_{(0)}$ obtained as in Section 2.2. We then choose an orthonormal basis in the principal subspace, that is, a $p \times k$ matrix $\mathbf{V}_{(0)}$ with orthonormal columns such that $\mathbf{V}_{(0)} \mathbf{V}_{(0)}^T = \mathbf{P}_{(0)}$. We start the algorithm from $\mathbf{V}_{(0)}$, yielding a $\widehat{\mathbf{V}}_n$ for each sample $\{\mathbf{x}_1, \mathbf{x}_2, \dots, \mathbf{x}_n\}$. We know that $\mathbf{V}_{(0)}$ is not unique, but it is shown in Section E of the Supplementary Material that the resulting estimates $\widehat{\mathbf{P}}_n$ are the same no matter which $\mathbf{V}_{(0)}$ was chosen. Let us assume that $\widehat{\mathbf{V}}_n$ converges in probability to the population version $\mathbf{V}(H)$. We now denote

$$\widehat{\Lambda}_n(\mathbf{V}) := \frac{1}{n} \sum_{i=1}^n \boldsymbol{\Psi}(\mathbf{x}_i, \mathbf{V}) \quad \text{and} \quad \Lambda(\mathbf{V}) := \text{E}_H \boldsymbol{\Psi}(\mathbf{x}, \mathbf{V})$$

where $\Psi(\mathbf{x}_i, \mathbf{V}) = (\Psi_1(\mathbf{x}_i, \mathbf{V}), \dots, \Psi_{pk}(\mathbf{x}_i, \mathbf{V}))^T = \text{vec}(\mathbf{W}_i(\mathbf{x}_i - \mathbf{V}\mathbf{u}_i)\mathbf{u}_i^T)$, $\mathbf{u}_i = \mathbf{V}^T \mathbf{x}_i^0$, and \mathbf{x}_i^0 satisfies $(\mathbf{P}\mathbf{W}_i\mathbf{P})\mathbf{x}_i^0 = \mathbf{P}\mathbf{W}_i\mathbf{x}_i^0$. Then $\widehat{\Lambda}_n(\widehat{\mathbf{V}}_n) = \mathbf{0}$ and $\Lambda(\mathbf{V}(H)) = \mathbf{0}$.

Proposition 3. *Assume that Ψ is twice differentiable with respect to \mathbf{V} with bounded second derivatives, and that $\dot{\Psi}_\ell = \frac{\partial \Psi_\ell}{\partial \text{vec}(\mathbf{V})}$ exists and satisfies*

$$|\dot{\Psi}_\ell(\mathbf{x}, \mathbf{V})| \leq K(\mathbf{x}) \text{ with } \mathbb{E}_H[K(\mathbf{x})] < \infty$$

for any $\ell = 1, \dots, pk$, \mathbf{V} and \mathbf{x} . Then $\widehat{\mathbf{P}}_n \rightarrow \mathbf{P}(H)$ in probability, and

$$\sqrt{n} \text{vec}(\widehat{\mathbf{P}}_n - \mathbf{P}(H)) \rightarrow N_{p^2}(\mathbf{0}, \Theta)$$

in distribution, where $\Theta = \mathbb{E}_H [\text{IF}_{\text{case}}(\mathbf{x}, \mathbf{P}) \text{IF}_{\text{case}}(\mathbf{x}, \mathbf{P})^T]$ does not depend on the parametrization of \mathbf{P} .

4 Practical extensions of the methodology

4.1 Selecting the rank k

The rank k of the PCA model (4) is rarely given in advance, one typically needs to select it based on the data. In classical PCA one defines the proportion of explained variance, given by $1 - \nu_s/\nu_0$ where $\nu_s := \|\mathbf{X} - \widehat{\mathbf{X}}_s\|_F^2$ in which $\widehat{\mathbf{X}}_s$ is the best approximation of \mathbf{X} of rank s . In particular $\nu_0 = \|\mathbf{X} - \mathbf{1}_n \bar{\mathbf{x}}^T\|_F^2$ where $\bar{\mathbf{x}}$ is the sample mean. This ν_s is computed for a range of s values. One can then make a plot of ν_s versus s , which is called a scree plot. The rank k may be selected by looking for an ‘elbow’ in the scree plot (Jolliffe, 2011). The elbow can be selected visually, or in an automatic way by means of the Kneedle algorithm (Satopaa et al., 2011).

Here we define ν_s as the objective (8) of the cellPCA fit of rank s . For ν_0 we compute (8) on the cellwise residuals $x_{ij} - \text{median}_{\ell=1}^n(x_{\ell j})$. Afterward we can again search for an elbow in the scree plot of ν_s versus s by the Kneedle algorithm.

4.2 Imputation

When one or more cells of a data point \mathbf{x}_i get cell weights below 1, it means that the method considers those cells as contaminated. In such a situation it may be useful to produce an

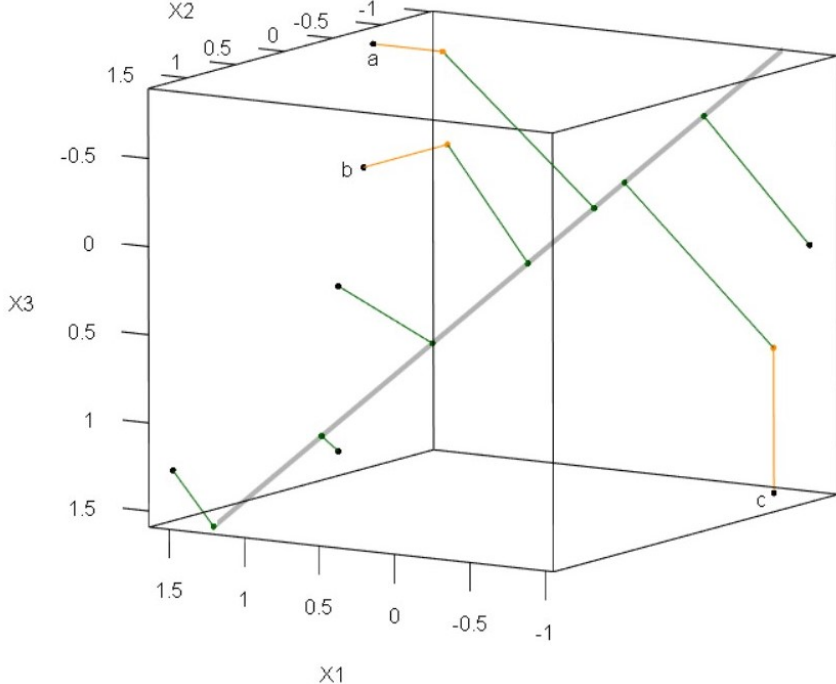


Figure 5: Illustration of imputation for $p = 3$ and $k = 1$. The first cell of point a was imputed before projecting it on the principal subspace, the second cell of b , and the third cell of c .

imputed version of that point, in which suspicious cells are cleaned and missing cells are filled in, whereas the other cells are kept as they are. So we want to obtain a point $\mathbf{x}_i^{\text{imp}}$ whose cells are $x_{ij}^{\text{imp}} = x_{ij}$ for all j with $w_{ij} = 1$, and with different cells x_{ij}^{imp} where $w_{ij} < 1$. We would like the modified cells to be such that $\mathbf{x}_i^{\text{imp}}$ is closer to the PCA subspace, and such that the orthogonal projection of $\mathbf{x}_i^{\text{imp}}$ coincides with the fitted $\hat{\mathbf{x}}_i$.

We do this as follows. From (22) and $\hat{\mathbf{x}}_i = \mathbf{V}\mathbf{u}_i + \boldsymbol{\mu}$ we know that $(\widetilde{\mathbf{W}}_i(\mathbf{x}_i - \hat{\mathbf{x}}_i))^T \mathbf{V} = \mathbf{0}$, so $\widetilde{\mathbf{W}}_i(\mathbf{x}_i - \hat{\mathbf{x}}_i)$ is orthogonal to the PCA subspace. We then construct the imputed point

$$\mathbf{x}_i^{\text{imp}} := \hat{\mathbf{x}}_i + \widetilde{\mathbf{W}}_i(\mathbf{x}_i - \hat{\mathbf{x}}_i) \quad (35)$$

so that its orthogonal projection on the PCA subspace equals $\hat{\mathbf{x}}_i$. Note that every imputed cell $x_{ij}^{\text{imp}} = \hat{x}_{ij} + w_{ij}^{\text{cell}} m_{ij}(x_{ij} - \hat{x}_{ij})$ lies between the original x_{ij} and the fitted cell \hat{x}_{ij} .

Figure 5 illustrates imputation for a 1-dimensional principal subspace in 3-dimensional space. Most points are projected orthogonally on the fitted subspace, but the first cell of point a is imputed before projecting it, and the second cell of b , and the third cell of c . None of these cells would be considered outlying in their individual variables.

4.3 Estimating a center and principal directions

So far our estimation targets were the principal subspace $\mathbf{\Pi}$ and the fit $\widehat{\mathbf{X}}$. This is often sufficient, e.g. for face recognition, computer vision, signal processing, and data compression (Vaswani et al., 2018). However, in many other applications one may wish to obtain major directions in the principal subspace, as well as a good estimate of the center of the fitted data. These may facilitate interpretation of the PCA scores in \mathbf{U} .

Note that the matrix \mathbf{V} obtained by the algorithm in Section 2.3 need not have orthonormal columns. But this can be fixed by carrying out an SVD of \mathbf{V} and putting its right singular vectors in the new $p \times k$ matrix $\tilde{\mathbf{V}}$. From this we also immediately obtain a set of k -variate scores $\tilde{\mathbf{U}} = \mathbf{U}\mathbf{V}^T\tilde{\mathbf{V}}$, and we denote $\tilde{\boldsymbol{\mu}} := \boldsymbol{\mu}$.

This initial parametrization $(\tilde{\mathbf{V}}, \tilde{\mathbf{U}}, \tilde{\boldsymbol{\mu}})$ is not yet satisfactory, because the columns of $\tilde{\mathbf{V}}$ do not reflect the shape of the point cloud, and $\tilde{\boldsymbol{\mu}}$ does not have to lie in its center. In order to obtain principal axes in the PCA subspace, the algorithm carries out an additional step which estimates a center and a scatter matrix of the scores in $\tilde{\mathbf{U}}$. This needs to be done by a robust estimation method to avoid that outlying score vectors have a large effect on the result, as illustrated in Appendix A.1 of Hubert et al. (2019). For this estimation we use the fast and robust deterministic algorithm DetMCD of Hubert et al. (2012), yielding $\hat{\boldsymbol{\mu}}_{\tilde{\mathbf{U}}}$ and $\hat{\boldsymbol{\Sigma}}_{\tilde{\mathbf{U}}}$. The spectral decomposition of $\hat{\boldsymbol{\Sigma}}_{\tilde{\mathbf{U}}}$ yields a $k \times k$ loading matrix $\hat{\mathbf{V}}_{\tilde{\mathbf{U}}}$ and eigenvalues $\hat{\lambda}_1 \geq \hat{\lambda}_2 \geq \dots \geq \hat{\lambda}_k$. We set the final parameter estimates to $\hat{\boldsymbol{\mu}} := \tilde{\boldsymbol{\mu}} + \hat{\mathbf{V}}_{\tilde{\mathbf{U}}}\hat{\boldsymbol{\mu}}_{\tilde{\mathbf{U}}}$, $\hat{\mathbf{V}} := \tilde{\mathbf{V}}\hat{\mathbf{V}}_{\tilde{\mathbf{U}}}$, and $\hat{\mathbf{U}} := (\tilde{\mathbf{U}} - \mathbf{1}_n\hat{\boldsymbol{\mu}}_{\tilde{\mathbf{U}}})\hat{\mathbf{V}}_{\tilde{\mathbf{U}}}$.

4.4 Out-of-sample prediction

The cellPCA estimation in Section 2 can be seen as a training stage. There can also be an out-of-sample stage, where a new datapoint \mathbf{x}^* arrives and we wish to predict its $\hat{\mathbf{x}}^*$. For instance, in chemometrics one often carries out a principal component regression when there are more regressors (say, intensities at many wavelengths) than cases. In the training stage, also called calibration, a PCA model of low rank k is fitted to the regressors, after which the response is regressed on the low-dimensional scores. Afterward, when a new data point arrives, it is an \mathbf{x}^* without response. If \mathbf{x}^* is clean we can simply project it on the principal subspace to obtain its scores, and predict the response from them.

However, this task becomes nontrivial when \mathbf{x}^* contains NAs and/or cellwise outliers. Then we cannot just project \mathbf{x}^* . Instead we need to estimate its scores vector \mathbf{u}^* for the given \mathbf{V} and $\boldsymbol{\mu}$. For this purpose we minimize the inner part of the objective (8) for a single $\mathbf{x}_i = \mathbf{x}^*$. That is, we minimize

$$\sum_{j=1}^p m_j^* \widehat{\sigma}_{1,j}^2 \rho_1 \left(\frac{x_j^* - \mu_j - \mathbf{v}_j^T \mathbf{u}}{\widehat{\sigma}_{1,j}} \right) \quad (36)$$

where \mathbf{V} and $\boldsymbol{\mu}$ are now known and x_{ij} was replaced by x_j^* and m_{ij} by m_j^* . When all m_j^* are zero we set \mathbf{u}^* and $\widehat{\mathbf{x}}^*$ to NA. If not, (36) becomes a sum over $J = \{j ; m_j^* = 1\}$ so

$$\mathbf{u}^* = \operatorname{argmin}_{\mathbf{u}} \sum_{j \in J} \widehat{\sigma}_{1,j}^2 \rho_1 \left(\frac{\tilde{x}_j - \mathbf{v}_j^T \mathbf{u}}{\widehat{\sigma}_{1,j}} \right) \quad (37)$$

where $\tilde{x}_j := x_j^* - \mu_j$. So \mathbf{u}^* is the slope vector of a robust regression without intercept of the column vector $\tilde{\mathbf{x}}_J = (\tilde{x}_j ; j \in J)$ on the matrix $\mathbf{V}_J = [\mathbf{v}_j^T ; j \in J]$. Note that \mathbf{V}_J has no outliers since all $|v_{j\ell}| \leq 1$. The IRLS algorithm uses the first order condition (22) and alternates updating \mathbf{u}^* according to (23) with updating the cellwise weights (16) by

$$w_j^* = \psi_1 \left(\frac{r_j}{\widehat{\sigma}_{1,j}} \right) / \frac{r_j}{\widehat{\sigma}_{1,j}} \quad \text{for } j \text{ in } J \quad (38)$$

and $w_j^* = 0$ for j not in J . The iterations continue until convergence (the pseudocode is in Section I of the Supplementary Material). Upon convergence we put $\widehat{x}_j^* := \mu_j + \mathbf{v}_j^T \mathbf{u}^*$. When \mathbf{x}^* happens to be equal to some in-sample \mathbf{x}_i it follows that $\widehat{\mathbf{x}}^* = \widehat{\mathbf{x}}_i$.

5 Displaying outliers graphically

We will now construct some graphical displays to visualize outlying cells or cases when they occur. As an illustration we consider the `ionosphere` data in the `R` package `rrcov` (Todorov and Filzmoser, 2009). This real dataset contains $n = 351$ cases with $p = 32$ numerical variables. The data were collected by the Space Physics Group of Johns Hopkins as described by Sigillito et al. (1989). The dataset contains two classes, and we restrict attention to the 225 cases labeled “good”. We applied cellPCA. The procedure in Section 4.1 yielded $k = 2$, with both components together explaining 84% of the total variability.

Figure 6 shows six cases (purple curves) together with their fitted (green) and imputed (dashed orange) curves. The bottom row shows cases that received a large casewise weight

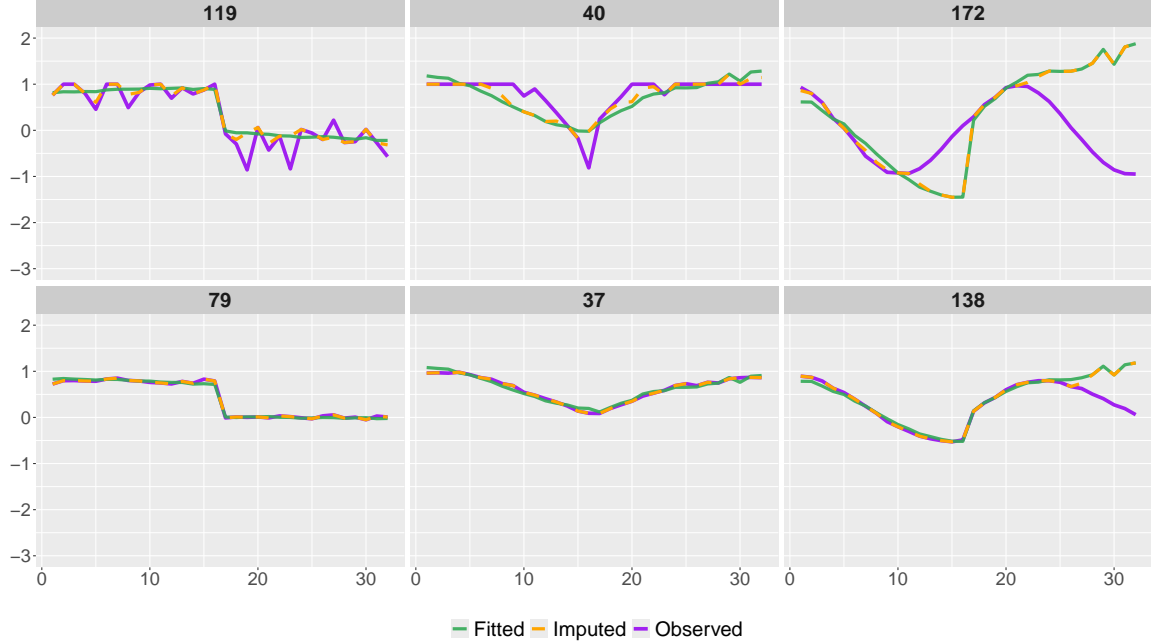


Figure 6: Observed (purple), fitted (green) and imputed (orange dashed) curves of six cases in the ionosphere data.

($w_{79}^{\text{case}} = w_{37}^{\text{case}} = w_{138}^{\text{case}} = 1$) whereas the top row plots curves with low ($w_{119}^{\text{case}} = 0.44$) and zero casewise weight ($w_{40}^{\text{case}} = w_{172}^{\text{case}} = 0$). The fitted values of the latter differ strongly from their observed values in most cells. According to (35) the imputed values agree with the observed ones in cells with cell weight $w_{ij}^{\text{cell}} = 1$, whereas they align with the fitted values when $w_{ij}^{\text{cell}} = 0$. Cell weights between 0 and 1 yield intermediate imputed values. Supplementary Material K illustrates this interpolation in detail.

In the final residual matrix $\mathbf{R} = \mathbf{X} - \widehat{\mathbf{X}} = \mathbf{X} - (\widehat{\mathbf{U}}\widehat{\mathbf{V}}^T + \mathbf{1}_n\widehat{\boldsymbol{\mu}}^T)$ we estimate the scale of each column by the M-scale (11) with the function $\rho_{b,c}$ of (18). Dividing each column of \mathbf{R} by its scale yields the standardized residuals $\widetilde{\mathbf{R}} = \{\tilde{r}_{ij}\} = [\tilde{\mathbf{r}}_1, \dots, \tilde{\mathbf{r}}_n]^T$. We can then visualize $\widetilde{\mathbf{R}}$, or some of its rows and columns, by a *residual cellmap* as in Figure 7. Cells with $|\tilde{r}_{ij}| < \sqrt{\chi^2_{1,0.99}} = 2.57$ are considered regular and colored yellow, whereas any missing values would be white. Outlying positive residuals receive a color which ranges from light orange to dark red (here, when $\tilde{r}_{ij} > 6$) and outlying negative residuals from light purple to dark blue (when $\tilde{r}_{ij} < -6$).

We see at a glance that cases 79 and 37 have no outlying cells, and that the last cells of case 138 have much lower values than expected. The cases at the bottom have cells with

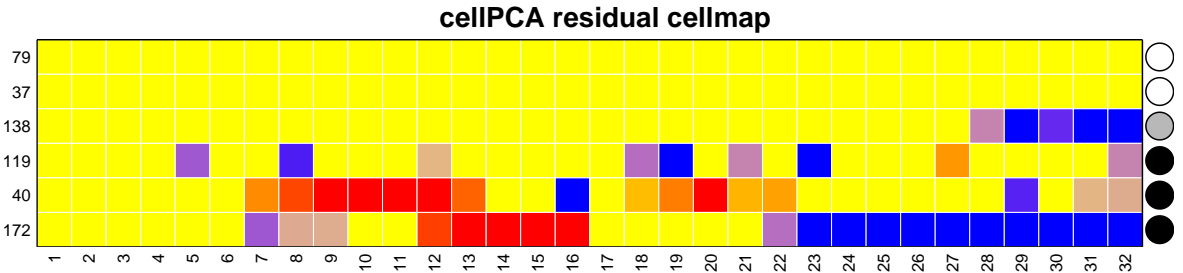


Figure 7: cellPCA residual cellmap of the six cases in Figure 6.

unexpectedly high values as well as cells with unexpectedly low values. To this residual cellmap we add information about casewise outlyingness, by coloring a circle to the right of each row according to its standardized casewise total deviation \tilde{t}_i . For this we compute t_i from $\tilde{\mathbf{r}}_i$ using (10), and divide it by its M-scale (11) with the function $\rho_{b,c}$ of (18). The circle is colored black when $\tilde{t}_i > c_{\tilde{t},0.999}$, white when $\tilde{t}_i < c_{\tilde{t},0.99}$, and has an interpolated grayscale in between. The cutoff $c_{\tilde{t},\alpha}$ is the α -quantile of the distribution of \tilde{t} simulated for uncontaminated data. These colored circles indicate casewise outliers.

To focus more on the casewise outlyingness we propose an *enhanced outlier map*, inspired by the outlier map of Hubert et al. (2019). This plot displays for each observation the norm of its standardized residual $\|\tilde{\mathbf{r}}_i\|$ versus its score distance SD_i which is defined as the norm of $(\widehat{\mathbf{V}}^T(\mathbf{x}_i - \widehat{\mathbf{\mu}})) \odot [1/\sqrt{\widehat{\lambda}_1}, \dots, 1/\sqrt{\widehat{\lambda}_k}]^T$. Figure 8 shows the enhanced outlier map obtained by applying cellPCA to the ionosphere data. The vertical dotted line indicates the cutoff $c_{SD} = \sqrt{\chi^2_{k,0.99}}$ and the horizontal dotted line is at the cutoff c_r , the 0.99-quantile of the distribution of $\|\tilde{\mathbf{r}}\|$ simulated at uncontaminated data. Regular cases have a small $SD_i \leq c_{SD}$ and a small $\|\tilde{\mathbf{r}}_i\| \leq c_r$. Cases with large SD_i and small $\|\tilde{\mathbf{r}}_i\|$ are called good leverage points. The cases with large $\|\tilde{\mathbf{r}}_i\|$ can be divided into orthogonal outliers when their SD_i is small, and bad leverage points when their SD_i is large.

The size of each point i in Figure 8 is proportional to one minus the average of its cellwise weights, i.e. $1 - \bar{w}_i^{\text{cell}} = 1 - \frac{1}{p} \sum_{j=1}^p m_{ij} w_{ij}^{\text{cell}}$. Larger points thus correspond to cases with many outlying cells. The points get the same color as the circles in the residual cellmap. This enhanced outlier map thus combines information about the cellwise and casewise outlyingness of observations, and their position with respect to and within the fitted subspace. The curves in Figure 6 occupy different positions in this outlier map.

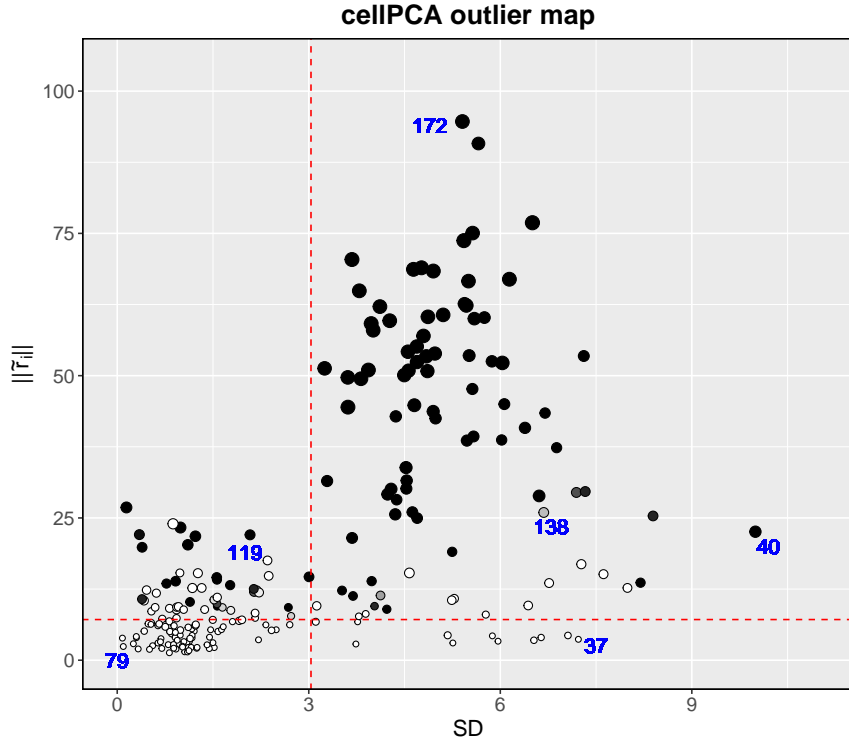


Figure 8: Enhanced outlier map of the ionosphere data.

6 Simulation study

We study the performance of cellPCA by Monte Carlo, with setup similar to (Hubert et al., 2019). The clean data are generated from a multivariate Gaussian with $\mu = \mathbf{0}$ and the covariance matrix Σ constructed as follows. Its eigenvectors are those of the matrix called A09 with entries $\Sigma_{j\ell} = (-0.9)^{|j-\ell|}$. For the eigenvalues we take numbers such that the first component explains 53% of the total variance, the first two together explain 90%, and all subsequent eigenvalues are tiny. We generate $n = 100$ data points in dimension $p = 20$ so that $n > p$, and in dimension $p = 200$ for which $n < p$.

Three contamination types are considered, according to models (1)-(3). In the cellwise outlier scenario we randomly replace $\varepsilon^{\text{cell}} = 20\%$ of the cells x_{ij} with $\gamma_{\text{cell}}\sigma_j$, where γ_{cell} varies from 0 to 6 and σ_j^2 is the j th diagonal element of Σ . In the casewise outlier setting $\varepsilon^{\text{case}} = 20\%$ of the cases are generated from $N(\gamma_{\text{case}}(\mathbf{e}_1 + \mathbf{e}_3), \Sigma/1.5)$, where \mathbf{e}_1 and \mathbf{e}_3 are the first and third eigenvectors of Σ , and γ_{case} varies from 0 to 9 when $p = 20$, and from 0 to 24 when $p = 200$. In the third scenario, the data is contaminated by $\varepsilon^{\text{cell}} = 10\%$ of cellwise outliers as well as $\varepsilon^{\text{case}} = 10\%$ of casewise outliers. Here $\gamma_{\text{case}} = 1.5\gamma_{\text{cell}}$ when

$p = 20$ and $\gamma_{\text{case}} = 4\gamma_{\text{cell}}$ when $p = 200$, where γ_{cell} again varies from 0 to 6.

We compare cellPCA with $k = 2$ to competing approaches that are robust to either cellwise outliers, casewise outliers, or both. We run the cellwise robust PCA method of Candès et al. (2011), called CANDES, the special case of cellPCA with $\rho_2(z) = z^2$ denoted as Only-cell, the casewise robust method of Hubert et al. (2005) called ROBPCA, and the special case of cellPCA with $\rho_1(z) = z^2$, called Only-case. We also run the MacroPCA method (Hubert et al., 2019), and include classical PCA (denoted as CPCa).

We measure performance by the angle between the estimated principal subspace and the true principal subspace. This angle is computed by the function `subspace()` of the R package `pracma` (Borchers, 2022). We also compute the mean squared error given by

$$\text{MSE} = \frac{1}{|\mathcal{U}|} \sum_{i \in \mathcal{U}} \sum_{j=1}^p (x_{ij}^0 - \hat{x}_{ij})^2 \quad (39)$$

where \mathcal{U} is the set of uncontaminated cases, \hat{x}_{ij} is the prediction of x_{ij} , and x_{ij}^0 is the original value of the cell before any contamination took place. We report the median angle and MSE over 1000 replications.

Figure 9 shows the median angle and MSE in the presence of either cellwise outliers, casewise outliers, or both, for $p = 200$. The plots for $p = 20$ are very similar, see Figure 20 in Section L of the Supplementary material. As expected, CPCa did best on clean data ($\gamma = 0$), but outperformed cellPCA by a small margin only. The results with outliers are more interesting. When there are only cellwise outliers, CPCa, ROBPCA, and Only-case break down, because they were not designed for cellwise outliers. CANDES did well in this setting. Here cellPCA did best, and Only-cell almost coincided with it.

In the presence of casewise outliers, CPCa, CANDES and Only-cell break down, because they were not created for that situation. Also here cellPCA does well, only slightly outperformed by Only-case. Note that cellPCA also outperforms the casewise robust method ROBPCA, as well as MacroPCA, but the latter do not break down.

When cellwise outliers and casewise outliers are combined, cellPCA outperforms overall. It naturally beats the methods that are not robust to cellwise outliers (CPCA, Only-case, ROBPCA) or not robust to casewise outliers (CPCA, CANDES, Only-cell).

In all three settings cellPCA outperforms its predecessor MacroPCA, because it minimizes an objective function in which the cellwise and casewise weights adapt to the data.

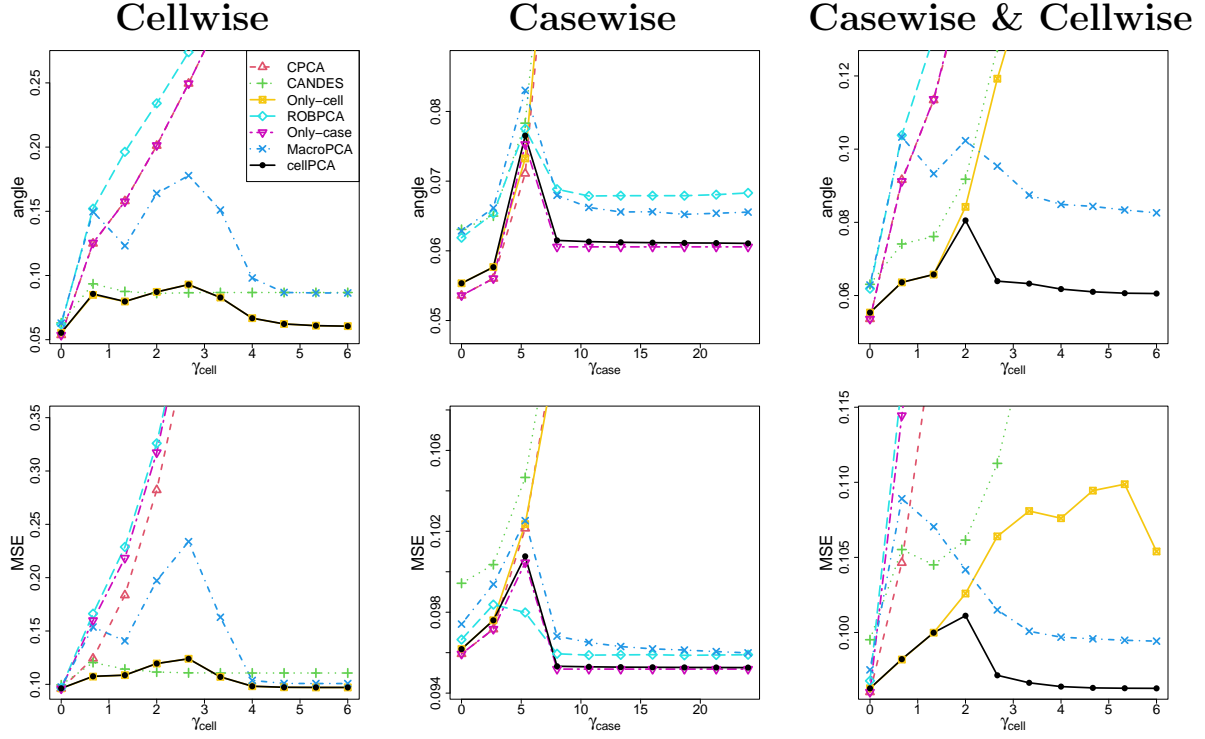


Figure 9: Median angle (top) and MSE (bottom) attained by CPCa, CANDES, Only-cell, ROBPCA, Only-case, MacroPCA, and cellPCA in the presence of either cellwise outliers, casewise outliers, or both. The covariance model was A09 with $n = 100$ and $p = 200$, without NAs.

To assess the performance in the presence of missing data, we repeated the three scenarios but also randomly set $\varepsilon^{\text{obs}} = 20\%$ of the cells to NA. In this situation we cannot run CANDES or ROBPCA which are unable to deal with missing data, and for CPCa we use the ICPCA method of Kiers (1997) that can. The resulting Figure 10 looks quite similar to Figure 9. Again cellPCA performs best overall, and outperforms MacroPCA. The remaining methods break down under the combination of cellwise outliers, casewise outliers and NAs.

Section L of the Supplementary material repeats the entire simulation where the covariance matrix A09 is replaced by more diverse random covariance matrices based on Agostinelli et al. (2015). The results in Figures 22 and 23 are very similar to those shown here, with the same conclusions. The performance of the methods is further compared in the presence of *structured cellwise outliers* as introduced in Raymaekers and Rousseeuw (2021b). The results are shown in Figure 24 and Figure 25 and show that cellPCA signifi-

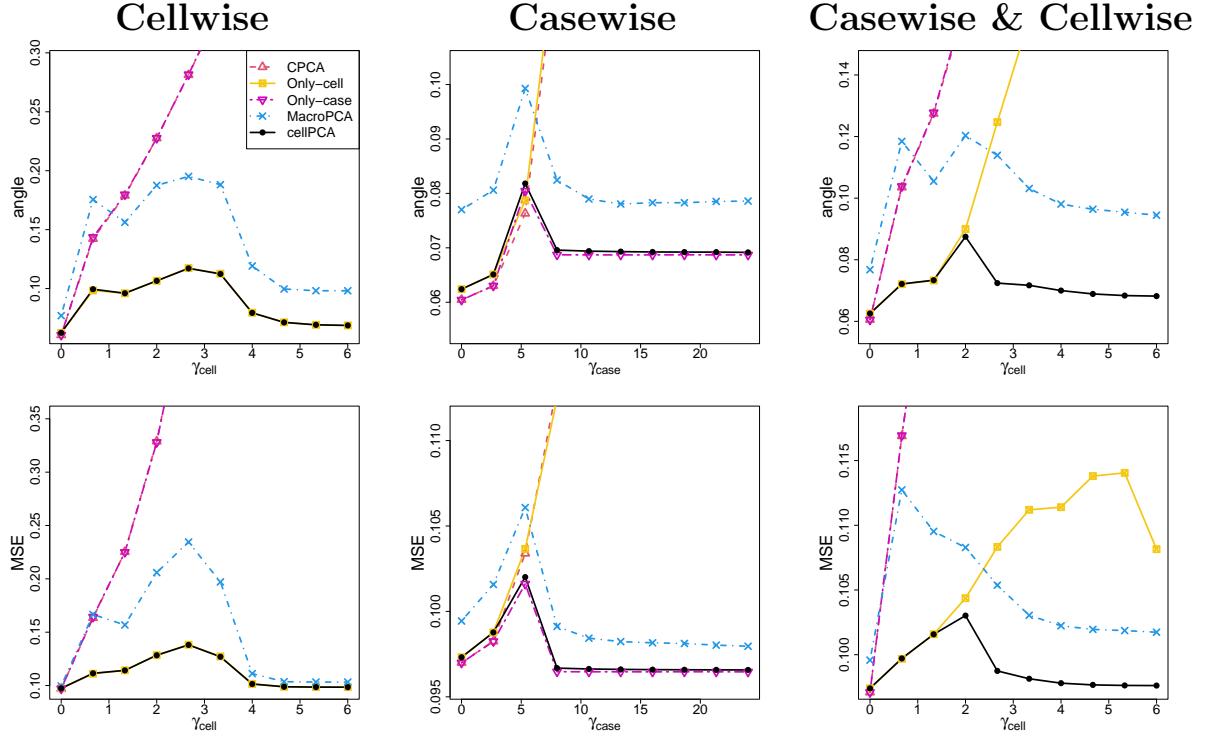


Figure 10: Median angle (top) and MSE (bottom) attained by CPCa, Only-cell, Only-case, MacroPCA, and cellPCA in the presence of either cellwise outliers, casewise outliers, or both. The covariance model was A09 with $n = 100$ and $p = 200$, and 20% of randomly selected cells were set to NA.

cantly outperforms its competitors in this more challenging setting. In Figures 26 and 27 we compare the methods under varying percentages of contamination, and in Figures 28–30 under varying percentages of NAs. In these situations cellPCA continues to outperform. Figure 31 shows that cellPCA provides a more accurate prediction of $\hat{\mathbf{x}}$ than MacroPCA, and Figure 32 does the same for imputations. In the simulation summarized in Figure 33, cellPCA typically found the natural rank k .

We now investigate how well cellPCA and MacroPCA detect outliers. For data generated with only cellwise outliers, we consider the absolute cellwise residuals obtained by both. The left panel of Figure 11 shows the total area under the receiver operating characteristic (ROC) curve, referred to as AUC, which measures how well the absolute cellwise residual predicts whether the cell is outlying. The AUC is a well-known measure of the overall performance of a binary classification method. The middle panel of Figure 11

shows the AUC for the casewise total deviation in cellPCA and the orthogonal distance of MacroPCA, which does not have the concept of casewise total deviation. In the right panel the data are contaminated by both cellwise and casewise outliers, and then the AUCs for both types of outliers are averaged. In all three panels we see that cellPCA outperforms MacroPCA, especially when both types of outliers occur together.

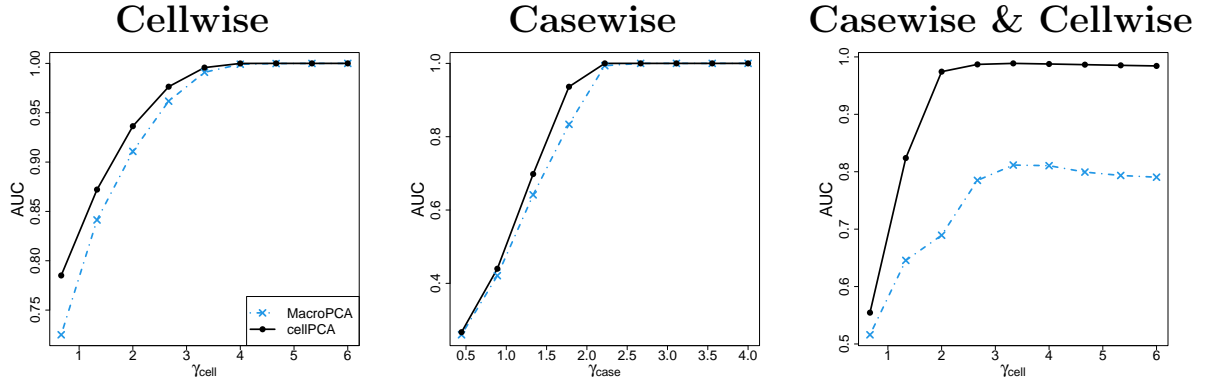


Figure 11: Median AUC of outlier detection by MacroPCA and cellPCA for either cellwise outliers, casewise outliers, or both. The covariance model was A09 with $n = 100$ and $p = 20$.

7 Real data example

Campi Flegrei is an active volcanic field partly underlying the city of Naples, Italy. It is monitored from six permanent ground stations, one of which is located at the Vesuvius crater (Sansivero and Vilardo, 2022). They record thermal infrared (TIR) images to investigate volcanic plumes and gases, lava flows, lava lakes, and fumaroles, which are vents of hot gas. The goal is to track surface thermal anomalies that may reveal a renewal of eruptive activity (Vilardo et al., 2015). The Solfatara data are available at <https://figshare.com/s/82bcfb64d5130712aeeef>. They consist of TIR images of 200×200 pixels acquired from May to November 2022 by the remote station of Solfatara 1. Vectorizing each frame yields an ultra-high dimensional data matrix with $n = 205$ and $p = 40,000$. We have applied cellPCA, with $k = 2$ obtained from Section 4.1.

Figure 12 shows the resulting enhanced outlier map. We see that many residuals have $\|\tilde{r}_i\|$ far above the horizontal cutoff line, and there are quite many casewise outliers (black

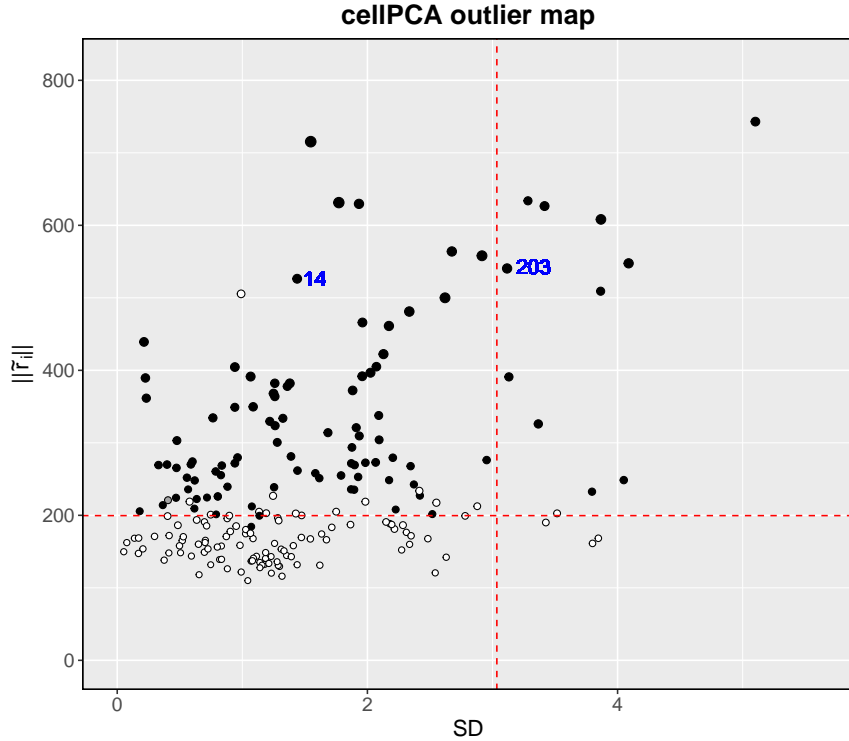


Figure 12: Enhanced outlier map of the Solfatara data.

points). The size of these points indicates that many of their cells have low weight. By way of illustration we look at one of them, case 14.

Figure 13 shows some results for frame 14. The top left panel is the observed frame, with cooler regions in blue and warmer regions in yellow to red. The predicted frame is slightly different, and overall a bit less cool. The standardized residuals are shown in the bottom panel. This is the part of the residual cellmap of the Solfatara data belonging to frame 14. The entire residual cellmap is much bigger, and has a row with 40000 cells for case 14. These cells are more easily visualized in this 200 by 200 square form corresponding to frame 14 itself. The blue region in the cellmap indicates where the observed temperature was lower than expected. It points to the condensation of hot water vapor in plumes from the volcanic fumaroles, which partly hides the heat underneath. This behavior is not visible in the raw observed frame, but it deviates from the overall linear relations described by the principal subspace.

The outlier map of Figure 12 shows where case 14 is located, and the results for case 203 are shown in section M of the Supplementary Material. Inspection showed that the casewise outliers in the outlier map were mainly among the first 23 and the last 65 cases,

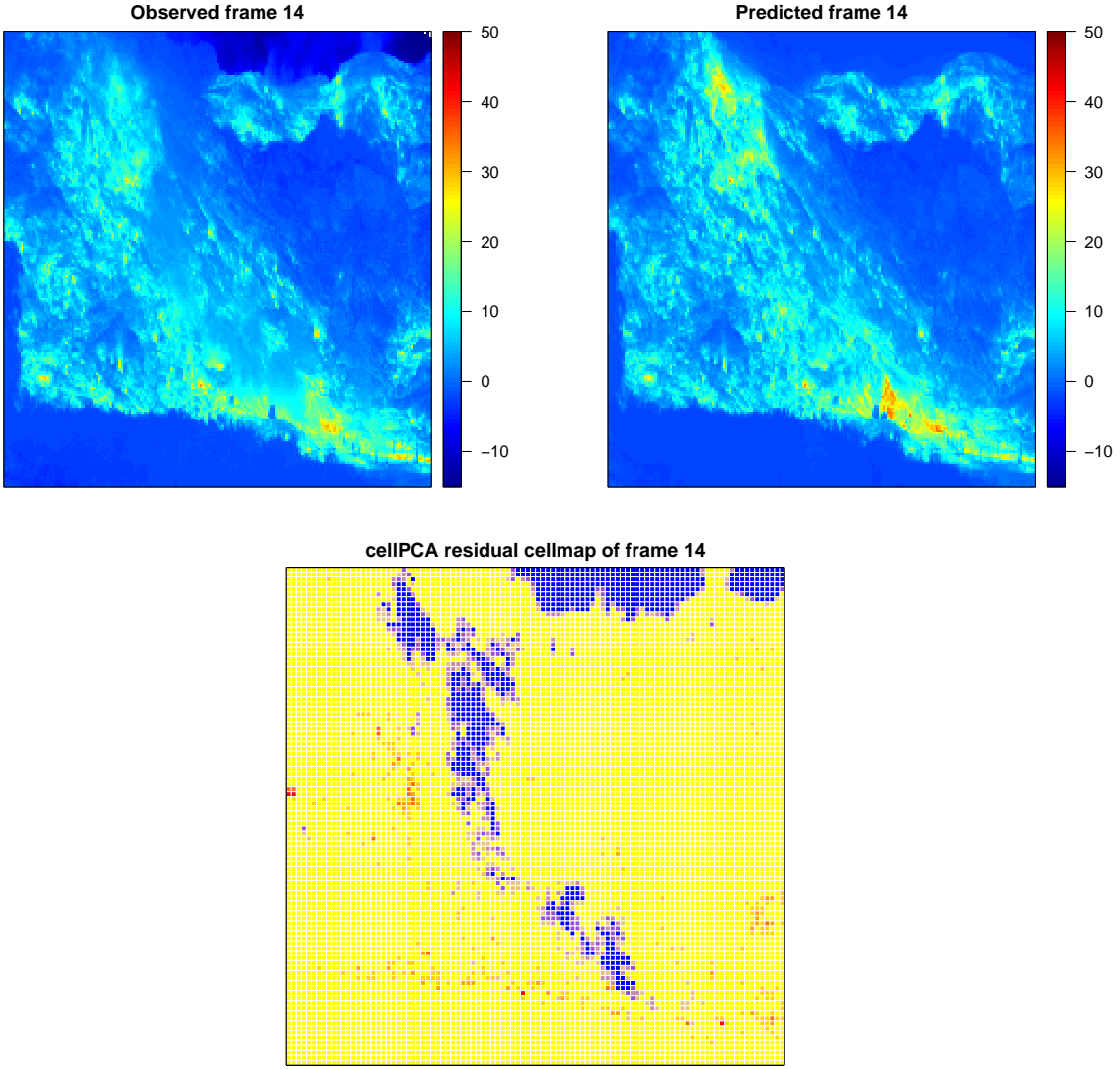


Figure 13: Solfatara data: (top left) observed frame 14, (top right) its prediction, and (bottom) its residual cellmap.

that correspond to TIR frames acquired in May, October, and November. By visually examining the frames we observed that the majority of the anomalous images exhibit temperature patterns distinctly different from those of the regular frames. As in frame 14 the residual frames often show extensive blurred regions, which have been attributed to the condensation of water vapor. This effect is most pronounced during the winter season, due to higher air humidity levels.

Moreover, we assess the performance of cellPCA to deal with missing data by replacing a random subset of 20% of the cells with NAs. Then the median absolute error (MAE) is

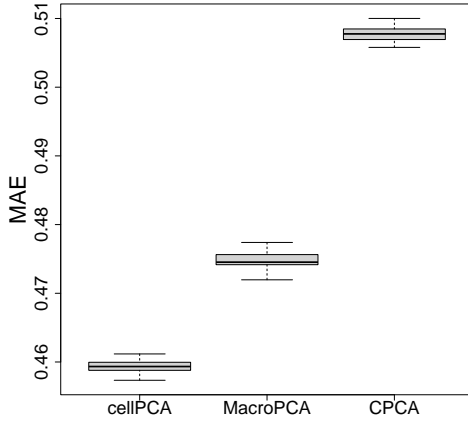


Figure 14: Boxplots of the MAE for cellPCA, MacroPCA, and CPCCA that are obtained by replacing a random subset of 20% of the Solfatara data cells with NAs.

calculated, i.e., the median absolute difference between the known values of the missing cells and the corresponding predicted values. This is repeated 50 times for cellPCA, MacroPCA, and CPCCA, and results are shown in Figure 14. The proposed method clearly outperforms the competing ones in prediction accuracy.

8 Conclusions

We have introduced a new contamination model that includes casewise outliers, cellwise outliers and missing values simultaneously. We proposed the cellPCA method, that can handle data generated by this model. The main novelty of this method is that it minimizes a single objective function. Its algorithm assigns a weight to each cell in the data, as well as to each case. The unifying objective function allowed us to derive both the cellwise and the casewise influence function of the projection matrix, as well as the asymptotic distribution of the latter. The cellwise and casewise weights allowed us to better visualize outliers in residual cellmaps and outlier maps. The method also provides imputed data that can be used in further analyses. The performance of cellPCA was showcased in a simulation study, and the method was illustrated on interesting datasets.

This work opens several directions for further research. One of those is an extension to principal component regression, and related methods like partial least squares that are often used in chemometrics. Another avenue is tensor data.

Software availability. R code for the proposed method and a script that reproduces the examples is available at <https://wis.kuleuven.be/statdatascience/robust>. The rather large Solfatara dataset that was analyzed in Section 7 can be downloaded from <https://figshare.com/s/82bcfb64d5130712aeeef>.

References

Agostinelli, C., A. Leung, V. J. Yohai, and R. H. Zamar (2015). Robust estimation of multivariate location and scatter in the presence of cellwise and casewise contamination. *Test* 24, 441–461.

Alfons, A. (2021). robustHD: An R package for robust regression with high-dimensional data. *Journal of Open Source Software* 6(67), 3786.

Alqallaf, F., S. Van Aelst, V. J. Yohai, and R. H. Zamar (2009). Propagation of outliers in multivariate data. *The Annals of Statistics* 37, 311–331.

Borchers, H. W. (2022). *pracma: Practical Numerical Math Functions*. CRAN. R package version 2.4.2.

Candès, E. J., X. Li, Y. Ma, and J. Wright (2011). Robust principal component analysis? *Journal of the ACM* 58(3), 1–37.

Croux, C., L. García-Escudero, A. Gordaliza, C. Ruwet, and R. S. Martín (2017). Robust principal component analysis based on trimming around affine subspaces. *Statistica Sinica* 27, 1437–1459.

De Klerk, J. (2015). Time series outlier detection using the trajectory matrix in singular spectrum analysis with outlier maps and ROBPCA. *South African Statistical Journal* 49, 61–76.

De La Torre, F. and M. J. Black (2003). A framework for robust subspace learning. *International Journal of Computer Vision* 54, 117–142.

Debruyne, M. and M. Hubert (2009). The influence function of the Stahel–Donoho covariance estimator of smallest outlyingness. *Statistics & Probability Letters* 79(3), 275–282.

Engelen, S. and M. Hubert (2011). Detecting outlying samples in a parallel factor analysis model. *Analytica Chimica Acta* 705, 155–165.

Gabriel, K. R. (1978). Least squares approximation of matrices by additive and multiplicative models. *Journal of the Royal Statistical Society Series B* 40(2), 186–196.

Hampel, F. R., E. M. Ronchetti, and P. J. Rousseeuw (1981). The Change-of-Variance Curve and Optimal Redescending M-Estimators. *Journal of the American Statistical Association* 76, 643–648.

Hampel, F. R., E. M. Ronchetti, P. J. Rousseeuw, and W. A. Stahel (1986). *Robust Statistics: the Approach based on Influence Functions*. Wiley.

Huber, P. J. (1981). *Robust Statistics*. John Wiley & Sons.

Hubert, M., T. Reynkens, E. Schmitt, and T. Verdonck (2016). Sparse PCA for High-Dimensional Data With Outliers. *Technometrics* 58, 424–434.

Hubert, M., P. J. Rousseeuw, and W. Van Den Bossche (2019). MacroPCA: An All-in-One PCA Method Allowing for Missing Values as Well as Cellwise and Rowwise Outliers. *Technometrics* 61(4), 459–473.

Hubert, M., P. J. Rousseeuw, and K. Vanden Branden (2005). ROBPCA: A New Approach to Robust Principal Component Analysis. *Technometrics* 47, 64–79.

Hubert, M., P. J. Rousseeuw, and T. Verdonck (2012). A deterministic algorithm for robust location and scatter. *Journal of Computational and Graphical Statistics* 21(3), 618–637.

Jolliffe, I. (2011). *Principal Component Analysis*. Springer.

Kiers, H. A. (1997). Weighted least squares fitting using ordinary least squares algorithms. *Psychometrika* 62, 251–266.

Locantore, N., J. Marron, D. Simpson, N. Tripoli, J. Zhang, K. Cohen, G. Boente, R. Fraiman, B. Brumback, C. Croux, et al. (1999). Robust principal component analysis for functional data. *Test* 8(1), 1–73.

Maronna, R. A., R. D. Martin, V. J. Yohai, and M. Salibián-Barrera (2019). *Robust Statistics: Theory and Methods (with R)*. Wiley.

Maronna, R. A. and V. J. Yohai (2008). Robust Low-Rank Approximation of Data Matrices With Elementwise Contamination. *Technometrics* 50(3), 295–304.

Öllerer, V., A. Alfons, and C. Croux (2016). The shooting S -estimator for robust regression. *Computational Statistics* 31(3), 829–844.

Puchhammer, P., I. Wilms, and P. Filzmoser (2025). A smooth multi-group Gaussian Mixture Model for cellwise robust covariance estimation. *arXiv* preprint arXiv:2504.02547.

Raymaekers, J. and P. J. Rousseeuw (2021a). Fast Robust Correlation for High-Dimensional Data. *Technometrics* 63, 184–198.

Raymaekers, J. and P. J. Rousseeuw (2021b). Handling cellwise outliers by sparse regression and robust covariance. *Journal of Data Science, Statistics, and Visualisation* 1(3), 1–29.

Raymaekers, J. and P. J. Rousseeuw (2024a). The Cellwise Minimum Covariance Determinant estimator. *Journal of the American Statistical Association* 119, 2610–2621.

Raymaekers, J. and P. J. Rousseeuw (2024b). The Cellwise Minimum Covariance Determinant Estimator. *Journal of the American Statistical Association* 119, 2610–2621.

Raymaekers, J. and P. J. Rousseeuw (2025). Challenges of cellwise outliers. *Econometrics and Statistics*, to appear, <https://doi.org/10.1016/j.ecosta.2024.02.002>.

Rieser, C., K. Fačevicová, and P. Filzmoser (2023). Cell-wise robust covariance estimation for compositions, with application to geochemical data. *Journal of Geochemical Exploration* 253, 107299.

Rousseeuw, P. J. and A. Leroy (1987). *Robust Regression and Outlier Detection*. Wiley.

Rousseeuw, P. J. and W. Van den Bossche (2018). Detecting Deviating Data Cells. *Technometrics* 60(2), 135–145.

Rousseeuw, P. J. and K. Van Driesssen (1999). A Fast Algorithm for the Minimum Covariance Determinant Estimator. *Technometrics* 41, 212–223.

Sansivero, F. and G. Vilardo (2022). *Ground-based thermal/IR images acquired by TIRNet permanent volcanic surveillance network*. Istituto Nazionale di Geofisica e Vulcanologia (INGV).

Satopaa, V., J. Albrecht, D. Irwin, and B. Raghavan (2011). Finding a “kneedle” in a haystack: Detecting knee points in system behavior. In *31st International Conference on Distributed Computing Systems Workshop*, pp. 166–171. IEEE.

Serneels, S. and T. Verdonck (2008). Principal component analysis for data containing outliers and missing elements. *Computational Statistics & Data Analysis* 52(3), 1712–1727.

She, Y., S. Li, and D. Wu (2016). Robust Orthogonal Complement Principal Component Analysis. *Journal of the American Statistical Association* 111(514), 763–771.

Sigillito, V. G., S. P. Wing, L. V. Hutton, and K. B. Baker (1989). Classification of radar returns from the ionosphere using neural networks. *Johns Hopkins APL Technical Digest* 10(3), 262–266.

Todorov, V. and P. Filzmoser (2009). An object-oriented framework for robust multivariate analysis. *Journal of Statistical Software* 32(3), 1–47.

Vaswani, N., T. Bouwmans, S. Javed, and P. Narayanamurthy (2018). Robust subspace learning: Robust PCA, robust subspace tracking, and robust subspace recovery. *IEEE Signal Processing* 35(4), 32–55.

Vilardo, G., F. Sansivero, and G. Chiodini (2015). Long-term TIR imagery processing for spatiotemporal monitoring of surface thermal features in volcanic environment: A case study in the Campi Flegrei (Southern Italy). *Journal of Geophysical Research: Solid Earth* 120(2), 812–826.

Zaccaria, G., L. A. García-Escudero, F. Greselin, and A. Mayo-Íscar (2025). Cell-wise outlier detection in heterogeneous populations. *Technometrics*, to appear, <https://doi.org/10.1080/00401706.2025.2497822>.

Supplementary Material to: Robust Principal Components by Casewise and Cellwise Weighting

A The masking effect in the diagnostic approach

To illustrate how diagnostic methods for handling outliers can be affected by the masking problem, we consider the `octane` dataset available in the `R` package `rrcov` (Todorov and Filzmoser, 2009). It contains near infrared (NIR) absorbance spectra of $n = 39$ gasoline samples over $p = 226$ wavelengths ranging from 1102 nm to 1552 nm, with measurements every two nanometers. The six gasoline samples 25, 26, and 36–39 contain added ethanol, resulting in highly deviating absorbance values in the last 80 wavelengths, as can be seen in Figure 15.

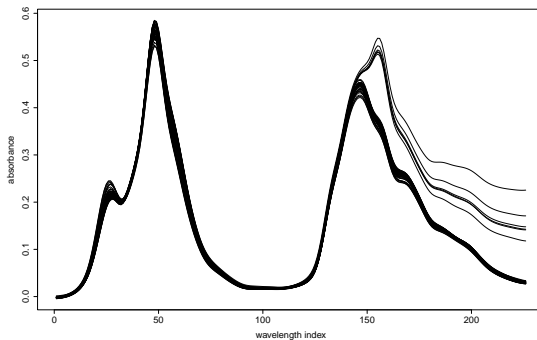


Figure 15: Raw absorbance spectra of the octane data.

The dimensionality of this dataset can be reduced by PCA. To account for the possible presence of outliers, a typical diagnostic approach repeatedly applies classical PCA to the data, and flags and removes anomalies by identifying cases with either orthogonal distance (OD) or score distance (SD) exceeding specific thresholds. The OD measures how far a point lies from the PCA estimated subspace, whereas the SD is the Mahalanobis distance between the projection of the point onto the subspace and the center. Figure 16 displays the outlier maps, which plot the OD against the SD with the corresponding thresholds, obtained using the diagnostic approach. After two iterations, no additional observations are flagged, and observations 18, 26, 32 and 38 are identified as outliers. Therefore, this method fails to detect four of the known outliers, thereby suffering from the masking effect.

Moreover, some regular observations are incorrectly flagged as outliers, so this diagnostic approach also suffers from the swamping effect.

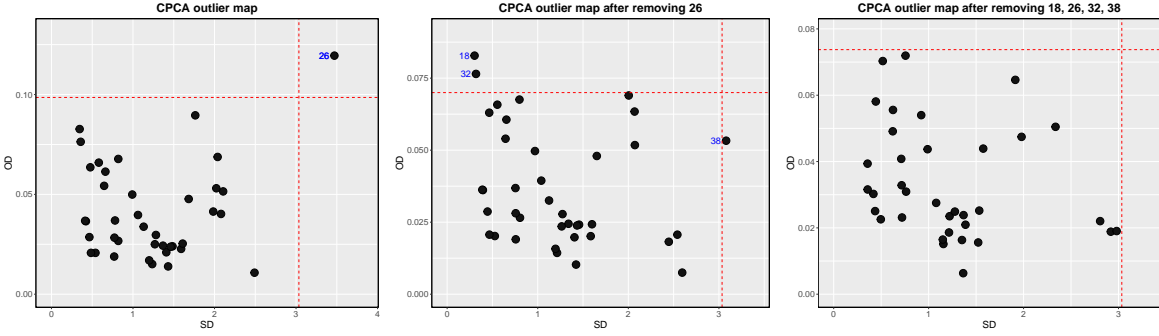


Figure 16: Outlier maps of the octane data obtained with the diagnostic approach.

Figure 17 shows the enhanced outlier map obtained by our proposed cellPCA method. Similarly to the classical outlier map, this plot displays, for each observation, the norm of the standardized residuals $\|\tilde{r}_i\|$ against its SD, with the corresponding thresholds indicated by horizontal and vertical lines. Additional details about the enhanced outlier map are provided in Section 5. All the outliers are clearly identified and have no impact on the final estimates, demonstrating the advantage of the robust approach over the diagnostic approach.

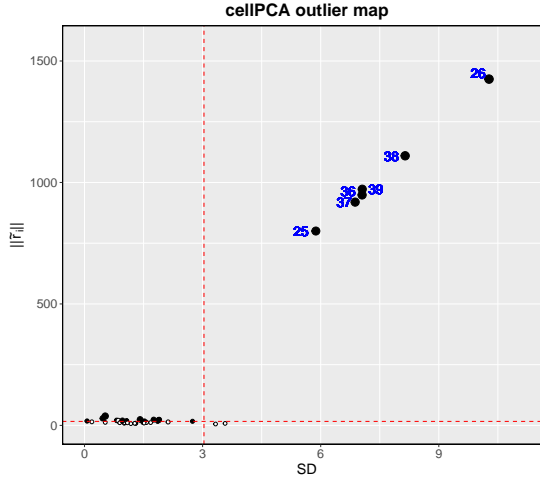


Figure 17: cellPCA enhanced outlier map of the octane data.

B Equivalent parametrizations of \mathbf{V}

The principal subspace is of the form $\mathbf{\Pi} = \mathbf{\Pi}_0 + \boldsymbol{\mu}$ where \mathbf{P}_0 is a linear subspace of dimension k which is characterized by the $p \times p$ projection matrix \mathbf{P} . We saw in Section 2.1 that \mathbf{P} can be written as $\mathbf{P} = \mathbf{V}\mathbf{V}^T$ where the $p \times k$ matrix \mathbf{V} has orthonormal columns, which form an orthonormal basis of $\mathbf{\Pi}_0$.

The only disadvantage of working with \mathbf{V} is that, unlike \mathbf{P} , it is not unique. Indeed, we could take any other orthonormal basis of $\mathbf{\Pi}_0$ corresponding to a matrix $\tilde{\mathbf{V}}$, and then $\tilde{\mathbf{V}}\tilde{\mathbf{V}}^T = \mathbf{P}$ as well. But then there must be a nonsingular $k \times k$ matrix \mathbf{A} such that $\tilde{\mathbf{V}} = \mathbf{V}\mathbf{A}$. Left multiplying by \mathbf{V}^T yields $\mathbf{V}^T\tilde{\mathbf{V}} = \mathbf{V}^T\mathbf{V}\mathbf{A} = \mathbf{A}$. We can also go in the opposite direction by $\mathbf{V} = \tilde{\mathbf{V}}\mathbf{A}^{-1}$ and then left multiply by $\tilde{\mathbf{V}}^T$ yielding $\tilde{\mathbf{V}}^T\mathbf{V} = \tilde{\mathbf{V}}^T\tilde{\mathbf{V}}\mathbf{A}^{-1} = \mathbf{A}^{-1}$. Then $\mathbf{A}^{-1} = \tilde{\mathbf{V}}^T\mathbf{V} = (\mathbf{V}^T\tilde{\mathbf{V}})^T = \mathbf{A}^T$ so \mathbf{A} is an orthogonal matrix. Therefore we can write $\tilde{\mathbf{V}} = \mathbf{V}\mathbf{O}$ where $\mathbf{O} = \mathbf{A}$ is an orthogonal $k \times k$ matrix. This shows that \mathbf{V} is only determined up to right multiplication by an orthogonal matrix.

However, we will see in the sequel that whichever parametrization \mathbf{V} is chosen, the final algorithmic and theoretical results on \mathbf{P} are the same.

C M-estimation and robustness

The M-scale $\hat{\sigma}$ given by (11) as the solution $\hat{\sigma}$ of the equation

$$\frac{1}{n} \sum_{i=1}^n \rho\left(\frac{z_i}{\sigma}\right) = \delta$$

belongs to the class of M-estimators, see e.g. Section 2.5 of Maronna et al. (2019). Here z_1, \dots, z_n is a univariate dataset and $\rho(0)$ is zero, ρ is an even function in the sense that $\rho(-z) = \rho(z)$, and $\rho(z)$ is nondecreasing for $z \geq 0$.

The robustness of $\hat{\sigma}$ depends on the boundedness of ρ . When ρ is unbounded, a single far outlier z_1 can make $\hat{\sigma}$ arbitrarily large, which is a form of breakdown. For instance, the L^1 function $\rho(z) = |z|$ yields the mean deviation $\hat{\sigma} = (n\delta)^{-1} \sum_{i=1}^n |z_i|$ which goes to infinity when $|z_1|$ grows while z_2, \dots, z_n remain the same. The same is true for the L^2 function $\rho(z) = z^2$ yielding the root mean square. Moreover, the influence function of $\hat{\sigma}$ has the shape of ρ , so ρ needs to be bounded in order for the influence function to be bounded.

The number of outliers that $\hat{\sigma}$ can withstand depends on the value of δ . The *explosion breakdown value* of $\hat{\sigma}$ is the smallest percentage of outliers in the dataset that can make $\hat{\sigma}$

arbitrarily large, and equals $\delta / \max(\rho)$. On the other hand, the *implosion breakdown value* of $\widehat{\sigma}$ is the smallest percentage of outliers that can bring $\widehat{\sigma}$ arbitrarily close to zero, and equals $(\max(\rho) - \delta) / \max(\rho)$. Since we don't want either type of breakdown to occur, the best choice is thus to take $\delta = \max(\rho)/2$. Then it would take almost 50% of outliers to destroy $\widehat{\sigma}$, so we are quite safe.

We will often want our scale estimator to be consistent for the scale parameter of a Gaussian distribution. In order to achieve that we include a consistency factor a in (11), yielding

$$\frac{1}{n} \sum_{i=1}^n \rho\left(\frac{z_i}{a\sigma}\right) = \delta \quad (\text{A.1})$$

which is a special case of (11) in which ρ is rescaled in the horizontal direction. We choose a such that $E[\rho(z/a)] = \delta$ for $z \sim N(0, 1)$, the standard Gaussian distribution. In the cellPCA algorithm we use the M-scale given by the function $\rho_{1.5,4}$ shown in the top left panel of Figure 2, for which $\max(\rho) = 3.7622$ so we put $\delta = 1.8811$ and obtain $a = 0.3431$.

In the cellPCA algorithm of Section 2.3 both the cellwise weights (16) and the casewise weights (17) use the derivative of $\rho_{b,c}$ which is denoted as $\psi_{b,c}$ and shown in the top right panel of Figure 2. Since $\rho_{b,c}$ is bounded it follows that $\psi_{b,c}(z)$ goes to zero for large positive and large negative values of z . Such functions ψ are called redescending. They were first used in M-estimators of location for univariate data, given by minimizing the objective function

$$\sum_{i=1}^n \rho\left(\frac{z_i - \mu}{\widehat{\sigma}}\right) \quad (\text{A.2})$$

in μ , where we assume that $\widehat{\sigma}$ is given. The first order condition of this minimization states that the derivative of the objective function is zero, so

$$\sum_{i=1}^n \psi\left(\frac{z_i - \widehat{\mu}}{\widehat{\sigma}}\right) = 0. \quad (\text{A.3})$$

It turns out that the influence function of $\widehat{\mu}$ has the shape of ψ . This implies that the effect of a far outlier goes to zero, which aids the robustness of the estimator. Note that the cellPCA objective (8) contains parts similar to (A.2). Moreover, univariate M-estimators of location can be computed by an algorithm that uses casewise weights based on their function ψ , as described in Section 2.8.1 of Maronna et al. (2019).

D First-order Conditions

In the following, the derivation of the first-order necessary conditions from (8) is presented.

Rewriting (8) in terms of the parameters \mathbf{V} and \mathbf{U} yields

$$L_{\rho_1, \rho_2}(\mathbf{X}, \mathbf{V}, \mathbf{U}, \boldsymbol{\mu}) := \frac{\widehat{\sigma}_2^2}{m} \sum_{i=1}^n m_i \rho_2 \left(\frac{1}{\widehat{\sigma}_2} \sqrt{\frac{1}{m_i} \sum_{j=1}^p m_{ij} \widehat{\sigma}_{1,j}^2 \rho_1 \left(\frac{x_{ij} - \mu_j - (\mathbf{U}\mathbf{V}^T)_{ij}}{\widehat{\sigma}_{1,j}} \right)} \right).$$

We start with the gradient of L_{ρ_1, ρ_2} with respect to \mathbf{v}_j which is

$$\begin{aligned} \mathbf{0} = \frac{\partial}{\partial \mathbf{v}_j} L_{\rho_1, \rho_2} &= \frac{\widehat{\sigma}_2^2}{m} \sum_{i=1}^n m_i \rho_2' \left(t_i / \widehat{\sigma}_2 \right) \frac{1}{\widehat{\sigma}_2} \frac{\partial}{\partial \mathbf{v}_j} \sqrt{\frac{1}{m_i} \sum_{j=1}^p m_{ij} \widehat{\sigma}_{1,j}^2 \rho_1 \left(\frac{x_{ij} - \widehat{x}_{ij}}{\widehat{\sigma}_{1,j}} \right)} \\ &= \frac{1}{m} \sum_{i=1}^n m_i \frac{\psi_2(t_i / \widehat{\sigma}_2)}{t_i / \widehat{\sigma}_2} \frac{1}{2m_i} \frac{\partial}{\partial \mathbf{v}_j} \left(\sum_{j=1}^p m_{ij} \widehat{\sigma}_{1,j}^2 \rho_1 \left(\frac{x_{ij} - \widehat{x}_{ij}}{\widehat{\sigma}_{1,j}} \right) \right) \\ &= \frac{1}{2m} \sum_{i=1}^n w_i^{\text{case}} \widehat{\sigma}_{1,j}^2 \psi_1(r_{ij} / \widehat{\sigma}_{1,j}) \frac{m_{ij}}{\widehat{\sigma}_{1,j}} \frac{\partial}{\partial \mathbf{v}_j} (x_{ij} - \mu_j - \mathbf{u}_i^T \mathbf{v}_j) \\ &= \frac{-1}{2m} \sum_{i=1}^n w_i^{\text{case}} \widehat{\sigma}_{1,j} \frac{\psi_1(r_{ij} / \widehat{\sigma}_{1,j})}{r_{ij} / \widehat{\sigma}_{1,j}} \frac{m_{ij}}{\widehat{\sigma}_{1,j}} r_{ij} \mathbf{u}_i \\ &= \frac{-1}{2m} \sum_{i=1}^n \mathbf{u}_i w_i^{\text{case}} w_{ij}^{\text{cell}} m_{ij} (x_{ij} - \mu_j - \mathbf{u}_i^T \mathbf{v}_j) \\ &= \frac{-1}{2m} \sum_{i=1}^n \mathbf{u}_i w_{ij} (x_{ij} - \mu_j - \mathbf{u}_i^T \mathbf{v}_j) \\ &= \frac{-1}{2m} (\mathbf{U}^T \mathbf{W}^j (\mathbf{x}^j - \mu_j \mathbf{1}_n) - \mathbf{U}^T \mathbf{W}^j \mathbf{U} \mathbf{v}_j). \end{aligned}$$

The gradient of L_{ρ_1, ρ_2} with respect to \mathbf{u}_i is

$$\begin{aligned}
\mathbf{0} = \frac{\partial}{\partial \mathbf{u}_i} L_{\rho_1, \rho_2} &= \frac{\widehat{\sigma}_2^2}{m} m_i \rho'_2(t_i/\widehat{\sigma}_2) \frac{1}{\widehat{\sigma}_2} \frac{\partial}{\partial \mathbf{u}_i} \sqrt{\frac{1}{m_i} \sum_{j=1}^p m_{ij} \widehat{\sigma}_{1,j}^2 \rho_1 \left(\frac{x_{ij} - \widehat{x}_{ij}}{\widehat{\sigma}_{1,j}} \right)} \\
&= \frac{1}{2m} \frac{\psi_2(t_i/\widehat{\sigma}_2)}{t_i/\widehat{\sigma}_2} \frac{\partial}{\partial \mathbf{u}_i} \left(\sum_{j=1}^p m_{ij} \widehat{\sigma}_{1,j}^2 \rho_1 \left(\frac{x_{ij} - \widehat{x}_{ij}}{\widehat{\sigma}_{1,j}} \right) \right) \\
&= \frac{1}{2m} \sum_{j=1}^p w_i^{\text{case}} \widehat{\sigma}_{1,j}^2 \psi_1(r_{ij}/\widehat{\sigma}_{1,j}) \frac{m_{ij}}{\widehat{\sigma}_{1,j}} \frac{\partial}{\partial \mathbf{u}_i} (x_{ij} - \mu_j - \mathbf{v}_j^T \mathbf{u}_i) \\
&= \frac{-1}{2m} \sum_{j=1}^p \mathbf{v}_j w_i^{\text{case}} \widehat{\sigma}_{1,j} \frac{\psi_1(r_{ij}/\widehat{\sigma}_{1,j})}{r_{ij}/\widehat{\sigma}_{1,j}} \frac{m_{ij}}{\widehat{\sigma}_{1,j}} r_{ij} \\
&= \frac{-1}{2m} \sum_{j=1}^p \mathbf{v}_j w_i^{\text{case}} w_{ij}^{\text{cell}} m_{ij} (x_{ij} - \mu_j - \mathbf{v}_j^T \mathbf{u}_i) \\
&= \frac{-1}{2m} (\mathbf{V}^T \mathbf{W}_i (\mathbf{x}_i - \boldsymbol{\mu}) - \mathbf{V}^T \mathbf{W}_i \mathbf{V} \mathbf{u}_i).
\end{aligned}$$

Finally, the derivative of L_{ρ_1, ρ_2} with respect to μ_j is

$$\begin{aligned}
\frac{\partial}{\partial \mu_j} L_{\rho_1, \rho_2} &= \frac{\widehat{\sigma}_2^2}{m} \sum_{i=1}^n m_i \rho'_2(t_i/\widehat{\sigma}_2) \frac{1}{\widehat{\sigma}_2} \frac{\partial}{\partial \mu_j} \sqrt{\frac{1}{m_i} \sum_{j=1}^p m_{ij} \widehat{\sigma}_{1,j}^2 \rho_1 \left(\frac{x_{ij} - \widehat{x}_{ij}}{\widehat{\sigma}_{1,j}} \right)} \\
&= \frac{1}{2m} \sum_{i=1}^n \frac{\psi_2(t_i/\widehat{\sigma}_2)}{t_i/\widehat{\sigma}_2} \frac{\partial}{\partial \mu_j} \left(\sum_{j=1}^p m_{ij} \widehat{\sigma}_{1,j}^2 \rho_1 \left(\frac{x_{ij} - \widehat{x}_{ij}}{\widehat{\sigma}_{1,j}} \right) \right) \\
&= \frac{1}{2m} \sum_{i=1}^n w_i^{\text{case}} \widehat{\sigma}_{1,j}^2 \psi_1(r_{ij}/\widehat{\sigma}_{1,j}) \frac{m_{ij}}{\widehat{\sigma}_{1,j}} \frac{\partial}{\partial \mu_j} (x_{ij} - \mu_j - \mathbf{u}_i^T \mathbf{v}_j) \\
&= \frac{-1}{2m} \sum_{i=1}^n w_i^{\text{case}} \widehat{\sigma}_{1,j} \frac{\psi_1(r_{ij}/\widehat{\sigma}_{1,j})}{r_{ij}/\widehat{\sigma}_{1,j}} \frac{m_{ij}}{\widehat{\sigma}_{1,j}} r_{ij} \\
&= \frac{-1}{2m} \sum_{i=1}^n w_i^{\text{case}} w_{ij}^{\text{cell}} m_{ij} (x_{ij} - \mu_j - \mathbf{u}_i^T \mathbf{v}_j)
\end{aligned}$$

so the gradient with respect to the vector $\boldsymbol{\mu}$ becomes

$$\mathbf{0} = \frac{\partial}{\partial \boldsymbol{\mu}} L_{\rho_1, \rho_2} = \frac{-1}{2m} \sum_{i=1}^n \mathbf{W}_i (\mathbf{x}_i - \boldsymbol{\mu} - \mathbf{V} \mathbf{u}_i).$$

We also derive the first order conditions of the weighted PCA objective function

$$\tilde{L} = \sum_{i=1}^n \sum_{j=1}^p w_{ij} (x_{ij} - \mu_j - \mathbf{u}_i^T \mathbf{v}_j)^2.$$

We start with the gradient of \tilde{L} with respect to \mathbf{v}_j which is

$$\begin{aligned}\mathbf{0} &= \frac{\partial}{\partial \mathbf{v}_j} \tilde{L} = \sum_{i=1}^n w_{ij} \frac{\partial}{\partial \mathbf{v}_j} (x_{ij} - \mu_j - \mathbf{u}_i^T \mathbf{v}_j)^2 \\ &= -2 \sum_{i=1}^n \mathbf{u}_i w_{ij} (x_{ij} - \mu_j - \mathbf{u}_i^T \mathbf{v}_j) \\ &= -2 (\mathbf{U}^T \mathbf{W}^j (\mathbf{x}^j - \mu_j \mathbf{1}_n) - \mathbf{U}^T \mathbf{W}^j \mathbf{U} \mathbf{v}_j).\end{aligned}$$

The gradient of \tilde{L} with respect to \mathbf{u}_i is

$$\begin{aligned}\mathbf{0} &= \frac{\partial}{\partial \mathbf{u}_i} \tilde{L} = \sum_{j=1}^p w_{ij} \frac{\partial}{\partial \mathbf{u}_i} (x_{ij} - \mu_j - \mathbf{u}_i^T \mathbf{v}_j)^2 \\ &= -2 \sum_{j=1}^p \mathbf{v}_j w_{ij} (x_{ij} - \mu_j - \mathbf{v}_j^T \mathbf{u}_i) \\ &= -2 (\mathbf{V}^T \mathbf{W}_i (\mathbf{x}_i - \boldsymbol{\mu}) - \mathbf{V}^T \mathbf{W}_i \mathbf{V} \mathbf{u}_i).\end{aligned}$$

Finally, the derivative of \tilde{L} with respect to μ_j is

$$\begin{aligned}\frac{\partial}{\partial \mu_j} \tilde{L} &= \sum_{i=1}^n w_{ij} \frac{\partial}{\partial \mu_j} (x_{ij} - \mu_j - \mathbf{u}_i^T \mathbf{v}_j)^2 \\ &= -2 \sum_{i=1}^n w_{ij} (x_{ij} - \mu_j - \mathbf{v}_j^T \mathbf{u}_i)\end{aligned}$$

so the gradient with respect to the vector $\boldsymbol{\mu}$ becomes

$$\mathbf{0} = \frac{\partial}{\partial \boldsymbol{\mu}} \tilde{L} = -2 \sum_{i=1}^n \mathbf{W}_i (\mathbf{x}_i - \boldsymbol{\mu} - \mathbf{V} \mathbf{u}_i).$$

E Description of the Algorithm

In each step of the algorithm we optimize the objective function of the weighted principal subspace objective (20) by adjusting the components \mathbf{V} , \mathbf{U} and $\boldsymbol{\mu}$ one after the other, by means of the first-order optimality conditions (12)–(14). This is all done for a fixed weight function. Afterward, the weight function is updated too.

The IRLS algorithm starts from our initial estimate $(\mathbf{V}_{(0)}, \mathbf{U}_{(0)}, \boldsymbol{\mu}_{(0)})$. Then, for each $q = 0, 1, 2, \dots$, we obtain $(\mathbf{V}_{(q+1)}, \mathbf{U}_{(q+1)}, \boldsymbol{\mu}_{(q+1)})$ from $(\mathbf{V}_{(q)}, \mathbf{U}_{(q)}, \boldsymbol{\mu}_{(q)})$ by a four-step procedure.

(a) Minimize (20) with respect to \mathbf{V} by applying (12) with $\mathbf{U}_{(q)}$, $\boldsymbol{\mu}_{(q)}$, and $\mathbf{W}_{(q)}$, the weight matrix based on $(\mathbf{V}_{(q)}, \mathbf{U}_{(q)}, \boldsymbol{\mu}_{(q)})$. Condition (12) says

$$(\mathbf{U}_{(q)}^T \mathbf{W}_{(q)}^j \mathbf{U}_{(q)}) \mathbf{v}_j = \mathbf{U}_{(q)}^T \mathbf{W}_{(q)}^j (\mathbf{x}^j - (\boldsymbol{\mu}_{(q)})_j \mathbf{1}_n) \quad j = 1, \dots, p. \quad (\text{A.4})$$

For a fixed j we now want to find the best column vector \mathbf{v}_j in the sense of minimizing the objective function (20), in particular the term

$$\begin{aligned} \sum_{i=1}^n (\mathbf{W}_{(q)}^j)_{ii} (x_{ij} - (\boldsymbol{\mu}_{(q)})_j - \hat{x}_{ij})^2 &= \sum_{i=1}^n (\mathbf{W}_{(q)}^j)_{ii} (x_{ij} - (\boldsymbol{\mu}_{(q)})_j - (\mathbf{U}_{(q)} \mathbf{V}^T)_{ij})^2 \\ &= \|(\mathbf{W}_{(q)}^j)^{1/2} (\mathbf{x}^j - (\boldsymbol{\mu}_{(q)})_j \mathbf{1}_n) - (\mathbf{W}_{(q)}^j)^{1/2} \mathbf{U}_{(q)} \mathbf{v}_j\|^2 \end{aligned} \quad (\text{A.5})$$

that depends on \mathbf{v}_j . This is the objective of the least squares regression of $(\mathbf{W}_{(q)}^j)^{1/2} (\mathbf{x}^j - (\boldsymbol{\mu}_{(q)})_j \mathbf{1}_n)$ on $(\mathbf{W}_{(q)}^j)^{1/2} \mathbf{U}_{(q)}$, so the optimum is reached at

$$\begin{aligned} \mathbf{v}_j &= \left[(\mathbf{W}_{(q)}^j)^{1/2} \mathbf{U}_{(q)} \right]^T (\mathbf{W}_{(q)}^j)^{1/2} \mathbf{U}_{(q)} \left[(\mathbf{W}_{(q)}^j)^{1/2} \mathbf{U}_{(q)} \right]^T (\mathbf{W}_{(q)}^j)^{1/2} (\mathbf{x}^j - (\boldsymbol{\mu}_{(q)})_j \mathbf{1}_n) \\ &= (\mathbf{U}_{(q)}^T \mathbf{W}_{(q)}^j \mathbf{U}_{(q)})^\dagger \mathbf{U}_{(q)}^T \mathbf{W}_{(q)}^j (\mathbf{x}^j - (\boldsymbol{\mu}_{(q)})_j \mathbf{1}_n) \end{aligned} \quad (\text{A.6})$$

where † stands for the Moore-Penrose generalized inverse. Repeating this for all $j = 1, \dots, p$ yields a new matrix $\mathbf{V}_{(q+1)}$ with rows $\tilde{\mathbf{v}}_1, \dots, \tilde{\mathbf{v}}_p$, which attains the lowest objective when everything else remains fixed.

Note that the initial $\mathbf{V}_{(0)}$ that we started the algorithm from was not unique, and could be replaced by $\tilde{\mathbf{V}}_{(0)} = \mathbf{V}_{(0)} \mathbf{O}$ for any $k \times k$ orthogonal matrix \mathbf{O} . It may seem that the resulting $\mathbf{P}_{(1)}, \dots, \mathbf{P}_{(q+1)}, \dots$ need not be unique, but we will show that they are. We will show this by induction. For $q = 0$ we note that the score matrix $\mathbf{U}_{(0)}$ becomes

$\tilde{\mathbf{U}}_{(0)} = (\mathbf{U}_{(0)} \mathbf{V}_{(0)}^T) \tilde{\mathbf{V}}_{(0)} = \mathbf{U}_{(0)} \mathbf{V}_{(0)}^T \mathbf{V}_{(0)} \mathbf{O} = \mathbf{U}_{(0)} \mathbf{O}$. The right-hand side of (A.6) becomes

$$\begin{aligned} & (\mathbf{O}^T \mathbf{U}_{(0)}^T \mathbf{W}_{(0)}^j \mathbf{U}_{(0)} \mathbf{O})^\dagger \mathbf{O}^T \mathbf{U}_{(0)}^T \mathbf{W}_{(0)}^j (\mathbf{x}^j - (\boldsymbol{\mu}_{(0)})_j \mathbf{1}_n) \\ &= \mathbf{O}^T (\mathbf{U}_{(0)}^T \mathbf{W}_{(0)}^j \mathbf{U}_{(0)})^\dagger \mathbf{U}_{(0)}^T \mathbf{W}_{(0)}^j (\mathbf{x}^j - (\boldsymbol{\mu}_{(0)})_j \mathbf{1}_n) \end{aligned}$$

because \mathbf{O} has orthonormal columns and $\mathbf{O}^\dagger = \mathbf{O}^{-1} = \mathbf{O}^T$. So $\tilde{\mathbf{V}}_{(1)} = \mathbf{V}_{(1)} \mathbf{O}$. The step from $\mathbf{V}_{(q)}$ to $\mathbf{V}_{(q+1)}$ is analogous, so by induction we know that for all q it holds that $\tilde{\mathbf{V}}_{(q+1)} = \mathbf{V}_{(q+1)} \mathbf{O}$ and $\tilde{\mathbf{V}}_{(q+1)} \tilde{\mathbf{V}}_{(q+1)}^T = \mathbf{V}_{(q+1)} \mathbf{V}_{(q+1)}^T$ hence $\mathbf{P}_{(q+1)}^* = \mathbf{P}_{(q+1)}$.

(b) Minimize (20) with respect to \mathbf{U} by (13) with the new $\mathbf{V}_{(q+1)}$ and the old $\boldsymbol{\mu}_{(q)}$ and $\mathbf{W}_{(q)}$. For this we use the first order condition (13), which says

$$(\mathbf{V}_{(q+1)}^T (\mathbf{W}_{(q)})_i \mathbf{V}_{(q+1)}) \mathbf{u}_i = \mathbf{V}_{(q+1)}^T (\mathbf{W}_{(q)})_i (\mathbf{x}_i - \boldsymbol{\mu}_{(q)}), \quad i = 1, \dots, n. \quad (\text{A.7})$$

For a fixed i our goal is find the \mathbf{u}_i that minimizes the corresponding term

$$\|(\mathbf{W}_{(q)})_i^{1/2} (\mathbf{x}_i - \boldsymbol{\mu}_{(q)}) - (\mathbf{W}_{(q)})_i^{1/2} \mathbf{V}_{(q+1)} \mathbf{u}_i\|^2 \quad (\text{A.8})$$

of the objective (20). We instead minimize

$$\|(\tilde{\mathbf{W}}_{(q)})_i^{1/2} (\mathbf{x}_i - \boldsymbol{\mu}_{(q)}) - (\tilde{\mathbf{W}}_{(q)})_i^{1/2} \mathbf{V}_{(q+1)} \mathbf{u}_i\|^2. \quad (\text{A.9})$$

This is the least squares regression of $(\tilde{\mathbf{W}}_{(q)})_i^{1/2} (\mathbf{x}_i - \boldsymbol{\mu}_{(q)})$ on $(\tilde{\mathbf{W}}_{(q)})_i^{1/2} \mathbf{V}_{(q+1)}$ with solution

$$\begin{aligned} (\mathbf{u}_{(q+1)})_i &= \left([(\tilde{\mathbf{W}}_{(q)})_i^{1/2} \mathbf{V}_{(q+1)}]^T (\tilde{\mathbf{W}}_{(q)})_i^{1/2} \mathbf{V}_{(q+1)} \right)^\dagger \left[(\tilde{\mathbf{W}}_{(q)})_i^{1/2} \mathbf{V}_{(q+1)} \right]^T (\tilde{\mathbf{W}}_{(q)})_i^{1/2} (\mathbf{x}_i - \boldsymbol{\mu}_{(q)}) \\ &= \left(\mathbf{V}_{(q+1)}^T (\tilde{\mathbf{W}}_{(q)})_i \mathbf{V}_{(q+1)} \right)^\dagger \mathbf{V}_{(q+1)}^T (\tilde{\mathbf{W}}_{(q)})_i (\mathbf{x}_i - \boldsymbol{\mu}_{(q)}). \end{aligned} \quad (\text{A.10})$$

Note that this solution also minimizes (A.8) which equals w_i^{case} times (A.9). When the casewise weight w_i^{case} is strictly positive these minimizations are equivalent, and when $w_i^{\text{case}} = 0$ the norm (A.8) attains its lower bound of zero anyway. Repeating this for all i yields $\mathbf{U}_{(q+1)}$ and therefore $\mathbf{X}_{(q+1)}^0 := \mathbf{U}_{(q+1)} \mathbf{V}_{(q+1)}^T$.

As in step (a) we note that $\mathbf{V}_{(q+1)}$ is not unique so neither is $\mathbf{U}_{(q+1)}$, but their product $\mathbf{X}_{(q+1)}^0 := \mathbf{U}_{(q+1)} \mathbf{V}_{(q+1)}^T$ is unique. We show this as follows. Writing $\tilde{\mathbf{V}}_{(q+1)} = \mathbf{V}_{(q+1)} \mathbf{O}$ and $\tilde{\mathbf{U}}_{(q+1)} = \mathbf{U}_{(q+1)} \mathbf{O}$ the right-hand side of (A.10) becomes

$$\mathbf{O}^\dagger \left(\mathbf{V}_{(q+1)}^T (\tilde{\mathbf{W}}_{(q)})_i \mathbf{V}_{(q+1)} \right)^\dagger \mathbf{V}_{(q+1)}^T (\tilde{\mathbf{W}}_{(q)})_i (\mathbf{x}_i - \boldsymbol{\mu}_{(q)}) \quad \text{so} \quad \tilde{\mathbf{U}}_{(q+1)} = \mathbf{U}_{(q+1)} \mathbf{O},$$

and $\tilde{\mathbf{X}}_{(q+1)}^0 = \tilde{\mathbf{U}}_{(q+1)} \tilde{\mathbf{V}}_{(q+1)}^T = \mathbf{U}_{(q+1)} \mathbf{O} \mathbf{O}_{(q)}^T \mathbf{V}_{(q+1)}^T = \mathbf{U}_{(q+1)} \mathbf{V}_{(q+1)}^T = \mathbf{X}_{(q+1)}^0$.

(c) **Minimize** (20) **with respect to** $\boldsymbol{\mu}$ with the new $\mathbf{V}_{(q+1)}$ and $\mathbf{U}_{(q+1)}$ and the old $\mathbf{W}_{(q)}$. For each $j = 1, \dots, p$ the term of the objective function (20) involving μ_j is the weighted sum of squares

$$\begin{aligned} & \|(\mathbf{W}_{(q)})_j^{1/2}(\mathbf{x}^j - (\boldsymbol{\mu}_{(q)})_j \mathbf{1}_n - (\mathbf{U}_{(q+1)} \mathbf{V}_{(q+1)}^T)^j)\|^2 \\ &= \sum_{i=1}^n (\mathbf{W}_{(q)})_{ij} \left(x_{ij} - \mu_j - (\mathbf{U}_{(q+1)} \mathbf{V}_{(q+1)}^T)_{ij} \right)^2 \end{aligned} \quad (\text{A.11})$$

where \mathbf{x}^j is the j th column of \mathbf{X} , which is minimized by the weighted mean

$$(\boldsymbol{\mu}_{(q+1)})_j = \frac{\sum_{i=1}^n (\mathbf{W}_{(q)})_{ij} (x_{ij} - (\mathbf{U}_{(q+1)} \mathbf{V}_{(q+1)}^T)_{ij})}{\sum_{i=1}^n (w_{(q)})_{ij}}. \quad (\text{A.12})$$

Repeating this for all j yields the column vector $\boldsymbol{\mu}_{(q+1)}$.

(d) **Update** $\mathbf{W}_{(q)}$ according to (15), (16), and (17) with the new $\mathbf{V}_{(q+1)}$, $\mathbf{U}_{(q+1)}$ and $\boldsymbol{\mu}_{(q+1)}$.

The use of the generalized inverse in steps (a) and (b) of the algorithm deserves some explanation. In (A.6) it could happen that the matrix $\mathbf{U}_{(q)}^T \mathbf{W}_{(q)}^j \mathbf{U}_{(q)}$ is singular, especially when k is not much smaller than n . In that case we cannot invert $\mathbf{U}_{(q)}^T \mathbf{W}_{(q)}^j \mathbf{U}_{(q)}$, but its generalized inverse still exists. The matrix $\mathbf{V}_{(q+1)}^T (\mathbf{W}_{(q)})_i \mathbf{V}_{(q+1)}$ in (A.7) can also be singular. This occurs for instance when \mathbf{x}_i is considered as a casewise outlier so $w_i^{\text{case}} = 0$. Then the matrix $(\mathbf{W}_{(q)})_i$ becomes zero so that $(\mathbf{V}_{(q+1)}^T (\mathbf{W}_{(q)})_i \mathbf{V}_{(q+1)})^\dagger$ is zero too, yielding $(\mathbf{u}_{(q+1)})_i = \mathbf{0}$ so $\mathbf{x}_i^0 = \mathbf{0}$ hence $\widehat{\mathbf{x}}_i = \boldsymbol{\mu}_{(q+1)}$. During the course of the algorithm we monitor the fraction of zero weights in each variable j . We do not want this fraction to be too high, because this could make it hard to identify the robust correlation between variables, making the estimation of \mathbf{P} imprecise or even impossible. So we impose a maximal fraction of zero weights per column, which is 25% by default. In case this fraction is exceeded, the iteration stops and the code returns the results of the previous iteration step, together with a warning that it may be better to remove that variable.

The update formula (A.12) does not compute the generalized inverse of $\sum_{i=1}^n (w_{(q)})_{ij}$ because it is strictly positive under the same condition. If $\sum_{i=1}^n (w_{(q)})_{ij}$ were zero this would mean all cells x_{ij} of variable j received zero weight.

F Proof of Proposition 1

In this section Proposition 1 is proved, which ensures that each step of the algorithm decreases the objective function (8). In order to prove Proposition 1 we need three lemmas.

Lemma 1. *For a given weight matrix $\mathbf{W}_{(q)}$, each of the update steps (a), (b), and (c) of the algorithm in Section B decreases the weighted PCA objective function (20).*

Proof. The objective function (20) we want to minimize is

$$\sum_{i=1}^n \sum_{j=1}^p w_{ij} (x_{ij} - \mu_j - (\mathbf{U}\mathbf{V}^T)_{ij})^2 \quad (\text{A.13})$$

where $w_{ij} = W_{(q)ij}$ is fixed. We start from the triplet $(\mathbf{V}_{(q)}, \mathbf{U}_{(q)}, \boldsymbol{\mu}_{(q)})$ with objective

$$\sum_{i=1}^n \sum_{j=1}^p w_{ij} (x_{ij} - (\boldsymbol{\mu}_{(q)})_j - (\mathbf{U}_{(q)}\mathbf{V}_{(q)}^T)_{ij})^2. \quad (\text{A.14})$$

Step (a) minimizes the squared norm (A.5), which after summing over $j = 1, \dots, p$ becomes the objective (20) in the new triplet $(\mathbf{V}_{(q+1)}, \mathbf{U}_{(q)}, \boldsymbol{\mu}_{(q)})$.

Next, step (b) minimizes the squared norm (A.8), which after summing over $i = 1, \dots, n$ becomes the objective (20) in the new triplet $(\mathbf{V}_{(q+1)}, \mathbf{U}_{(q+1)}, \boldsymbol{\mu}_{(q)})$.

Finally, step (c) minimizes the squared norm (A.11), whose sum over $j = 1, \dots, p$ is the objective (20) in the new triplet $(\mathbf{V}_{(q+1)}, \mathbf{U}_{(q+1)}, \boldsymbol{\mu}_{(q+1)})$. \square

We will denote a potential fit to (8) as $\boldsymbol{\theta} = \widehat{\mathbf{X}} = \mathbf{X}^0 \mathbf{P} + \boldsymbol{\mu}$ where the matrices have the appropriate dimensions. We introduce the notation $\mathbf{f}(\boldsymbol{\theta})$ for $\text{vec}((\mathbf{X} - \boldsymbol{\theta}) \odot (\mathbf{X} - \boldsymbol{\theta}))$ where $\text{vec}(\cdot)$ turns a matrix into a column vector. The vector $\mathbf{f}(\boldsymbol{\theta})$ has np entries, which are the values $(\mathbf{X}_{ij} - \boldsymbol{\theta}_{ij})^2$ for $i = 1, \dots, n$ and $j = 1, \dots, p$. We can then write the cellPCA objective function (8) as $L(\mathbf{f}(\boldsymbol{\theta})) := L_{\rho_1, \rho_2}(\mathbf{X}, \mathbf{V}, \mathbf{U}, \boldsymbol{\mu})$.

Lemma 2. *The function $\mathbf{f} \rightarrow L(\mathbf{f})$ is concave.*

Proof. We first show that the univariate function $h : \mathbb{R}_+ \rightarrow \mathbb{R}_+ : z \rightarrow \rho_{b,c}(\sqrt{z})$, in which $\rho_{b,c}$ is the wrapping ρ -function, is concave as suggested in Figure 2. Note that the derivative h' is continuous, and differentiable except in the points b^2 and c^2 . Its derivative $h''(z)$ is zero on the intervals $(0, b^2)$ and (c^2, ∞) , and on (b^2, c^2) we obtain

$$h''(z) = \frac{-z^{3/2}}{4} q_1 \tanh(q_2(c - \sqrt{z})) - \frac{q_1 q_2}{4z} \operatorname{sech}^2(q_2(c - \sqrt{z})) \leq 0.$$

Since the function $h'(z)$ is continuous and on each of the three open intervals its derivative $h''(z)$ is nonpositive, it is nonincreasing everywhere. Therefore h is concave.

By the definition of concavity of a multivariate function, we now need to prove that for any column vectors \mathbf{f}, \mathbf{g} in \mathbb{R}_+^{np} and any λ in $(0, 1)$ it holds that $L(\lambda\mathbf{f} + (1 - \lambda)\mathbf{g}) \geq \lambda L(\mathbf{f}) + (1 - \lambda)L(\mathbf{g})$. This works out as

$$\begin{aligned}
L(\lambda\mathbf{f} + (1 - \lambda)\mathbf{g}) &= \frac{\widehat{\sigma}_2^2}{m} \sum_{i=1}^n h_2 \left(\frac{1}{m_i \widehat{\sigma}_2^2} \sum_{j=1}^p m_{ij} \widehat{\sigma}_{1,j}^2 h_1 \left(\frac{\lambda f_{ij} + (1 - \lambda)g_{ij}}{\widehat{\sigma}_{1,j}^2} \right) \right) \\
&\geq \frac{\widehat{\sigma}_2^2}{m} \sum_{i=1}^n h_2 \left(\frac{1}{m_i \widehat{\sigma}_2^2} \sum_{j=1}^p m_{ij} \widehat{\sigma}_{1,j}^2 [\lambda h_1(f_{ij}/\widehat{\sigma}_{1,j}^2) + (1 - \lambda)h_1(g_{ij}/\widehat{\sigma}_{1,j}^2)] \right) \\
&= \frac{\widehat{\sigma}_2^2}{m} \sum_{i=1}^n h_2 \left(\lambda \frac{1}{m_i \widehat{\sigma}_2^2} \sum_{j=1}^p m_{ij} \widehat{\sigma}_{1,j}^2 h_1(f_{ij}/\widehat{\sigma}_{1,j}^2) \right. \\
&\quad \left. + (1 - \lambda) \frac{1}{m_i \widehat{\sigma}_2^2} \sum_{j=1}^p m_{ij} \widehat{\sigma}_{1,j}^2 h_1(g_{ij}/\widehat{\sigma}_{1,j}^2) \right) \\
&\geq \frac{\widehat{\sigma}_2^2}{m} \sum_{i=1}^n \left[\lambda h_2 \left(\frac{1}{m_i \widehat{\sigma}_2^2} \sum_{j=1}^p m_{ij} \widehat{\sigma}_{1,j}^2 h_1(f_{ij}/\widehat{\sigma}_{1,j}^2) \right) \right. \\
&\quad \left. + (1 - \lambda) h_2 \left(\frac{1}{m_i \widehat{\sigma}_2^2} \sum_{j=1}^p m_{ij} \widehat{\sigma}_{1,j}^2 h_1(g_{ij}/\widehat{\sigma}_{1,j}^2) \right) \right] \\
&= \lambda L(\mathbf{f}) + (1 - \lambda)L(\mathbf{g}).
\end{aligned}$$

The first inequality derives from the concavity of h_1 and the fact that h_2 is nondecreasing. The second inequality is due to the concavity of h_2 . Therefore L is a concave function. \square

We can also write the weighted PCA objective (20) as a function of \mathbf{f} . We will denote it as $L_{\mathbf{W}}(\mathbf{f}) := (\text{vec}(\mathbf{W}))^T \mathbf{f}$, so \mathbf{W} was turned into a vector in the same way as was done to obtain the column vector \mathbf{f} . The next lemma makes a connection between the weighted PCA objective $L_{\mathbf{W}}$ and the original objective L .

Lemma 3. *If two column vectors \mathbf{f}, \mathbf{g} in \mathbb{R}_+^{np} satisfy $L_{\mathbf{W}}(\mathbf{f}) \leq L_{\mathbf{W}}(\mathbf{g})$, then $L(\mathbf{f}) \leq L(\mathbf{g})$.*

Proof. From Lemma 2 we know that $L(\mathbf{f})$ is concave as a function of \mathbf{f} , and it is also differentiable because h_1 and h_2 are. Therefore

$$L(\mathbf{f}) \leq L(\mathbf{g}) + (\nabla L(\mathbf{g}))^T (\mathbf{f} - \mathbf{g})$$

where the column vector $\nabla L(\mathbf{g})$ is the gradient of L in \mathbf{g} . But $\nabla L(\mathbf{g})$ is proportional to $\nabla L_{\mathbf{W}}(\mathbf{g})$ which equals $\text{vec}(\mathbf{W})$ by construction, so $(\nabla L(\mathbf{g}))^T(\mathbf{f} - \mathbf{g})$ is proportional to $L_{\mathbf{W}}(\mathbf{f}) - L_{\mathbf{W}}(\mathbf{g}) \leq 0$. Therefore $L(\mathbf{f}) \leq L(\mathbf{g})$. \square

With this preparation we can prove Proposition 1.

Proof of Proposition 1. When we go from $\boldsymbol{\theta}_{(q)}$ to $\boldsymbol{\theta}_{(q+1)}$, Lemma 1 ensures that $L_{\mathbf{W}_{(q)}}(\mathbf{f}(\boldsymbol{\theta}_{(q+1)})) \leq L_{\mathbf{W}_{(q)}}(\mathbf{f}(\boldsymbol{\theta}_{(q)}))$, so Lemma 3 implies $L(\mathbf{f}(\boldsymbol{\theta}_{(q+1)})) \leq L(\mathbf{f}(\boldsymbol{\theta}_{(q)}))$. \square

G Proofs of influence functions

We consider the contamination model (25) where $H_Z = \Delta_{\mathbf{z}}$ is the distribution that puts all of its mass in a fixed p -variate vector $\mathbf{z} = (z_1, \dots, z_p)^T$, given by

$$X_{\varepsilon} = A \odot X + (\mathbf{1}_p - A) \odot \mathbf{z}$$

with $A = (A_1, \dots, A_p)^T \sim G_{\varepsilon}$.

Under both the dependent and independent contamination models with $P(A_j^{\text{cell}} = 1) = 1 - \varepsilon^{\text{cell}}$ for all $j = 1, \dots, p$, the distribution of A satisfies $P(A_j = 1) = 1 - \varepsilon$, $j = 1, \dots, p$, and (ii) for any sequence (j_1, j_2, \dots, j_p) of zeroes and ones with $p - \ell$ ones and ℓ zeroes, $P(A_1 = j_1, \dots, A_p = j_p)$ has the same value, denoted as $\delta_{\ell}(\varepsilon)$. Obviously, $\varepsilon = \varepsilon^{\text{case}}$ under the fully dependent contamination model (FDCM) and $\varepsilon = \varepsilon^{\text{cell}}$ under the fully independent contamination model (FICM). Under FDCM we have that $P(A_1 = \dots = A_p) = 1$, and then $\delta_0(\varepsilon) = (1 - \varepsilon)$, $\delta_1(\varepsilon) = \dots = \delta_{p-1}(\varepsilon) = 0$, and $\delta_p(\varepsilon) = \varepsilon$. In that situation the distribution of X_{ε} simplifies to $(1 - \varepsilon)H_0 + \varepsilon\Delta_{\mathbf{z}}$ where $\Delta_{\mathbf{z}}$ is the distribution which puts all of its mass in the point \mathbf{z} . FICM instead assumes that A_1, \dots, A_p are independent, hence

$$\delta_{\ell}(\varepsilon) = \binom{p}{\ell} (1 - \varepsilon)^{p-\ell} \varepsilon^{\ell}, \quad \ell = 0, 1, \dots, p.$$

The distribution G_{ε} is denoted as G_{ε}^D in the dependent model, and as G_{ε}^I in the independent model.

The proof of Proposition 2 is based on the implicit function theorem, see e.g. Rio Branco de Oliveira (2012):

Theorem 1 (Implicit Function Theorem). *Let $\mathbf{f}(x, \boldsymbol{\theta}) = (f_1, \dots, f_p)$ be a function from $\mathbb{R} \times \mathbb{R}^p$ to \mathbb{R}^p that is continuous in $(x_0, \tilde{\boldsymbol{\theta}}) \in \mathbb{R} \times \mathbb{R}^p$ with $\mathbf{f}(x_0, \tilde{\boldsymbol{\theta}}) = \mathbf{0}$. Suppose the*

derivative of \mathbf{f} exists in a neighbourhood N of $(x_0, \tilde{\boldsymbol{\theta}})$ and is continuous at $(x_0, \tilde{\boldsymbol{\theta}})$, and that the derivative matrix $\partial \mathbf{f} / \partial \boldsymbol{\theta}$ is nonsingular at $(x_0, \tilde{\boldsymbol{\theta}})$. Then there are neighbourhoods N_1 of x_0 and N_p of $\tilde{\boldsymbol{\theta}}$ with $N_1 \times N_p \subset N$, such that for every x in N_1 there is a unique $\boldsymbol{\theta} = \mathbf{T}(x)$ in N_p for which $\mathbf{f}(x, \mathbf{T}(x)) = \mathbf{0}$. In addition, \mathbf{T} is differentiable in x_0 with derivative matrix given by

$$\frac{\partial \mathbf{T}(x)}{\partial x} \Big|_{x=x_0} = - \left(\frac{\partial \mathbf{f}(x_0, \boldsymbol{\theta})}{\partial \boldsymbol{\theta}} \Big|_{\boldsymbol{\theta}=\tilde{\boldsymbol{\theta}}} \right)^{-1} \frac{\partial \mathbf{f}(x, \tilde{\boldsymbol{\theta}})}{\partial x} \Big|_{x=x_0}.$$

Proof of Proposition 2. From (27), the IF of \mathbf{P} at a distribution H_0 is defined as

$$\text{IF}_H(\mathbf{z}, \mathbf{P}) = \text{vec} \left(\frac{\partial}{\partial \varepsilon} \mathbf{P}(H(G_\varepsilon, \mathbf{z})) \Big|_{\varepsilon=0} \right).$$

For $\varepsilon = 0$ we obtain $\mathbf{P}(H(G_0, \mathbf{z})) = \mathbf{P}(H_0) = \mathbf{P}_0$. We can then parametrize $\mathbf{P}_0 = \mathbf{V}_0 \mathbf{V}_0^T$ where \mathbf{V}_0 has orthonormal columns, corresponding to an orthonormal basis of the linear subspace $\boldsymbol{\Pi}_0$. Note that \mathbf{V}_0 is not unique, but we will see later that different choices lead to the same influence function of \mathbf{P} . When the distribution H_0 is contaminated by FDCM or FICM to $H(G_\varepsilon, \mathbf{z})$ we define $\mathbf{V}(H(G_\varepsilon, \mathbf{z}))$ as the result of the algorithm of Section E above, translated from finite samples to population distributions and starting from \mathbf{V}_0 . This construction makes $\mathbf{V}(H(G_\varepsilon, \mathbf{z}))$ unique, and it has to satisfy the first-order condition (29) saying

$$E_H[\mathbf{W}_x(\mathbf{V}\mathbf{u}_x - \mathbf{x})\mathbf{u}_x^T] = \mathbf{0} \quad (\text{A.15})$$

hence

$$\mathbf{g}(H(G_\varepsilon, \mathbf{z}), \mathbf{T}(\varepsilon), \boldsymbol{\sigma}(H(G_\varepsilon, \mathbf{z}))) = \text{vec} \left(\mathbf{E}_{H(G_\varepsilon, \mathbf{z})} [\mathbf{W}_x(\mathbf{V}\mathbf{u}_x - \mathbf{x})\mathbf{u}_x^T] \right) = \mathbf{0} \quad (\text{A.16})$$

where the pk -variate column vector \mathbf{g} is written as a function of the pk -variate column vector $\mathbf{T}(\varepsilon) := \text{vec}(\mathbf{V}(H(G_\varepsilon, \mathbf{z})))$. In order to compute $\text{vec} \left(\frac{\partial}{\partial \varepsilon} \mathbf{V}(H(G_\varepsilon, \mathbf{z})) \Big|_{\varepsilon=0} \right)$ we would like to apply the implicit function theorem in the point $\varepsilon = 0$, but the contaminated distribution $H(G_\varepsilon, \mathbf{z})$ is only defined for $\varepsilon > 0$. To circumvent this issue we extend the definition of \mathbf{g} to negative ε by defining a function \mathbf{f} from $\mathbb{R} \times \mathbb{R}^{pk}$ to \mathbb{R}^{pk} as

$$\mathbf{f}(\varepsilon, \boldsymbol{\theta}) = \begin{cases} \mathbf{g}(H(G_\varepsilon, \mathbf{z}), \boldsymbol{\theta}, \boldsymbol{\sigma}(H(G_\varepsilon, \mathbf{z}))) & \text{for } \varepsilon \geq 0 \\ 2\mathbf{g}(H_0, \boldsymbol{\theta}, \boldsymbol{\sigma}(H_0)) - \mathbf{g}(H(|\varepsilon|, \mathbf{z}), \boldsymbol{\theta}, \boldsymbol{\sigma}(H(|\varepsilon|, \mathbf{z}))) & \text{for } \varepsilon < 0. \end{cases}$$

We now put $\varepsilon_0 = 0$ and $\tilde{\boldsymbol{\theta}} = \mathbf{T}(0) = \text{vec}(\mathbf{V}_0)$. Then $\mathbf{f}(\varepsilon_0, \boldsymbol{\theta}) = \mathbf{f}(0, \mathbf{T}(0)) = \mathbf{0}$, and assuming that \mathbf{g} is sufficiently smooth for the differentiability requirements of the implicit function theorem, we can conclude that $\mathbf{T}(\varepsilon)$ is uniquely defined for small ε and that

$$\begin{aligned}\frac{\partial \mathbf{T}(\varepsilon)}{\partial \varepsilon}\Big|_{\varepsilon=0} &= -\left(\frac{\partial \mathbf{f}(0, \mathbf{T})}{\partial \mathbf{T}}\Big|_{\mathbf{T}=\mathbf{T}(0)}\right)^{-1} \frac{\partial \mathbf{f}(\varepsilon, \mathbf{T}(0))}{\partial \varepsilon}\Big|_{\varepsilon=0} \\ &= -\left(\frac{\partial \mathbf{g}(0, \mathbf{T})}{\partial \mathbf{T}}\Big|_{\mathbf{T}=\mathbf{T}(0)}\right)^{-1} \frac{\partial \mathbf{g}(\varepsilon, \mathbf{T}(0))}{\partial \varepsilon}\Big|_{\varepsilon=0}.\end{aligned}$$

Note that the left hand side is $\text{vec}\left(\frac{\partial}{\partial \varepsilon} \mathbf{V}(H(G_\varepsilon, \mathbf{z}))\Big|_{\varepsilon=0}\right)$. We now have to work out the right hand side. For the first factor we denote the matrix

$$\mathbf{B} := \frac{\partial \mathbf{g}(H_0, \mathbf{T}, \sigma_0)}{\partial \mathbf{T}}\Big|_{\mathbf{T}=\text{vec}(\mathbf{V}_0)}$$

which does not depend on \mathbf{z} and will be computed numerically in Section H. For the second factor, from (A.16) we know that $\mathbf{g}(H(G_\varepsilon, \mathbf{z}), \boldsymbol{\theta}_\varepsilon, \boldsymbol{\sigma}_\varepsilon)$ is an expectation over the mixture distribution $H(G_\varepsilon, \mathbf{z})$, so we can write \mathbf{g} as a linear combination with coefficients $\delta_\ell(\varepsilon)$ for $k = 0, 1, \dots, p$. For the FDCM model we know that G_ε^D has $\delta_0(\varepsilon) = (1 - \varepsilon)$, $\delta_1(\varepsilon) = \dots = \delta_{p-1}(\varepsilon) = 0$ and $\delta_p(\varepsilon) = \varepsilon$, so \mathbf{g} can be written as

$$\begin{aligned}\mathbf{g}(H(G_\varepsilon^D, \mathbf{z}), \text{vec}(\mathbf{V}_0), \boldsymbol{\sigma}(H(G_\varepsilon^D, \mathbf{z}))) \\ &= \delta_0(\varepsilon)\mathbf{g}(H_0, \text{vec}(\mathbf{V}_0), \boldsymbol{\sigma}(H(G_\varepsilon^D, \mathbf{z}))) + \delta_p(\varepsilon)\mathbf{g}(H(G_\varepsilon^D, \mathbf{z}), \text{vec}(\mathbf{V}_0), \boldsymbol{\sigma}(H(G_\varepsilon^D, \mathbf{z}))) \\ &= (1 - \varepsilon)\mathbf{g}(H_0, \text{vec}(\mathbf{V}_0), \boldsymbol{\sigma}_\varepsilon) + \varepsilon\mathbf{g}(\Delta_{\mathbf{z}}, \text{vec}(\mathbf{V}_0), \boldsymbol{\sigma}_\varepsilon)\end{aligned}$$

which yields the derivative

$$\begin{aligned}-\mathbf{g}(H_0, \text{vec}(\mathbf{V}_0), \boldsymbol{\sigma}_0) + \frac{\partial}{\partial \varepsilon}\mathbf{g}(H_0, \text{vec}(\mathbf{V}_0), \boldsymbol{\sigma}_\varepsilon)\Big|_{\varepsilon=0} &+ \mathbf{g}(\Delta_{\mathbf{z}}, \text{vec}(\mathbf{V}_0), \boldsymbol{\sigma}_0) \\ &= \mathbf{0} + \frac{\partial \mathbf{g}}{\partial \boldsymbol{\sigma}}(H_0, \text{vec}(\mathbf{V}_0), \boldsymbol{\sigma})\Big|_{\boldsymbol{\sigma}=\boldsymbol{\sigma}_0} \frac{\partial \boldsymbol{\sigma}_\varepsilon}{\partial \varepsilon}\Big|_{\varepsilon=0} + \mathbf{g}(\Delta_{\mathbf{z}}, \text{vec}(\mathbf{V}_0), \boldsymbol{\sigma}_0) \\ &= \mathbf{S} \text{IF}_{\text{case}}(\mathbf{z}, \boldsymbol{\sigma}) + \mathbf{g}(\Delta_{\mathbf{z}}, \text{vec}(\mathbf{V}_0), \boldsymbol{\sigma}_0)\end{aligned}\tag{A.17}$$

where $\mathbf{S} := \frac{\partial}{\partial \boldsymbol{\sigma}}\mathbf{g}(H_0, \text{vec}(\mathbf{V}_0), \boldsymbol{\sigma})\Big|_{\boldsymbol{\sigma}=\boldsymbol{\sigma}_0}$ and $\text{IF}_{\text{case}}(\mathbf{z}, \boldsymbol{\sigma})$ is the influence function of $\boldsymbol{\sigma}$ under FDCM.

Under the FICM model the second factor is different. We have $\delta_0(\varepsilon) = (1 - \varepsilon)^p$, $\delta_0(0) = 1$, $\delta_1(\varepsilon) = p(1 - \varepsilon)^{p-1}\varepsilon$ so $\delta_1(0) = 0$ and $\delta_1'(0) = p$, and $\delta_\ell(0) = \delta_\ell'(0) = 0$ for $\ell \geq 2$.

Therefore \mathbf{g} can be written as the sum

$$\begin{aligned}
& \mathbf{g}(H(G_\varepsilon^I, \mathbf{z}), \text{vec}(\mathbf{V}_0), \boldsymbol{\sigma}(H(G_\varepsilon^I, \mathbf{z}))) \\
&= \delta_0(\varepsilon) \mathbf{g}(H_0, \text{vec}(\mathbf{V}_0), \boldsymbol{\sigma}(H(G_\varepsilon^I, \mathbf{z}))) + \delta_1(\varepsilon) \sum_{j=1}^p \mathbf{g}(H(G_1^j, \mathbf{z}), \text{vec}(\mathbf{V}_0), \boldsymbol{\sigma}(G_\varepsilon^I, \mathbf{z})) \\
&= (1 - \varepsilon)^p \mathbf{g}(H_0, \text{vec}(\mathbf{V}_0), \boldsymbol{\sigma}_\varepsilon) + p(1 - \varepsilon)^{p-1} \varepsilon \sum_{j=1}^p \mathbf{g}(H(G_1^j, \mathbf{z}), \text{vec}(\mathbf{V}_0), \boldsymbol{\sigma}(G_\varepsilon^I, \mathbf{z}))
\end{aligned}$$

where $H(G_1^j, \mathbf{z})$ is the distribution of $X \sim H_0$ but with its j th component fixed at the constant z_j . It is thus a degenerate distribution concentrated on the hyperplane $X_j = z_j$.

The derivative now becomes

$$\mathbf{S} \text{IF}_{\text{cell}}(\mathbf{z}, \boldsymbol{\sigma}) + p \sum_{j=1}^p \mathbf{g}(H(G_1^j, \mathbf{z}), \text{vec}(\mathbf{V}_0), \boldsymbol{\sigma}_0) \quad (\text{A.18})$$

where \mathbf{S} is the same as before but $\text{IF}_{\text{cell}}(\mathbf{z}, \boldsymbol{\sigma})$ is now the cellwise influence function of $\boldsymbol{\sigma}$.

Now that we have an expression for $\frac{\partial}{\partial \varepsilon} \mathbf{V}(H(G_\varepsilon, \mathbf{z}))$ we can use it to derive the IF of \mathbf{P} . Note that the columns of \mathbf{V}_0 were orthonormal, but the columns of $\mathbf{V}(H(G_\varepsilon, \mathbf{z}))$ do not have to be. Therefore the projection matrix $\mathbf{V}(H(G_\varepsilon, \mathbf{z}))$ is given by

$$\mathbf{P}(H(G_\varepsilon, \mathbf{z})) = \mathbf{V}(H(G_\varepsilon, \mathbf{z})) (\mathbf{V}(H(G_\varepsilon, \mathbf{z}))^T \mathbf{V}(H(G_\varepsilon, \mathbf{z})))^{-1} \mathbf{V}(H(G_\varepsilon, \mathbf{z}))^T.$$

Differentiating yields

$$\begin{aligned}
& \frac{\partial}{\partial \varepsilon} \mathbf{P}(H(G_\varepsilon, \mathbf{z})) \Big|_{\varepsilon=0} = \frac{\partial}{\partial \varepsilon} \mathbf{V}(H(G_\varepsilon, \mathbf{z})) (\mathbf{V}(H(G_\varepsilon, \mathbf{z}))^T \mathbf{V}(H(G_\varepsilon, \mathbf{z})))^{-1} \mathbf{V}(H(G_\varepsilon, \mathbf{z}))^T \Big|_{\varepsilon=0} \\
&= \frac{\partial}{\partial \varepsilon} \mathbf{V}(H(G_\varepsilon, \mathbf{z})) \Big|_{\varepsilon=0} (\mathbf{V}_0^T \mathbf{V}_0)^{-1} \mathbf{V}_0^T \\
&\quad - \mathbf{V}_0 (\mathbf{V}_0^T \mathbf{V}_0)^{-1} \frac{\partial}{\partial \varepsilon} \mathbf{V}(H(G_\varepsilon, \mathbf{z}))^T \Big|_{\varepsilon=0} \mathbf{V}_0 (\mathbf{V}_0^T \mathbf{V}_0)^{-1} \mathbf{V}_0^T \\
&\quad - \mathbf{V}_0 (\mathbf{V}_0^T \mathbf{V}_0)^{-1} \mathbf{V}_0^T \frac{\partial}{\partial \varepsilon} \mathbf{V}(H(G_\varepsilon, \mathbf{z})) \Big|_{\varepsilon=0} (\mathbf{V}_0^T \mathbf{V}_0)^{-1} \mathbf{V}_0^T \\
&\quad + \mathbf{V}_0 (\mathbf{V}_0^T \mathbf{V}_0)^{-1} \frac{\partial}{\partial \varepsilon} \mathbf{V}(H(G_\varepsilon, \mathbf{z}))^T \Big|_{\varepsilon=0}
\end{aligned}$$

where the derivative of $(\mathbf{V}(H(G_\varepsilon, \mathbf{z}))^T \mathbf{V}(H(G_\varepsilon, \mathbf{z})))^{-1}$ comes from the identity $\frac{\partial \mathbf{Y}^{-1}}{\partial x} = -\mathbf{Y}^{-1} \frac{\partial \mathbf{Y}}{\partial x} \mathbf{Y}^{-1}$ (Magnus and Neudecker, 2019). Since $\mathbf{V}_0^T \mathbf{V}_0 = \mathbf{I}_k$ is the identity matrix and

$\mathbf{V}_0 \mathbf{V}_0^T = \mathbf{P}$, the expression simplifies to

$$\begin{aligned}
\frac{\partial}{\partial \varepsilon} \mathbf{P}(H(G_\varepsilon, \mathbf{z})) \Big|_{\varepsilon=0} &= \frac{\partial}{\partial \varepsilon} \mathbf{V}(H(G_\varepsilon, \mathbf{z})) \Big|_{\varepsilon=0} \mathbf{V}_0^T - \mathbf{V}_0 \frac{\partial}{\partial \varepsilon} \mathbf{V}(H(G_\varepsilon, \mathbf{z}))^T \Big|_{\varepsilon=0} \mathbf{P}_0 \\
&\quad - \mathbf{P}_0 \frac{\partial}{\partial \varepsilon} \mathbf{V}(H(G_\varepsilon, \mathbf{z})) \Big|_{\varepsilon=0} \mathbf{V}_0^T + \mathbf{V}_0 \frac{\partial}{\partial \varepsilon} \mathbf{V}(H(G_\varepsilon, \mathbf{z}))^T \Big|_{\varepsilon=0} \\
&= (\mathbf{I}_p - \mathbf{P}_0) \frac{\partial}{\partial \varepsilon} \mathbf{V}(H(G_\varepsilon, \mathbf{z})) \Big|_{\varepsilon=0} \mathbf{V}_0^T + \mathbf{V}_0 \frac{\partial}{\partial \varepsilon} \mathbf{V}(H(G_\varepsilon, \mathbf{z}))^T \Big|_{\varepsilon=0} (\mathbf{I}_p - \mathbf{P}_0) . \quad (\text{A.19})
\end{aligned}$$

Since the second term is the transpose of the first we see that the derivative of $\mathbf{P}(H(G_\varepsilon, \mathbf{z}))$ is symmetric, as it should be.

Now suppose we had chosen a different orthonormal basis of Π_0 , corresponding to a matrix $\tilde{\mathbf{V}}_0$. We need to verify that this would yield the same result. First compute the $k \times k$ matrix $\mathbf{O} = (\tilde{\mathbf{V}}_0^{-1} \mathbf{V}_0)$. This matrix is orthogonal because $\mathbf{O}^T \mathbf{O} = \mathbf{V}_0^T (\tilde{\mathbf{V}}_0 \tilde{\mathbf{V}}_0^T)^{-1} \mathbf{V}_0 = \mathbf{V}_0^T \mathbf{V}_0 = \mathbf{I}_k$, and $\tilde{\mathbf{V}}_0 = \mathbf{V}_0 \mathbf{O}$. Then construct $\tilde{\mathbf{V}}(H(G_\varepsilon, \mathbf{z}))$ by running the algorithm starting from $\tilde{\mathbf{V}}_0$ instead of \mathbf{V}_0 . In Section E we saw that every step will have $\tilde{\mathbf{V}}_{(q+1)} = \mathbf{V}_{(q+1)} \mathbf{O}$, so this holds in the limit as well, hence $\tilde{\mathbf{V}}(H(G_\varepsilon, \mathbf{z})) = \mathbf{V}(H(G_\varepsilon, \mathbf{z})) \mathbf{O}$. Writing (A.19) with $\tilde{\mathbf{V}}(H(G_\varepsilon, \mathbf{z}))$ and $\tilde{\mathbf{V}}_0$ yields factors $\mathbf{O} \mathbf{O}^T$ that cancel, yielding (A.19) again.

Applying the vec operation to (A.19) gives the IF. Applying it to the first term yields

$$\text{vec} \left((\mathbf{I}_p - \mathbf{P}_0) \frac{\partial}{\partial \varepsilon} \mathbf{V}(H(G_\varepsilon, \mathbf{z})) \Big|_{\varepsilon=0} \mathbf{V}_0^T \right) = (\mathbf{V}_0 \otimes (\mathbf{I}_p - \mathbf{P}_0)) \text{vec} \left(\frac{\partial}{\partial \varepsilon} \mathbf{V}(H(G_\varepsilon, \mathbf{z})) \Big|_{\varepsilon=0} \right)$$

by the rule $\text{vec}(\mathbf{ABC}) = (\mathbf{C}^T \otimes \mathbf{A}) \text{vec}(\mathbf{B})$. For the second term we find

$$\text{vec} \left(\mathbf{V}_0 \frac{\partial}{\partial \varepsilon} \mathbf{V}(H(G_\varepsilon, \mathbf{z}))^T \Big|_{\varepsilon=0} (\mathbf{I}_p - \mathbf{P}_0) \right) = ((\mathbf{I}_p - \mathbf{P}_0) \otimes \mathbf{V}_0) \text{vec} \left(\left(\frac{\partial}{\partial \varepsilon} \mathbf{V}(H(G_\varepsilon, \mathbf{z})) \Big|_{\varepsilon=0} \right)^T \right)$$

by the same rule. The last factor is the vec of a transposed matrix, which can be written as

$$\text{vec} \left(\left(\frac{\partial}{\partial \varepsilon} \mathbf{V}(H(G_\varepsilon, \mathbf{z})) \Big|_{\varepsilon=0} \right)^T \right) = \mathbf{K}_{p,k} \text{vec} \left(\frac{\partial}{\partial \varepsilon} \mathbf{V}(H(G_\varepsilon, \mathbf{z})) \Big|_{\varepsilon=0} \right)$$

where $\mathbf{K}_{p,k}$ is a $pk \times pk$ permutation matrix that rearranges the entries of the column vector $\text{vec}(\frac{\partial}{\partial \varepsilon} \mathbf{V}(H(G_\varepsilon, \mathbf{z})) \Big|_{\varepsilon=0})$ to become those of $\text{vec}(\frac{\partial}{\partial \varepsilon} \mathbf{V}(H(G_\varepsilon, \mathbf{z}))^T \Big|_{\varepsilon=0})$. In all we can write

$$\text{vec} \left(\frac{\partial}{\partial \varepsilon} \mathbf{P}(H(G_\varepsilon, \mathbf{z})) \Big|_{\varepsilon=0} \right) = \mathbf{R}_0 \text{vec} \left(\frac{\partial}{\partial \varepsilon} \mathbf{V}(H(G_\varepsilon, \mathbf{z})) \Big|_{\varepsilon=0} \right) \quad (\text{A.20})$$

where \mathbf{R}_0 is the $p^2 \times pk$ matrix

$$\mathbf{R}_0 = \mathbf{V}_0 \otimes (\mathbf{I}_p - \mathbf{P}_0) + ((\mathbf{I}_p - \mathbf{P}_0) \otimes \mathbf{V}_0) \mathbf{K}_{(p,k)} . \quad (\text{A.21})$$

Combining (A.17) with $\mathbf{D} := \mathbf{R}_0 \mathbf{B}^{-1}$ yields (32), and left multiplying (A.18) by \mathbf{D} yields (33). \square

Proof of Proposition 3. For each $\ell = 1, \dots, pk$, call $\ddot{\Psi}_\ell = \frac{\partial^2 \Psi_\ell}{\partial \text{vec}(\mathbf{V}) \partial \text{vec}(\mathbf{V})}$ the matrix of second derivatives of Ψ_ℓ with respect to the entries of \mathbf{V} , and $\mathbf{C}_n(\mathbf{x}, \mathbf{V})$ the matrix with ℓ th row equal to $\text{vec}(\widehat{\mathbf{V}}_n - \mathbf{V}(H))^T \ddot{\Psi}_\ell(\mathbf{x}, \mathbf{V})$. A Taylor expansion yields

$$\begin{aligned} \mathbf{0} = \widehat{\Lambda}_n(\widehat{\mathbf{V}}_n) &= \frac{1}{n} \sum_{i=1}^n \left\{ \Psi(\mathbf{x}_i, \mathbf{V}(H)) + \dot{\Psi}(\mathbf{x}_i, \mathbf{V}(H)) \text{vec}(\widehat{\mathbf{V}}_n - \mathbf{V}(H)) \right. \\ &\quad \left. + \frac{1}{2} \mathbf{C}_n(\mathbf{x}_i, \mathbf{V}(H)) \text{vec}(\widehat{\mathbf{V}}_n - \mathbf{V}(H)) \right\}. \end{aligned}$$

In other words

$$\mathbf{0} = \mathbf{A}_n + (\mathbf{B}_n + \overline{\mathbf{C}}_n) \text{vec}(\widehat{\mathbf{V}}_n - \mathbf{V}(H)) \quad (\text{A.22})$$

with

$$\mathbf{A}_n = \frac{1}{n} \sum_{i=1}^n \Psi(\mathbf{x}_i, \mathbf{V}(H)), \quad \mathbf{B}_n = \frac{1}{n} \sum_{i=1}^n \dot{\Psi}(\mathbf{x}_i, \mathbf{V}(H)), \quad \overline{\mathbf{C}}_n = \frac{1}{2n} \sum_{i=1}^n \mathbf{C}_n(\mathbf{x}_i, \mathbf{V}(H)).$$

The ℓ th row of the matrix $\overline{\mathbf{C}}_n$ equals $\text{vec}(\widehat{\mathbf{V}}_n - \mathbf{V}(H))^T \overline{\ddot{\Psi}}_\ell$ where

$$\overline{\ddot{\Psi}}_\ell = \frac{1}{n} \sum_{i=1}^n \ddot{\Psi}_\ell(\mathbf{x}_i, \mathbf{V}(H))$$

which is bounded. Since $\widehat{\mathbf{V}}_n \rightarrow \mathbf{V}(H)$ in probability, this implies that $\overline{\mathbf{C}}_n \rightarrow \mathbf{0}$ in probability.

Note that for $i = 1, 2, \dots$ the vectors $\Psi(\mathbf{x}_i, \mathbf{V}(H))$ are i.i.d. with mean $\mathbf{0}$ (since $\Lambda(\mathbf{V}(H)) = \mathbf{0}$) and covariance matrix \mathbf{A} , where $\mathbf{A} = \text{E}_H[\Psi(\mathbf{x}, \mathbf{V}(H))\Psi(\mathbf{x}, \mathbf{V}(H))^T]$, and the matrices $\dot{\Psi}(\mathbf{x}_i, \mathbf{V}(H))$ are i.i.d. with mean \mathbf{B} , where $\mathbf{B} = \text{E}_H[\dot{\Psi}(\mathbf{x}, \mathbf{V}(H))]$. Hence when $n \rightarrow \infty$, the law of large numbers implies $\mathbf{B}_n \rightarrow \mathbf{B}$ in probability, which implies $\mathbf{B}_n + \overline{\mathbf{C}}_n \rightarrow \mathbf{B}$ in probability, and we assume that \mathbf{B} is nonsingular. The central limit theorem implies $\sqrt{n} \mathbf{A}_n \rightarrow N_p(\mathbf{0}, \mathbf{A})$ in distribution. Then from (A.22) and Slutsky's lemma we have that

$$\sqrt{n} \text{vec}(\widehat{\mathbf{V}}_n - \mathbf{V}(H)) \rightarrow_d N_{pk}(\mathbf{0}, \mathbf{B}^{-1} \mathbf{A} (\mathbf{B}^{-1})^T).$$

From $\widehat{\mathbf{V}}_n \rightarrow \mathbf{V}(H)$ in probability it follows that $\widehat{\mathbf{P}}_n \rightarrow \mathbf{P}(H)$ in probability. Consider the differentiable mapping $\mathbf{h}(\mathbf{M}) = \mathbf{M}(\mathbf{M}^T \mathbf{M})^{-1} \mathbf{M}^T$ on the set of $p \times k$ matrices \mathbf{M} of rank k . From the multivariate delta method, see e.g. Casella and Berger (2002), it follows that

$$\sqrt{n} \text{vec}(\mathbf{h}(\widehat{\mathbf{V}}_n) - \mathbf{h}(\mathbf{V}(H))) \rightarrow_d N_{p^2}(\mathbf{0}, \mathbf{R}_0 \mathbf{B}^{-1} \mathbf{A} \mathbf{B}^{-T} \mathbf{R}_0^T)$$

where $\mathbf{R}_0 = \frac{\partial \text{vec}(\mathbf{h}(\mathbf{V}))}{\partial \text{vec}(\mathbf{V})} \big|_{\mathbf{V}=\text{vec}(\mathbf{V}(H))}$ was defined in (A.21). Moreover $\mathbf{R}_0 \mathbf{B}^{-1} \mathbf{A} \mathbf{B}^{-T} \mathbf{R}_0^T = \Theta$ because $\text{IF}_{\text{case}}(\mathbf{x}, \mathbf{P}) = \mathbf{R}_0 \mathbf{B}^{-1} \Psi(\mathbf{x}, \mathbf{V}(H))$ by Proposition 2 with fixed $\boldsymbol{\sigma}$. Since $\text{IF}_{\text{case}}(\mathbf{x}, \mathbf{P})$ does not depend on the parametrization of \mathbf{P} , neither does $\Theta = E_H[\text{IF}_{\text{case}}(\mathbf{x}, \mathbf{P}) \text{IF}_{\text{case}}(\mathbf{x}, \mathbf{P})^T]$. \square

H Derivation of \mathbf{B} and \mathbf{S}

We now compute the $pk \times pk$ matrix $\mathbf{B} = \frac{\partial}{\partial \text{vec}(\mathbf{V})} g(H_0, \text{vec}(\mathbf{V}), \boldsymbol{\sigma}_0) \big|_{\text{vec}(\mathbf{V})=\text{vec}(\mathbf{V}(H))}$ and the $pk \times (p+1)$ matrix $\mathbf{S} = \frac{\partial}{\partial \boldsymbol{\sigma}} g(H_0, \text{vec}(\mathbf{V}(H)), \boldsymbol{\sigma}) \big|_{\boldsymbol{\sigma}=\boldsymbol{\sigma}_0}$.

Recall that $\boldsymbol{\mu}$ is known and equal to $\mathbf{0}$. Then

$$w_j^{\text{cell}} = \psi_1 \left(\frac{r_j}{\sigma_{1,j}} \right) / \frac{r_j}{\sigma_{1,j}} \quad r_j := x_j - \mathbf{v}_j^T \mathbf{u}_x \quad j = 1 \dots, p$$

and

$$w^{\text{case}} = \psi_2 \left(\frac{t}{\sigma_2} \right) / \frac{t}{\sigma_2} \quad t := \sqrt{\frac{1}{p} \sum_{j=1}^p \sigma_{1,j}^2 \rho_1 \left(\frac{r_j}{\sigma_{1,j}} \right)}.$$

For $j, l = 1, \dots, p$ and $h, m = 1, \dots, k$, we have that

$$-\frac{\partial}{\partial v_{lm}} E_{H_0} [w_j(x_j - \mathbf{v}_j^T \mathbf{u}_x) u_{x,h}] = -E_{H_0} \left[\frac{\partial w_j}{\partial v_{lm}} r_j u_{x,h} + w_j \frac{\partial r_j}{\partial v_{lm}} u_{x,h} + w_j r_j \frac{\partial u_{x,h}}{\partial v_{lm}} \right]$$

where

$$\frac{\partial r_j}{\partial v_{lm}} = - \left(\frac{\partial \mathbf{v}_j^T}{\partial v_{lm}} \mathbf{u}_x + \mathbf{v}_j^T \frac{\partial \mathbf{u}_x}{\partial v_{lm}} \right) = - \left(\delta_{j=l} u_{x,m} + \mathbf{v}_j^T \frac{\partial \mathbf{u}_x}{\partial v_{lm}} \right)$$

and $\delta_{j=l}$ is the Kronecker delta. Then

$$\begin{aligned} \frac{\partial w_j^{\text{cell}}}{\partial v_{lm}} &= \left(\frac{\psi'_1(r_j/\sigma_{1,j})}{\sigma_{1,j}} \left(\frac{\partial r_j}{\partial v_{lm}} \right) \frac{r_j}{\sigma_{1,j}} - \frac{\psi_1(r_j/\sigma_{1,j})}{\sigma_{1,j}} \left(\frac{\partial r_j}{\partial v_{lm}} \right) \right) / \frac{r_j^2}{\sigma_{1,j}^2} \\ &= \frac{\psi'_1(r_j/\sigma_{1,j})}{r_j} \left(\frac{\partial r_j}{\partial v_{lm}} \right) - \frac{\sigma_{1,j} \psi_1(r_j/\sigma_{1,j})}{r_j^2} \left(\frac{\partial r_j}{\partial v_{lm}} \right) \\ &= (w_j^{\text{cell}})' \left(\frac{\partial r_j}{\partial v_{lm}} \right) \end{aligned}$$

where $(w_j^{\text{cell}})' = \psi'_1(r_j/\sigma_{1,j})/r_j - \sigma_{1,j} \psi_1(r_j/\sigma_{1,j})/r_j^2$. Moreover

$$\begin{aligned} \frac{\partial w^{\text{case}}}{\partial v_{lm}} &= \left(\frac{\psi'_2(t/\sigma_2)}{\sigma_2} \frac{\partial t}{\partial v_{lm}} \frac{t}{\sigma_2} - \frac{\psi_2(t/\sigma_2)}{\sigma_2} \frac{\partial t}{\partial v_{lm}} \right) / \frac{t^2}{\sigma_2^2} \\ &= \left(\frac{\psi'_2(t/\sigma_2)}{t} - \frac{\sigma_2 \psi_2(t/\sigma_2)}{t^2} \right) \frac{\partial t}{\partial v_{lm}} \\ &= (w^{\text{case}})' \frac{\partial t}{\partial v_{lm}} \end{aligned}$$

where $(w^{\text{case}})' = \psi_2'(t/\sigma_2)/r - \sigma_2\psi_2(t/\sigma_2)/t^2$ and

$$\begin{aligned}\frac{\partial t}{\partial v_{lm}} &= \frac{1}{2pt} \sum_{s=1}^p \sigma_{1,s} \psi_1(r_s/\sigma_{1,s}) \left(\frac{\partial r_s}{\partial v_{lm}} \right) \\ &= \frac{1}{2pt} \sum_{s=1}^p w_s^{\text{cell}} r_s \left(\frac{\partial r_s}{\partial v_{lm}} \right).\end{aligned}$$

Then

$$\begin{aligned}\frac{\partial w_j}{\partial v_{lm}} &= \frac{\partial w_j^{\text{cell}}}{\partial v_{lm}} w^{\text{case}} + w_j^{\text{cell}} \frac{\partial w^{\text{case}}}{\partial v_{lm}} \\ &= w^{\text{case}} (w_j^{\text{cell}})' \left(\frac{\partial r_j}{\partial v_{lm}} \right) + w_j^{\text{cell}} (w^{\text{case}})' \frac{1}{2pt} \sum_{s=1}^p w_s^{\text{cell}} r_s \left(\frac{\partial r_s}{\partial v_{lm}} \right) \\ &= \sum_{s=1}^p \left(\frac{w_s^{\text{cell}} (w^{\text{case}})' w_s^{\text{cell}} r_s}{2pt} + \delta_{s=j} w^{\text{case}} (w_j^{\text{cell}})' \right) \left(\frac{\partial r_s}{\partial v_{lm}} \right).\end{aligned}$$

Then $\mathbf{B}(H_0, \text{vec}(\mathbf{V}(H)), \boldsymbol{\sigma}_0)$ is obtained from

$$\mathbf{B}(H_0, \text{vec}(\mathbf{V}(H)), \boldsymbol{\sigma}_0) = \{B_{\tilde{h}\tilde{m}}(H_0, \text{vec}(\mathbf{V}(H)), \boldsymbol{\sigma}_0)\},$$

where $B_{\tilde{h}\tilde{m}}(H_0, \text{vec}(\mathbf{V}(H)), \boldsymbol{\sigma}_0) = -\frac{\partial}{\partial v_{lm}} \mathbb{E}_{H_0} [w_j(x_j - \mathbf{v}_j^T \mathbf{u}_x) u_{x,h}] \Big|_{\text{vec}(\mathbf{V})=\text{vec}(\mathbf{V}(H))}$ with $\tilde{h} = (h-1)p + j$ and $\tilde{m} = (m-1)p + l$. Note that $\frac{\partial \mathbf{u}_x}{\partial v_{lm}}$ does not have a closed form, so it has to be computed numerically.

For $\mathbf{S}(H_0, \text{vec}(\mathbf{V}(H)), \boldsymbol{\sigma}_0)$ we compute

$$-\frac{\partial}{\partial \sigma_{1,j}} \mathbb{E}_{H_0} [w_j(x_j - \mathbf{v}_j^T \mathbf{u}_x) u_{x,h}] = -\mathbb{E}_{H_0} \left[\frac{\partial w_j}{\partial \sigma_{1,j}} r_j u_{x,h} + w_j \frac{\partial r_j}{\partial \sigma_{1,j}} u_{x,h} + w_j r_j \frac{\partial u_{x,h}}{\partial \sigma_{1,j}} \right]$$

where

$$\frac{\partial r_j}{\partial \sigma_{1,j}} = -\mathbf{v}_j^T \frac{\partial \mathbf{u}_x}{\partial \sigma_{1,j}}.$$

Then

$$\begin{aligned}\frac{\partial w_j^{\text{cell}}}{\partial \sigma_{1,j}} &= \left(\psi_1'(r_j/\sigma_{1,j}) \frac{\partial r_j/\sigma_{1,j}}{\partial \sigma_{1,j}} \frac{r_j}{\sigma_{1,j}} - \psi_1(r_j/\sigma_{1,j}) \frac{\partial r_j/\sigma_{1,j}}{\partial \sigma_{1,j}} \right) / \frac{r_j^2}{\sigma_{1,j}^2} \\ &= \left(\frac{\psi_1'(r_j/\sigma_{1,j})}{r_j} \sigma_{1,j} \frac{\partial r_j/\sigma_{1,j}}{\partial \sigma_{1,j}} - \sigma_{1,j}^2 \frac{\psi_1(r_j/\sigma_{1,j})}{r_j^2} \frac{\partial r_j/\sigma_{1,j}}{\partial \sigma_{1,j}} \right) \\ &= \sigma_{1,j} (w_j^{\text{cell}})' \frac{\partial r_j/\sigma_{1,j}}{\partial \sigma_{1,j}}.\end{aligned}$$

Moreover,

$$\begin{aligned}
\frac{\partial w^{\text{case}}}{\partial \sigma_{1,j}} &= \left(\frac{\psi'_2(t/\sigma_2)}{\sigma_2} \frac{\partial t}{\partial \sigma_{1,j}} \frac{t}{\sigma_2} - \frac{\psi_2(t/\sigma_2)}{\sigma_2} \frac{\partial t}{\partial \sigma_{1,j}} \right) / \frac{t^2}{\sigma_2^2} \\
&= \left(\frac{\psi'_2(t/\sigma_2)}{t} - \frac{\sigma_2 \psi_2(t/\sigma_2)}{t^2} \right) \frac{\partial t}{\partial \sigma_{1,j}} \\
&= (w^{\text{case}})' \frac{\partial t}{\partial \sigma_{1,j}}
\end{aligned}$$

where

$$\begin{aligned}
\frac{\partial t}{\partial \sigma_{1,j}} &= \frac{1}{2pt} \sum_{s=1}^p \left[\delta_{s=j} 2\sigma_{1,j} \rho_1 \left(\frac{r_j}{\sigma_{1,j}} \right) + \sigma_{1,s}^2 \psi_1 \left(\frac{r_s}{\sigma_{1,s}} \right) \frac{\partial r_s / \sigma_{1,s}}{\partial \sigma_{1,j}} \right] \\
&= \frac{1}{2pt} \sum_{s=1}^p \left[\delta_{s=j} 2\sigma_{1,j} \rho_1 \left(\frac{r_j}{\sigma_{1,j}} \right) + \sigma_{1,s} r_s w_s^{\text{cell}} \frac{\partial r_s / \sigma_{1,s}}{\partial \sigma_{1,j}} \right],
\end{aligned}$$

and

$$\frac{\partial r_s / \sigma_{1,s}}{\partial \sigma_{1,j}} = \frac{\partial r_s}{\partial \sigma_{1,j}} \frac{1}{\sigma_{1,s}} - \delta_{s=j} \frac{r_j}{\sigma_{1,j}^2}.$$

Then

$$\begin{aligned}
\frac{\partial w_j}{\partial \sigma_{1,j}} &= \frac{\partial w_j^{\text{cell}}}{\partial \sigma_{1,j}} w^{\text{case}} + w_j^{\text{cell}} \frac{\partial w^{\text{case}}}{\partial \sigma_{1,j}} \\
&= w^{\text{case}} \sigma_{1,j} (w_j^{\text{cell}})' \frac{\partial r_j / \sigma_{1,j}}{\partial \sigma_{1,j}} + \frac{w_j^{\text{cell}} (w^{\text{case}})'}{2pt} \sum_{s=1}^p \left[\delta_{s=j} 2\sigma_{1,j} \rho_1 \left(\frac{r_j}{\sigma_{1,j}} \right) + \sigma_{1,s} r_s w_s^{\text{cell}} \frac{\partial r_s / \sigma_{1,s}}{\partial \sigma_{1,j}} \right].
\end{aligned}$$

Moreover,

$$-\frac{\partial}{\partial \sigma_2} \mathbb{E}_{H_0} [w_j(x_j - \mathbf{v}_j^T \mathbf{u}_x) u_{x,h}] = -\mathbb{E}_{H_0} \left[\frac{\partial w_j}{\partial \sigma_2} r_j u_{x,h} + w_j \frac{\partial r_j}{\partial \sigma_2} u_{x,h} + w_j r_j \frac{\partial u_{x,h}}{\partial \sigma_2} \right]$$

where

$$\frac{\partial r_j}{\partial \sigma_2} = -\mathbf{v}_j^T \frac{\partial \mathbf{u}_x}{\partial \sigma_2}.$$

Then

$$\begin{aligned}
\frac{\partial w_j^{\text{cell}}}{\partial \sigma_2} &= \left(\psi'_1(r_j/\sigma_{1,j}) \frac{\partial r_j}{\partial \sigma_2} \frac{r_j}{\sigma_{1,j}^2} - \frac{\psi_1(r_j/\sigma_{1,j})}{\sigma_{1,j}} \frac{\partial r_j}{\partial \sigma_2} \right) / \frac{r_j^2}{\sigma_{1,j}^2} \\
&= \left(\frac{\psi'_1(r_j/\sigma_{1,j})}{r_j} \frac{\partial r_j}{\partial \sigma_2} - \sigma_{1,j} \frac{\psi_1(r_j/\sigma_{1,j})}{r_j^2} \frac{\partial r_j}{\partial \sigma_2} \right) \\
&= (w_j^{\text{cell}})' \frac{\partial r_j}{\partial \sigma_2}.
\end{aligned}$$

Moreover,

$$\begin{aligned}
\frac{\partial w^{\text{case}}}{\partial \sigma_2} &= \left(\psi'_2(t/\sigma_2) \frac{\partial t/\sigma_2}{\partial \sigma_2} \frac{t}{\sigma_2} - \psi_2(t/\sigma_2) \frac{\partial t/\sigma_2}{\partial \sigma_2} \right) / \frac{t^2}{\sigma_2^2} \\
&= \left(\sigma_2 \frac{\psi'_2(t/\sigma_2)}{t} - \sigma_2^2 \frac{\psi_2(t/\sigma_2)}{t^2} \right) \frac{\partial t/\sigma_2}{\partial \sigma_2} \\
&= \sigma_2 (w^{\text{case}})' \frac{\partial t/\sigma_2}{\partial \sigma_2}
\end{aligned}$$

where

$$\frac{\partial t/\sigma_2}{\partial \sigma_2} = \frac{\partial t}{\partial \sigma_2} \frac{1}{\sigma_2} - \frac{t}{\sigma_2^2}$$

and

$$\begin{aligned}
\frac{\partial t}{\partial \sigma_2} &= \frac{1}{2pt} \sum_{s=1}^p \sigma_{1,s} \psi_1 \left(\frac{r_j}{\sigma_{1,s}} \right) \frac{\partial r_s}{\partial \sigma_2} \\
&= \frac{1}{2pt} \sum_{s=1}^p \sigma_{1,s} r_s w_s^{\text{cell}} \frac{\partial r_s}{\partial \sigma_2}.
\end{aligned}$$

Then

$$\begin{aligned}
\frac{\partial w_j}{\partial \sigma_2} &= \frac{\partial w_j^{\text{cell}}}{\partial \sigma_2} w^{\text{case}} + w_j^{\text{cell}} \frac{\partial w^{\text{case}}}{\partial \sigma_2} \\
&= w^{\text{case}} (w_j^{\text{cell}})' \frac{\partial r_j}{\partial \sigma_2} + w_j^{\text{cell}} \sigma_2 (w^{\text{case}})' \left(\frac{1}{2pt} \sum_{s=1}^p \sigma_{1,s} r_s w_s^{\text{cell}} \frac{\partial r_s}{\partial \sigma_2} \frac{1}{\sigma_2} - \frac{t}{\sigma_2^2} \right).
\end{aligned}$$

Here $\frac{\partial \mathbf{u}_x}{\partial \sigma_{1,j}}$ and $\frac{\partial \mathbf{u}_x}{\partial \sigma_2}$ do not have not a closed form either, so they must be computed numerically as well.

I Pseudocode of the cellPCA algorithm

Algorithm 1 provides the pseudocode of the steps in Sections 2.2–2.3 of the main text.

Algorithm 1 IRLS algorithm for cellPCA

- 1: Initialize $\mathbf{V}_{(0)}$, $\mathbf{U}_{(0)}$, $\boldsymbol{\mu}_{(0)}$ by the MacroPCA initial fit.
- 2: Compute $\widehat{\sigma}_{1,j}$ and $\widehat{\sigma}_2$ according to Section 2.2.
- 3: Compute the initial weight matrix $\mathbf{W}_{(0)}$ using (15), (16), and (17).
- 4: Set $q = 0$.

5: **repeat**

- 6: (a) Update \mathbf{V} :

$$(\mathbf{v}_{(q+1)})_j = (\mathbf{U}_{(q)}^T \mathbf{W}_{(q)}^j \mathbf{U}_{(q)})^\dagger \mathbf{U}_{(q)}^T \mathbf{W}_{(q)}^j (\mathbf{x}^j - (\boldsymbol{\mu}_{(q)})_j \mathbf{1}_n) \quad j = 1, \dots, p.$$

- 7: (b) Update \mathbf{U} :

$$(\mathbf{u}_{(q+1)})_i = (\mathbf{V}_{(q+1)}^T (\widetilde{\mathbf{W}}_{(q)})_i \mathbf{V}_{(q+1)})^\dagger \mathbf{V}_{(q+1)}^T (\widetilde{\mathbf{W}}_{(q)})_i (\mathbf{x}_i - \boldsymbol{\mu}_{(q)}) \quad i = 1, \dots, n.$$

- 8: (c) Update $\boldsymbol{\mu}$:

$$\boldsymbol{\mu}_{(q+1)} = \left(\sum_{i=1}^n (\mathbf{W}_{(q)})_i \right)^{-1} \sum_{i=1}^n (\mathbf{W}_{(q)})_i (\mathbf{x}_i - \mathbf{V}_{(q+1)} (\mathbf{u}_{(q+1)})_i).$$

- 9: (d) Update \mathbf{W} : Compute $\mathbf{W}_{(q+1)}$ using (15), (16), and (17).

- 10: Increment q : $q = q + 1$.

- 11: **until** $\|\mathbf{U}_{(q)} \mathbf{V}_{(q)}^T - \mathbf{U}_{(q-1)} \mathbf{V}_{(q-1)}^T\|_F < \nu \|\mathbf{U}_{(q-1)} \mathbf{V}_{(q-1)}^T\|_F$ for some tolerance ν .

Algorithm 2 gives the pseudocode of the out-of-sample prediction in Section 4.4.

Algorithm 2 Out-of-Sample Prediction in cellPCA

- 1: Given a new data point \mathbf{x}^* with missingness indicator \mathbf{m}^* .
- 2: Retrieve the \mathbf{V} , $\boldsymbol{\mu}$ and $\widehat{\sigma}_{1,j}$ estimated in the training stage.
- 3: Set $J = \{j ; m_j^* = 1\}$.
- 4: **if** $J = \emptyset$ **then**
- 5: Set \mathbf{u}^* and $\widehat{\mathbf{x}}^*$ to NA.
- 6: **else**
- 7: Initialize $\mathbf{u}_{(0)}^*$ as $\mathbf{V}_J^T(\mathbf{x}_J^* - \boldsymbol{\mu}_J)$ where \mathbf{x}_J^* has the coordinates of \mathbf{x}^* in J .
- 8: Compute the initial weights $\mathbf{w}_{(0)}^*$ using (38).
- 9: Set $q = 0$.
- 10: **repeat**
- 11: Update \mathbf{u}^* by
$$\mathbf{u}_{(q+1)}^* = (\mathbf{V}^T \mathbf{W}_{(q)}^* \mathbf{V})^\dagger \mathbf{V}^T \mathbf{W}_{(q)}^* (\mathbf{x}^* - \boldsymbol{\mu})$$
where $\mathbf{W}_{(q)}^* = \text{diag}(\mathbf{w}_{(q)}^*)$.
- 12: Update cellwise weights by
$$(\mathbf{w}_{(q+1)}^*)_j = \psi_1\left(\frac{(r_{(q+1)})_j}{\widehat{\sigma}_{1,j}}\right) / \frac{(r_{(q+1)})_j}{\widehat{\sigma}_{1,j}} \quad \text{for } j \in J$$
and set $(\mathbf{w}_{(q+1)}^*)_j = 0$ for $j \notin J$, with $(r_{(q+1)})_j = x_j^* - \mu_j - \mathbf{v}_j^T \mathbf{u}_{(q+1)}^*$.
- 13: **until** $\|\mathbf{V}\mathbf{u}_{(q)}^* - \mathbf{V}\mathbf{u}_{(q-1)}^*\|_F < \nu \|\mathbf{V}\mathbf{u}_{(q-1)}^*\|_F$ for some tolerance ν .
- 14: Compute the final estimate $\widehat{\mathbf{x}}^* = (\widehat{x}_1^*, \dots, \widehat{x}_p^*)^T$ with $\widehat{x}_j^* := \mu_j + \mathbf{v}_j^T \mathbf{u}_{(q+1)}^*$.
- 15: **end if**

J Complexity of the cellPCA algorithm

We will first study the time complexity of the algorithm described in Sections 2.2–2.3 and 4.3.

Starting from the initial estimates of \mathbf{V} , \mathbf{U} and $\boldsymbol{\mu}$ we first have to compute the robust M-scales $\widehat{\sigma}_{1,j}$ for $j = 1, \dots, p$ as described in Section 2.2. Each M-scale can be computed in $O(n)$ time and we compute p of them, so the complexity is $O(np)$. The computation of the single M-scale $\widehat{\sigma}_2$ is $O(n)$ which does not increase the overall complexity $O(np)$ for all of these scale estimates.

Next we have to carry out the IRLS algorithm described in Section 2.3, which initializes \mathbf{W} and then updates \mathbf{V} , \mathbf{U} , $\boldsymbol{\mu}$ and \mathbf{W} . Initializing the $n \times p$ matrix \mathbf{W} according to (15)–(17) is an elementwise operation with complexity $O(np)$. The complexity for updating \mathbf{V} as in (21) is obtained as follows.

1. **Compute $\mathbf{x}^j - \boldsymbol{\mu}_j \mathbf{1}_n$.** Subtracting a scalar from an n -dimensional vector requires $O(n)$ operations.
2. **Compute $\mathbf{W}^j(\mathbf{x}^j - \boldsymbol{\mu}_j \mathbf{1}_n)$.** Matrix-vector multiplication of \mathbf{W}^j ($n \times n$) and this vector ($n \times 1$) would require $O(n^2)$ operations in general. However, as \mathbf{W}^j is diagonal the matrix by vector multiplication simplifies to elementwise multiplication, which requires $O(n)$ operations.
3. **Compute $\mathbf{U}^T \mathbf{W}^j(\mathbf{x}^j - \boldsymbol{\mu}_j \mathbf{1}_n)$.** Matrix-vector multiplication of \mathbf{U}^T ($k \times n$) and resulting vector ($n \times 1$) requires $O(nk)$ operations.
4. **Compute $\mathbf{U}^T \mathbf{W}^j \mathbf{U}$.** The matrix multiplication $\mathbf{W}^j \mathbf{U}$ of \mathbf{W}^j ($n \times n$) and \mathbf{U} ($n \times k$) would require $O(n^2k)$ operations in general, since each of the nk entries of the product matrix is a sum of n products of two scalars. However, because \mathbf{W}^j is diagonal it is only the number of entries in \mathbf{U} , so $O(nk)$ operations. To this we must add the complexity of multiplying \mathbf{U}^T ($k \times n$) and the resulting $\mathbf{W}^j \mathbf{U}$ ($n \times k$) which is $O(nk^2)$ which is bigger. Therefore the computation of $\mathbf{U}^T \mathbf{W}^j \mathbf{U}$ requires $O(nk^2)$ operations.
5. **Compute the pseudoinverse $(\mathbf{U}^T \mathbf{W}^j \mathbf{U})^\dagger$.** Computing the pseudoinverse of a $k \times k$ matrix by a singular value decomposition requires $O(k^3)$ operations.

6. **Carry out the final multiplication.** Multiplying the $k \times k$ pseudoinverse with the $k \times 1$ vector requires $O(k^2)$ operations.

Since (21) is repeated p times, adding up all the steps gives

$$\begin{aligned} & p(O(n) + O(n) + O(nk) + O(nk^2) + O(k^3) + O(k^2)) \\ &= O(npk) + O(npk^2) + O(pk^3) = O(npk^2 + pk^3) = O(npk^2) \end{aligned}$$

where the last equality follows from $npk^2 \geq pk^3$ due to $n \geq k$. Therefore, the time complexity for updating \mathbf{V} is $O(npk^2)$.

For updating \mathbf{U} we have to repeat (23) n times. By a totally similar reasoning we obtain the complexity

$$\begin{aligned} & n(O(p) + O(p) + O(pk) + O(pk^2) + O(k^3) + O(k^2)) \\ &= O(npk) + O(npk^2) + O(nk^3) = O(npk^2 + nk^3) = O(npk^2) \end{aligned}$$

where the last equality follows from $npk^2 \geq nk^3$ due to $p \geq k$. So the time complexity for updating \mathbf{U} is $O(npk^2)$ also.

Updating $\boldsymbol{\mu}$ consists of the following steps:

1. **Compute $\mathbf{x}_i - \mathbf{V}\mathbf{u}_i$.** Multiplying \mathbf{V} ($p \times k$) with \mathbf{u}_i ($k \times 1$) requires $O(pk)$ operations. Subtracting the resulting $p \times 1$ vector from \mathbf{x}_i ($p \times 1$) requires $O(p)$ operations. Repeating this for all $i = 1, \dots, n$ yields $O(np) + O(npk) = O(npk)$ operations.
2. **Compute $\mathbf{W}_i(\mathbf{x}_i - \mathbf{V}\mathbf{u}_i)$.** Since \mathbf{W}_i is a diagonal $p \times p$ matrix, the matrix by vector multiplication simplifies to elementwise multiplication, which requires $O(p)$ operations. For all i this becomes $O(np)$ operations.
3. **Sum over $i = 1, \dots, n$.** Summing n vectors ($p \times 1$) requires $O(np)$ operations.
4. **Compute $\sum_{i=1}^n \mathbf{W}_i$.** Adding n diagonal $p \times p$ matrices is performed by summing the diagonal elements. That is adding n vectors ($p \times 1$), which requires $O(np)$ operations.
5. **Compute the inverse $\left(\sum_{i=1}^n \mathbf{W}_i\right)^{-1}$.** Since $\sum_{i=1}^n \mathbf{W}_i$ is diagonal, the inversion simplifies to inverting each diagonal entry, which requires $O(p)$ operations.
6. **Multiply the inverse with the vector sum.** Multiplying the $p \times p$ diagonal inverse matrix with the $p \times 1$ vector requires $O(p)$ operations.

By adding up all the steps, the complexity for updating $\boldsymbol{\mu}$ becomes $O(npk) + O(np) + O(np) + O(np) + O(p) + O(p) = O(npk)$.

Finally, updating \mathbf{W} is again an elementwise operation with complexity $O(np)$.

Therefore, the total complexity of the algorithm in Sections 2.2–2.3 is $O(np) + O(npk^2) + O(npk^2) + O(npk)$ which equals $O(npk^2)$.

If we also want to estimate the principal directions as in Section 4.3 we need to carry out the DetMCD method (Hubert et al., 2012) for n points in k dimensions. This requires $O(n \log(n)k^2) + O(nk^2) = O(n \log(n)k^2)$ operations.

Therefore, all the computations in Sections 2.2–2.3 and 4.3 together have complexity $O((n \log(n) + np)k^2)$.

However, the cellPCA algorithm starts from the MacroPCA initial estimator, which has time complexity $O(np(\min(n, p) + \log(n) + \log(p)))$ as shown in (Hubert et al., 2019). Its complexity does not depend on k because MacroPCA requires $k \leq k_{max}$ where by default $k_{max} = 10$. Therefore, the rank k in the remainder of the cellPCA algorithm also cannot increase beyond k_{max} , so this part has complexity $O(n \log(n) + np)$. The overall complexity of cellPCA is thus

$$\begin{aligned} & O(np(\min(n, p) + \log(n) + \log(p))) + O(n \log(n) + np) \\ &= O(np(\min(n, p) + \log(n) + \log(p))) \end{aligned}$$

so the additional steps of cellPCA do not increase the time complexity beyond that of the initial estimator MacroPCA. In robust estimation it is indeed typical that the overall complexity remains that of the initial estimator.

Figure 18 shows the average computation times of the cellPCA components in seconds, as a function of n and p over 500 replications. These were measured on a workstation equipped with two 24-core sockets with an Intel® Xeon® Platinum 8160 processor with a clock frequency of 2.10GHz and 192GB of RAM. The top row in Figure 18 shows times in function of n , for fixed choices of (p, k) . The bottom row shows them in function of p , for fixed choices of (n, k) . The leftmost panels have the times for running the initial MacroPCA. In the middle we see the times for 10 iterations of the IRLS algorithm, which indeed look linear in both n and p . The rightmost panels show the total times of cellPCA, which are the sums of the leftmost and the middle panels. The shapes of its curves are similar to those of the initial MacroPCA method, as expected.

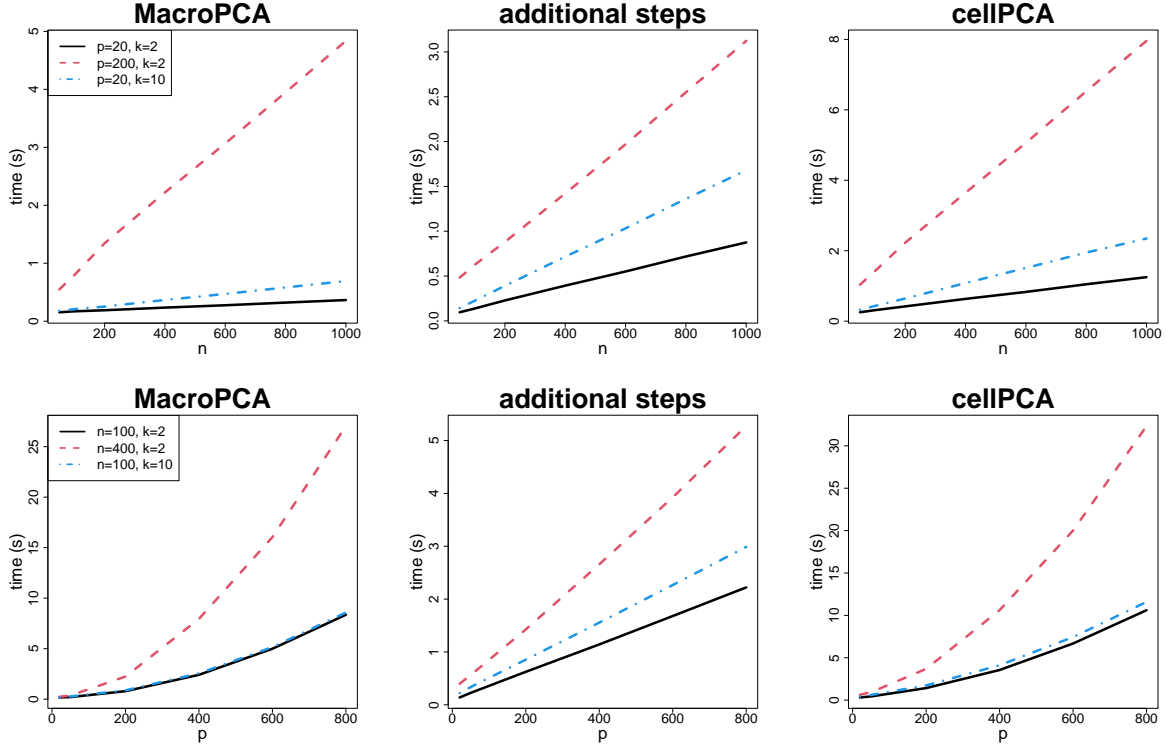


Figure 18: Average computation times in seconds of the different steps of cellPCA, as a function of the number of cases n (top row) and the dimension p (bottom row).

For the space complexity of cellPCA we look at each of its steps again. The first step of the initial estimator MacroPCA is the DDC method, whose space complexity is $O(np)$ for large n and p . The other steps of MacroPCA also have space complexity $O(np)$. Its DetMCD component requires $O(nk + k^2 + k)$, but since $k \leq \min(n, p)$ this is also at most $O(np)$. Therefore, the overall space complexity of MacroPCA remains $O(np)$. Similarly, updating $\mathbf{U}, \mathbf{V}, \boldsymbol{\mu}, \mathbf{W}$ requires $O(np)$ space. Computing robust scales has a space complexity of $O(p)$, while estimating the center and principal directions requires $O(np)$. Hence, the total space complexity of cellPCA is $O(np)$. Since this is also the space complexity of the dataset, the algorithm does not add to it.

K Additional Results for the Ionosphere Data

For cases 119 and 138 of the ionosphere data, Figure 19 illustrates that each imputed cell x_i^{imp} can be seen as a weighted average of the observed x_{ij} and the fitted \hat{x}_{ij} . Only a subset of the variables are shown. The plot also displays the cellwise weights w_{ij}^{cell} . The smaller the weight, the more the imputed value becomes close to the fitted value. For $w_{ij}^{\text{cell}} = 1$ the imputed cell is the observed value, and for $w_{ij}^{\text{cell}} = 0$ the imputed cell is the fitted value.

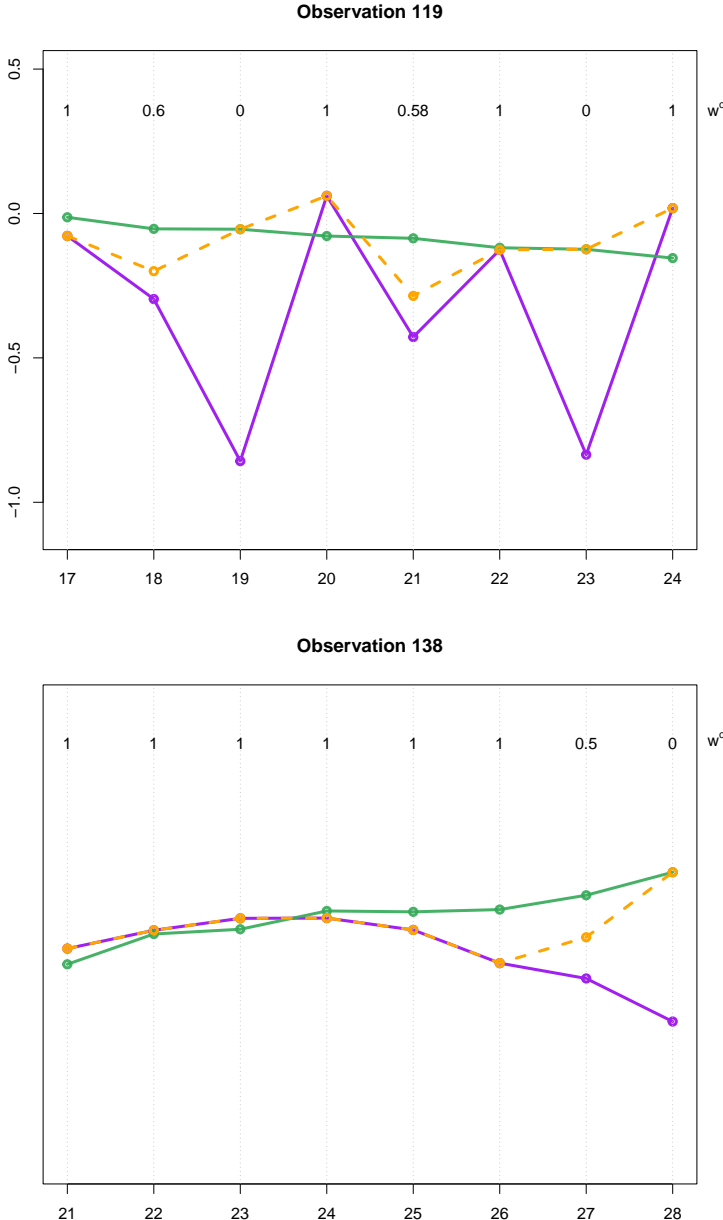


Figure 19: Observed (purple), fitted (green) and imputed (orange dashed) curves of cases 119 and 138 of the Ionosphere dataset. Above each cell we see its cellwise weight.

L Additional simulation results

Figure 20 shows the median angle and MSE for the A09-type covariance model in the presence of either cellwise outliers, casewise outliers, or both, without NAs, this time for $p = 20$. For $\gamma_{\text{cell}} = 0$ no cellwise outliers were generated, and for $\gamma_{\text{case}} = 0$ no casewise outliers. Figure 21 shows the corresponding results when $\varepsilon^{\text{obs}} = 20\%$ of randomly selected cells were made NA. All of these curves look a lot like those for $p = 200$ in Section 6 of the paper.

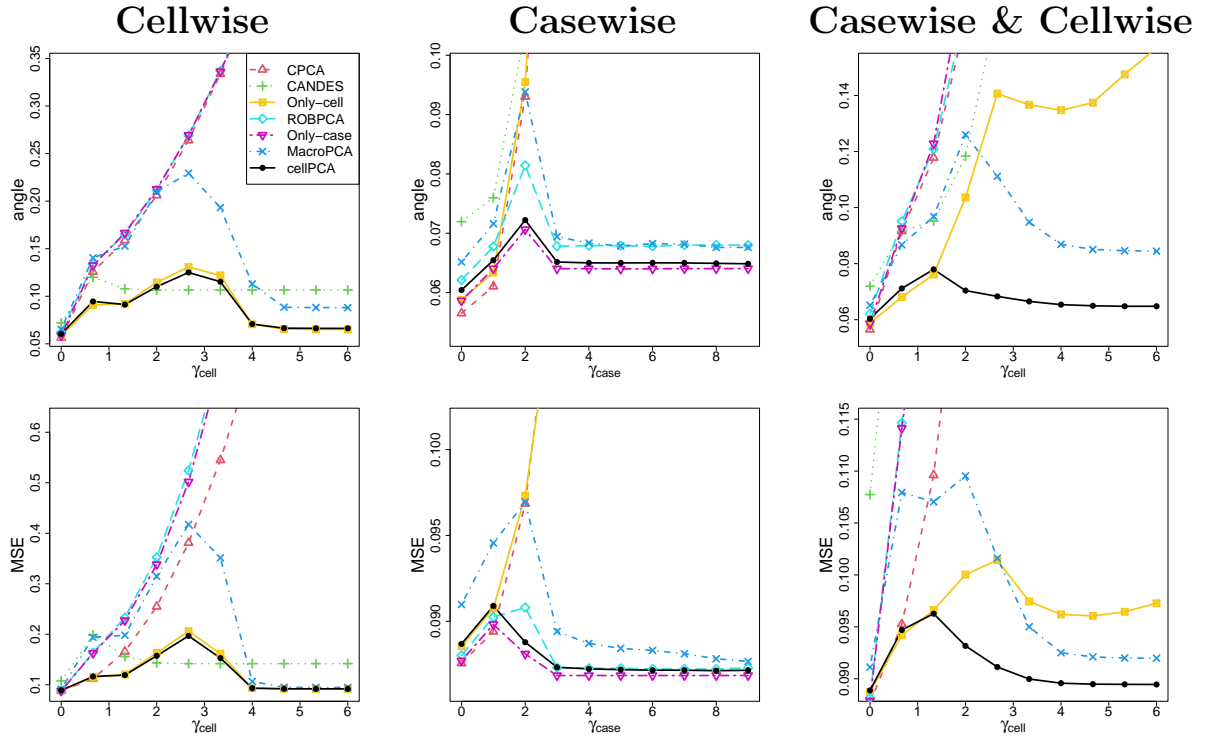


Figure 20: Median angle (top) and MSE (bottom) attained by CPCa, CANDES, Only-cell, ROBPCA, Only-case, MacroPCA, and cellPCA in the presence of either cellwise outliers, casewise outliers, or both. The covariance model was A09 with $n = 100$ and $p = 20$, without NAs.

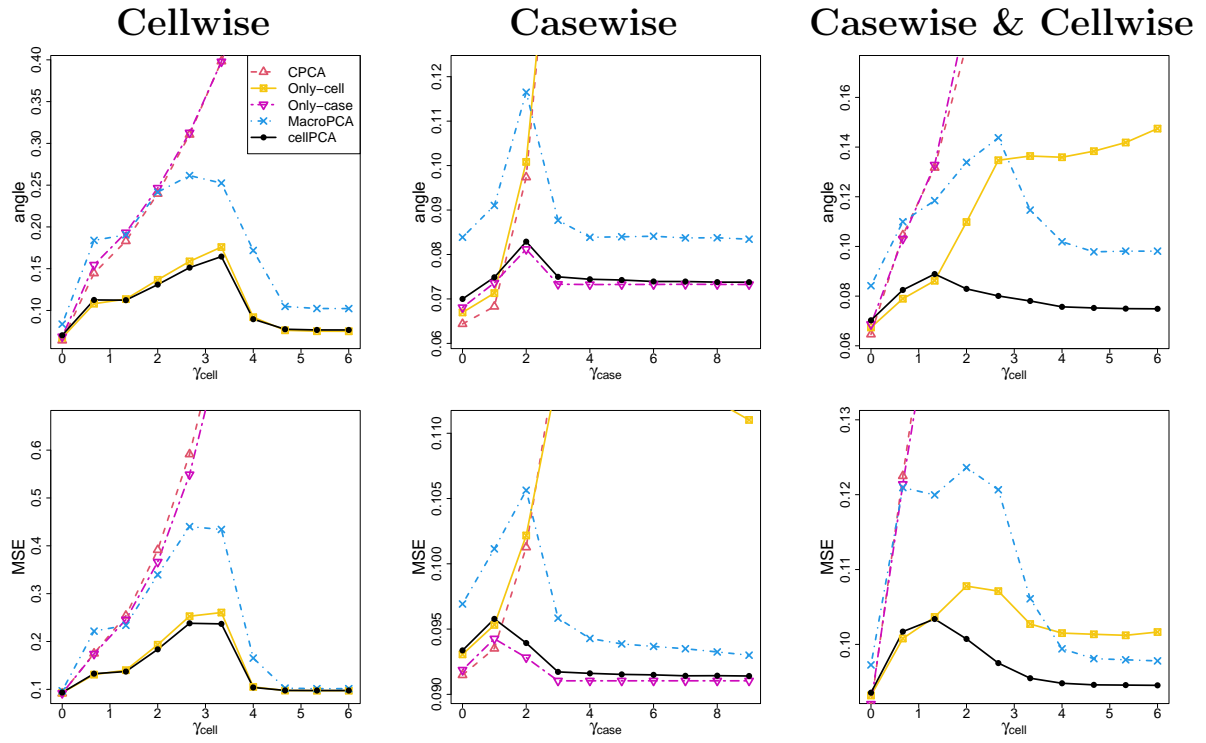


Figure 21: Median angle (top) and MSE (bottom) attained by CPCA, Only-cell, Only-case, MacroPCA, and cellPCA in the presence of either cellwise outliers, casewise outliers, or both. The covariance model was A09 with $n = 100$ and $p = 20$, and 20% of randomly selected cells were set to NA.

The second type of covariance matrix is based on the random correlation matrices of Agostinelli et al. (2015) and will be called ALYZ. These correlation matrices are turned into covariance matrices with other eigenvalues. More specifically, the matrix \mathbf{L} in the spectral decomposition $\mathbf{O}\mathbf{L}\mathbf{O}^T$ of the correlation matrix is replaced by $\text{diag}(9.57, 6.70, 0.11, 0.10, \dots, 0.10)$ for $p = 20$ and by $\text{diag}(104.86, 73.41, 0.11, 0.10, \dots, 0.10)$ for $p = 200$. These are the same eigenvalues as used in Figure 9 and Figures 20-21, but now the directions of the eigenvectors vary a lot. Again the first two components explain 90% of the variance, and we set $k = 2$ in the simulation.

Again three contamination types are considered. In the cellwise outlier scenario we randomly replace $\varepsilon^{\text{cell}} = 20\%$ of the cells x_{ij} with $\gamma_{\text{cell}}\sigma_j$, where γ_{cell} varies from 0 to 6 and σ_j^2 is the j th diagonal element of Σ . Note that the diagonal entries of this Σ are no longer 1 as in A09. In the casewise outlier setting $\varepsilon^{\text{case}} = 20\%$ of the cases are generated from $N(\gamma_{\text{case}}(\mathbf{e}_1 + \mathbf{e}_{k+1}), \Sigma/1.5)$, where \mathbf{e}_1 and \mathbf{e}_{k+1} are the first and $(k+1)$ -th eigenvectors of Σ , and γ_{case} varies from 0 to 9 when $p = 20$, and from 0 to 24 when $p = 200$. In the third scenario, the data is contaminated by $\varepsilon^{\text{cell}} = 10\%$ of cellwise outliers as well as $\varepsilon^{\text{case}} = 10\%$ of casewise outliers. Here $\gamma_{\text{case}} = 1.5\gamma_{\text{cell}}$ when $p = 20$ and $\gamma_{\text{case}} = 4\gamma_{\text{cell}}$ when $p = 200$, where γ_{cell} again varies from 0 to 6. When $\gamma_{\text{cell}} = \gamma_{\text{case}} = 0$ we do not contaminate the data.

Repeating the entire simulation with the ALYZ covariance model instead of A09 yields Figure 22 without NAs, and Figure 23 with NAs. These figures are qualitatively similar to those for A09, and yield the same conclusions.

The cellwise outliers considered in the simulation study in Section 6 are also referred to as *elementwise* outliers, since they occur in random individual entries of the data matrix. To further evaluate the performance of cellPCA, we examine a more challenging *structured cellwise* contamination scenario, where clean data, generated as in Section 6, are partially replaced by contaminated cells, with contamination percentages $\varepsilon_j^{\text{cell}}$ linearly varying across variables from 15% to 25%. For each column of the data matrix, we randomly sample the corresponding percentage of cell indices to be replaced. In each row, say (z_1, \dots, z_p) , we collect the indices of the cells selected for contamination. Denote this index set of size q by $Q = \{j_1, \dots, j_q\}$. We then replace the cells $(z_{j_1}, \dots, z_{j_q})$ with the q -dimensional vector $\gamma_{\text{cell}}\sqrt{q}\mathbf{v}_Q/(\mathbf{v}_Q^T \Sigma_Q^{-1} \mathbf{v}_Q)$, where Σ_Q denotes the covariance matrix Σ restricted to the indices in Q . The vector \mathbf{v}_Q is the normalized eigenvector of Σ_Q corresponding to its smallest eigenvalue. The contamination level γ_{cell} varies from 0 to 24 for $p = 20$ and from

0 to 12 for $p = 200$. In each row, the contaminated cells are structurally outlying in the subspace spanned by the variables in Q . Consequently, these cells are often not marginally outlying, especially when the size of Q is large and γ_{cell} is relatively small, which makes them difficult to detect. Moreover, since the probability of observing cellwise outliers depends on the variable, this contamination scenario does not fall under the standard notion of elementwise contamination. We also consider the scenario where the data is contaminated by a percentage of structured cellwise outliers that goes from 7.5% to 12.5% across variables, and by $\varepsilon^{\text{case}} = 10\%$ of casewise outliers generated as described in Section 6. Here γ_{cell} again varies from 0 to 24 with $\gamma_{\text{case}} = 2\gamma_{\text{cell}}$ when $p = 20$ and γ_{cell} again varies from 0 to 12 with $\gamma_{\text{case}} = 8\gamma_{\text{cell}}$ when $p = 200$.

Figure 24 and Figure 25 show the median angle and MSE in the presence of either structured cellwise outliers, or structured cellwise and casewise outliers, for $p = 20$ and $p = 200$. The results are even more convincing than those obtained for elementwise contamination. In this setting, cellPCA significantly outperforms the competitors across all scenarios. In particular, the CANDES approach is adversely affected by the presence of structured outliers, since its development relies on the assumption of elementwise contamination.

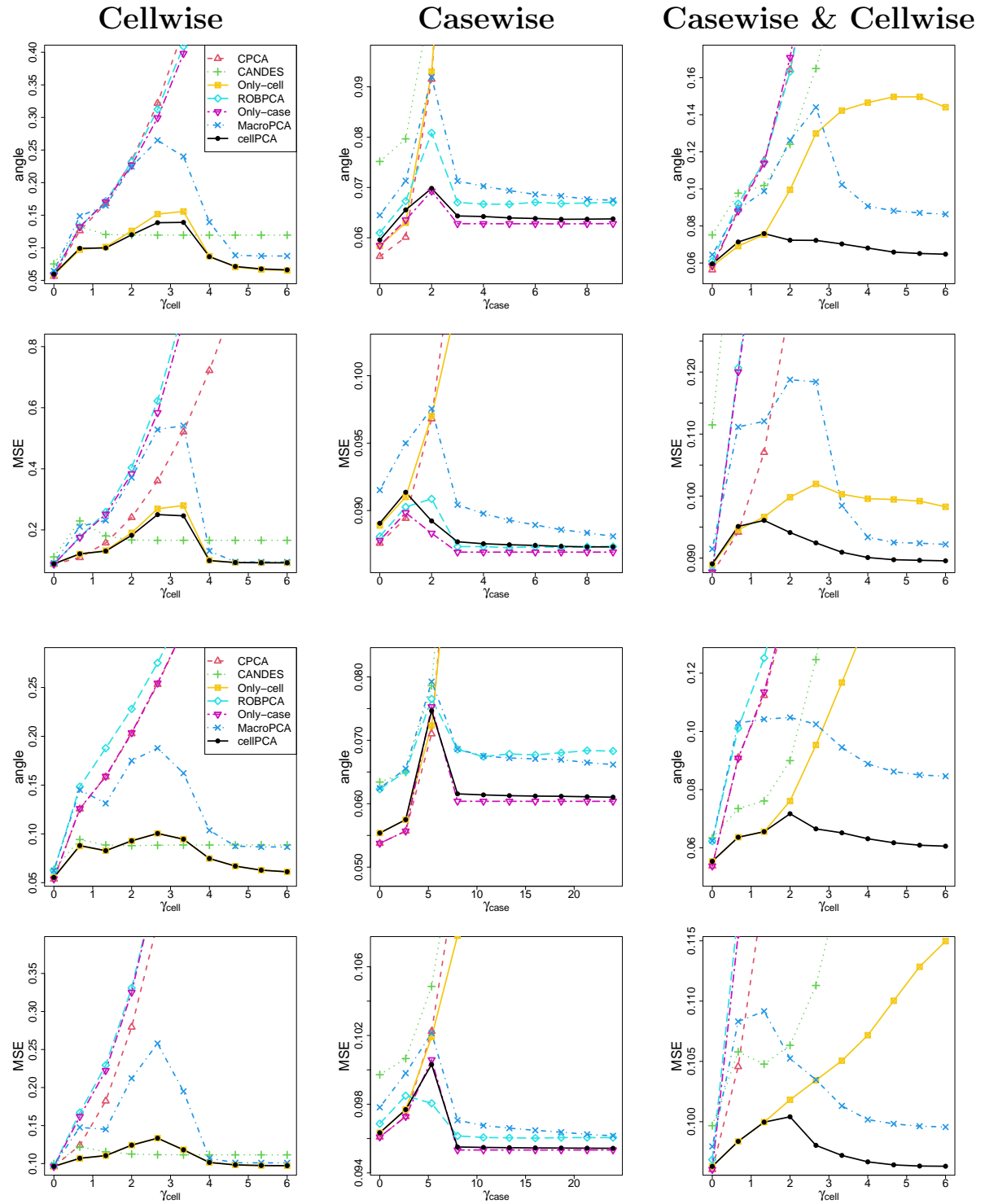


Figure 22: Median angle and MSE attained by CPCa, CANDES, Only-cell, ROBPCA, Only-case, MacroPCA, and cellPCA in the presence of either cellwise outliers, casewise outliers, or both. The covariance model was ALYZ with $n = 100$, without NAs. The top two rows are for $p = 20$, and the bottom two rows for $p = 200$.

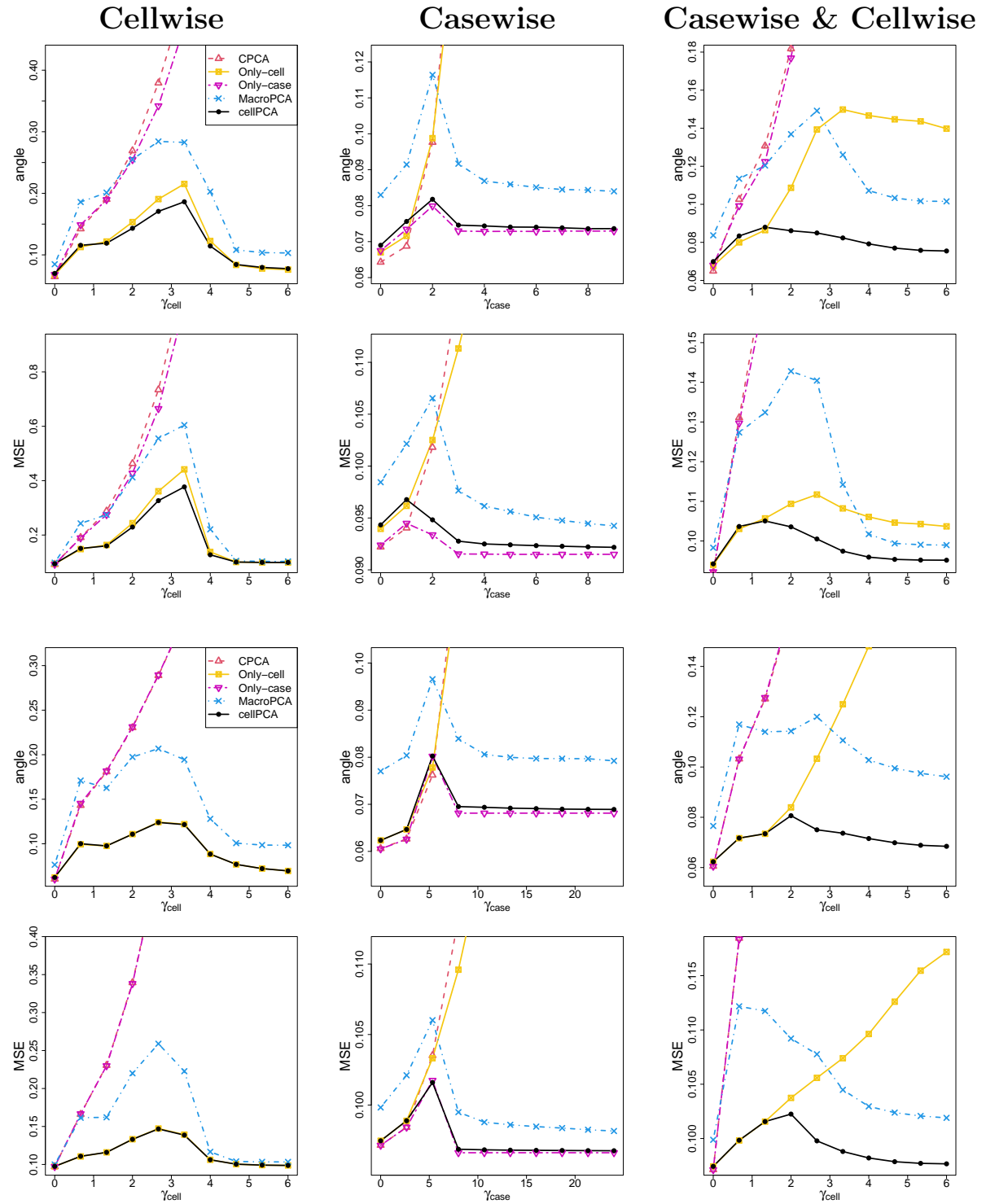


Figure 23: Median angle and MSE attained by CPCa, Only-cell, Only-case, MacroPCA, and cellPCA in the presence of either cellwise outliers, casewise outliers, or both. The covariance model was ALYZ with $n = 100$, and 20% of randomly selected cells were set to NA. The top two rows are for $p = 20$, and the bottom two rows for $p = 200$.

Structured Cellwise Casewise & Structured Cellwise

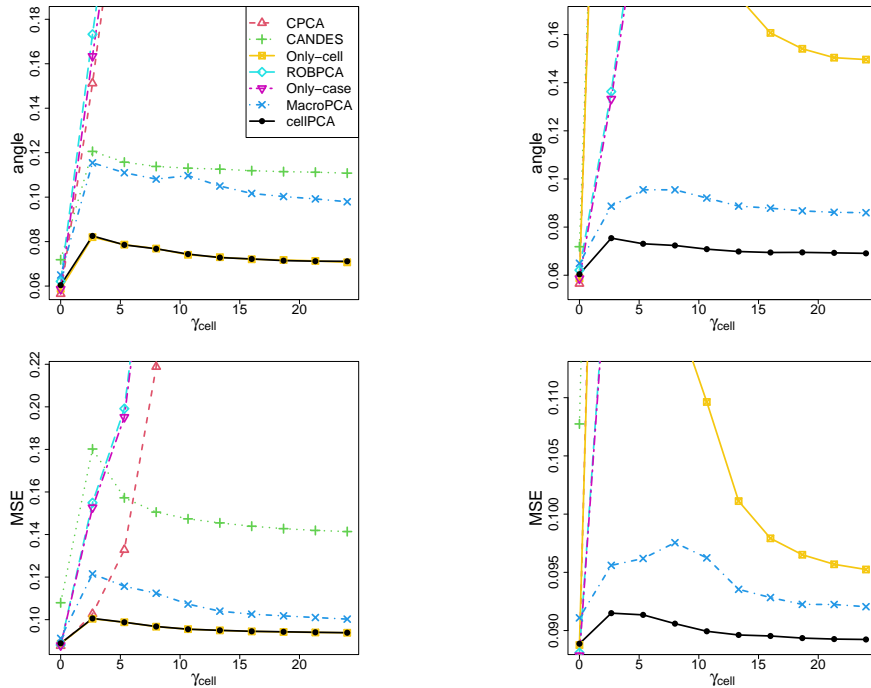


Figure 24: Median angle (top) and MSE (bottom) attained by CPCa, CANDES, Only-cell, ROBPCA, Only-case, MacroPCA, and cellPCA in the presence of structured cellwise outliers, and structured cellwise and casewise outliers. The covariance model was A09 with $n = 100$ and $p = 20$, without NAs.

Structured Cellwise Casewise & Structured Cellwise

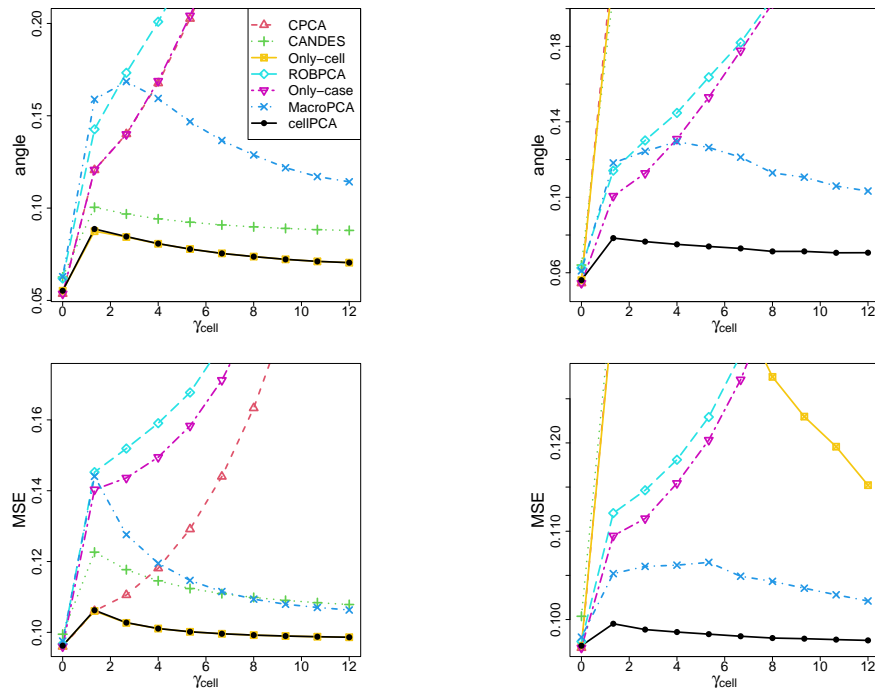


Figure 25: Median angle (top) and MSE (bottom) attained by CPCa, CANDES, Only-cell, ROBPCA, Only-case, MacroPCA, and cellPCA in the presence of structured cellwise outliers, and structured cellwise and casewise outliers. The covariance model was A09 with $n = 100$ and $p = 200$, without NAs.

To study the sensitivity of cellPCA and competing methods to the contamination fraction, Figures 26 and 27 show the median angle and MSE as a function of ε for data contaminated as in Section 6 with cellwise outliers generated with $\varepsilon^{\text{cell}} = \varepsilon$ and $\gamma_{\text{cell}} = \{3, 5\}$, casewise outliers generated with $\varepsilon^{\text{case}} = \varepsilon$ and $\gamma_{\text{case}} = \{3, 5\}$, and both together with $\varepsilon^{\text{cell}} = \varepsilon^{\text{case}} = \varepsilon/2$, $\gamma_{\text{cell}} = \{3, 5\}$ and γ_{case} obtained from γ_{cell} as in Figures 22 and 23. The covariance model was A09 with $n = 100$ and $p = 20$, without NAs. The two values of γ represent intermediate and far outliers.

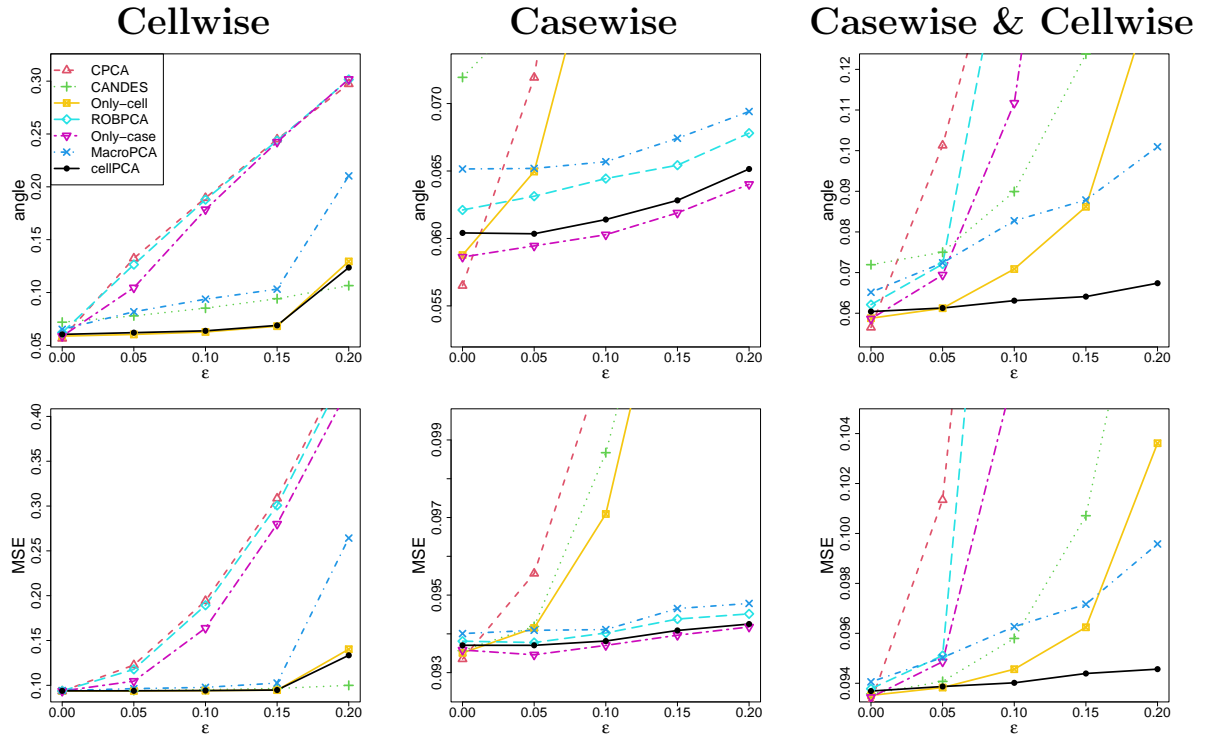


Figure 26: Median angle (top) and MSE (bottom) attained by CPCPA, CANDES, Only-cell, ROBPCA, Only-case, MacroPCA, and cellPCA as a function of ε in the presence of cellwise outliers generated with $\gamma_{\text{cell}} = 3$, casewise outliers generated with $\gamma_{\text{case}} = 3$, and both generated with $\gamma_{\text{cell}} = 3$. The covariance model was A09 with $n = 100$ and $p = 20$, without NAs.

In Figures 26 and 27 we see that, as expected, increasing ε hurts all methods, but not to the same extent. CellPCA did best in the presence of both cellwise and casewise outliers, and did very well also in the other settings.

Indeed, in the cellwise contamination setting, cellPCA performs similarly to Only-cell and CANDES, which are specifically designed to tackle this type of contamination. How-

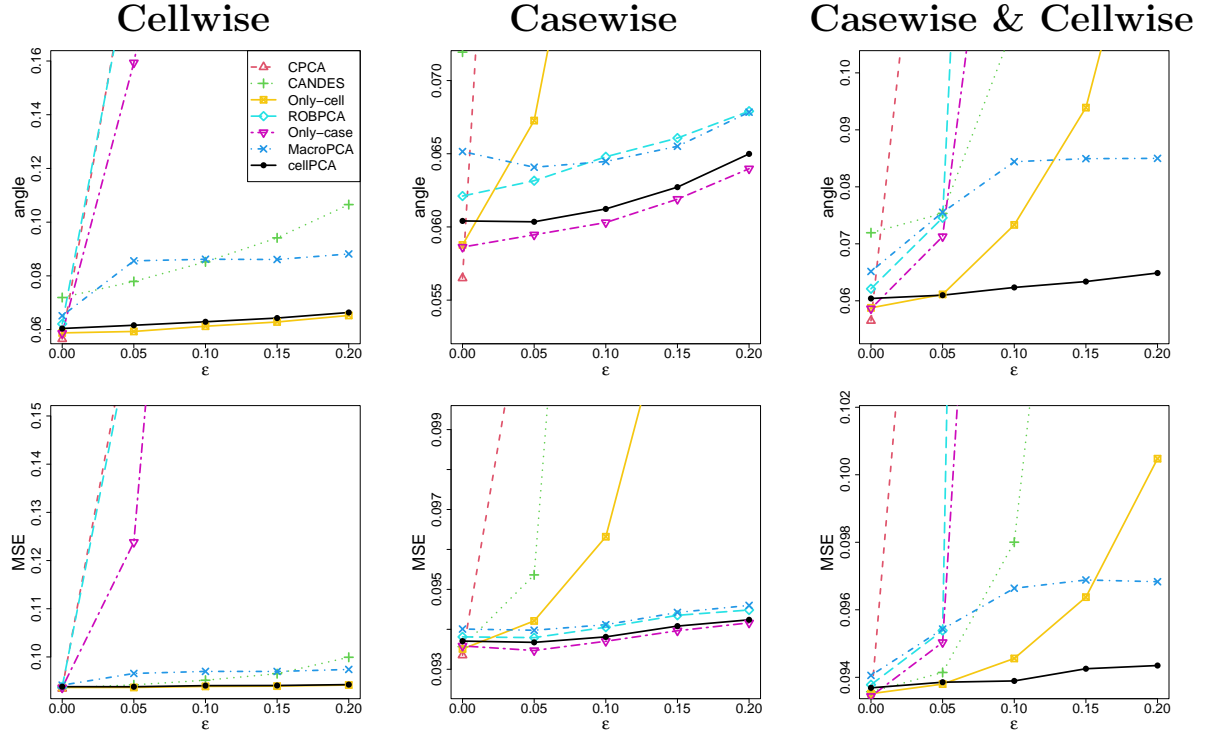


Figure 27: Median angle (top) and MSE (bottom) attained by CPCa, CANDES, Only-cell, ROBPCA, Only-case, MacroPCA, and cellPCA as a function of ε for data contaminated with cellwise outliers generated with $\gamma_{\text{cell}} = 5$, casewise outliers generated with $\gamma_{\text{case}} = 5$, and both generated with $\gamma_{\text{cell}} = 5$. The covariance model was A09 with $n = 100$ and $p = 20$, without NAs.

ever, in the casewise contamination setting the latter methods break down, whereas cellPCA still performs very well and is comparable to robust casewise methods such as Only-case and ROBPCA. In the presence of both types of contamination, cellPCA outperforms all other methods, including MacroPCA. As expected, differences in performance become more pronounced as the contamination fraction increases, with higher levels representing more challenging scenarios. Nevertheless, even for a small fraction of contamination, e.g., $\varepsilon = 0.05$, cellPCA is often the best, or among the best performing methods. Note that for very small values of ε , some methods are slightly more efficient than cellPCA. However, this reflects the common trade-off between robustness and efficiency. In real applications, however, the amount and type of contamination are rarely known in advance. This uncertainty further supports the use of the proposed method, which overall performs best across a wide range of settings.

To study the effect of different fractions ε^{obs} of missing values, Figures 28, 29, and 30 show the median angle and MSE as a function of ε^{obs} for uncontaminated data, data contaminated with cellwise outliers generated with $\gamma_{\text{cell}} = \{3, 5\}$, casewise outliers generated with $\gamma_{\text{case}} = \{2, 5\}$, and both with $\gamma_{\text{cell}} = \{3, 5\}$. The covariance model was A09 with $n = 100$ and $p = 20$, and contamination was added as described in Section 6.

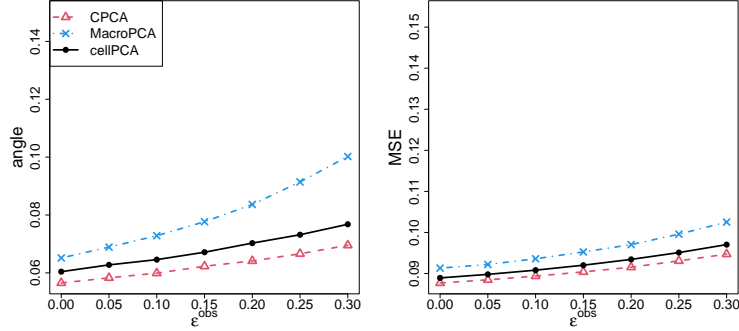


Figure 28: Median angle (left) and MSE (right) attained by CPCPA, MacroPCA, and cellPCA as a function of ε^{obs} for uncontaminated data. The covariance model was A09 with $n = 100$ and $p = 20$.

In Figure 28 we see that for uncontaminated data the classical method did best, as expected. It is followed by cellPCA, which outperforms its predecessor MacroPCA.

Figure 29 shows the effect of a varying percentage of NAs in the presence of intermediate outliers ($\gamma_{\text{cell}} = 3$ and/or $\gamma_{\text{case}} = 3$). Now cellPCA performs best, followed by MacroPCA, and CPCCA is the most affected.

The situation is similar in the presence of far outliers ($\gamma_{\text{cell}} = 5$ and/or $\gamma_{\text{case}} = 5$) in Figure 30, except that CPCCA now underperforms more substantially relative to the other methods.

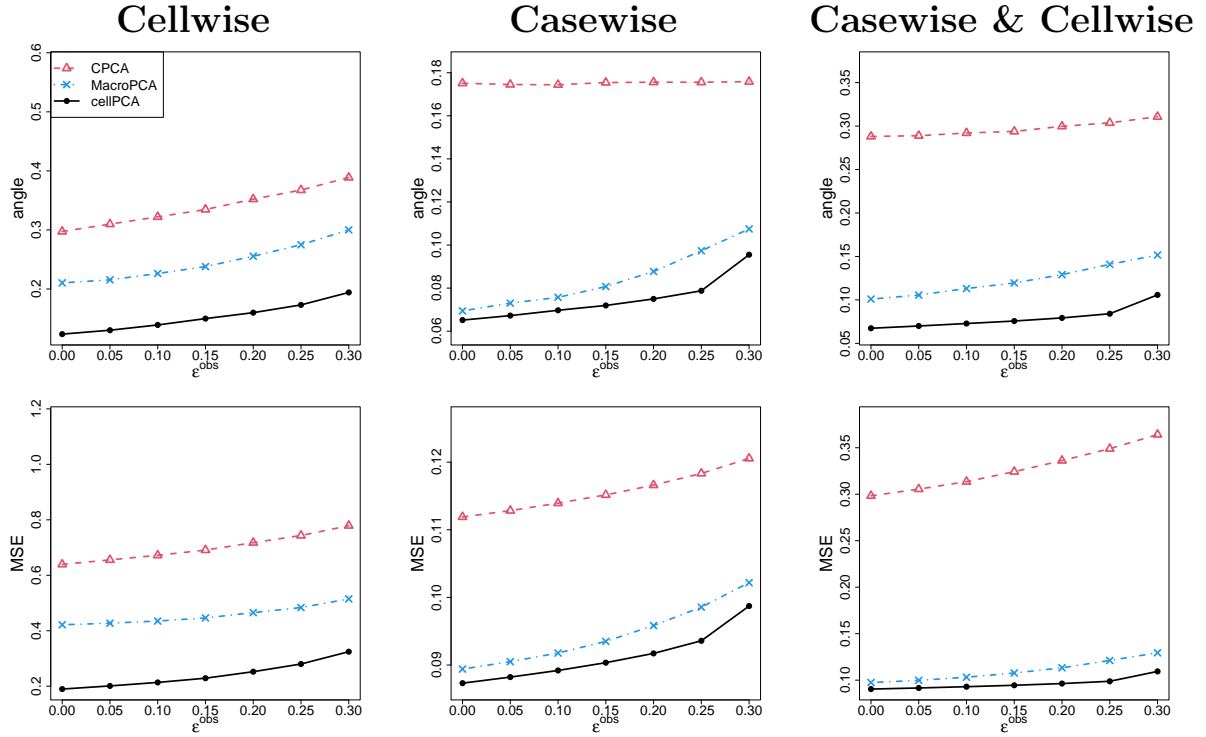


Figure 29: Median angle (top) and MSE (bottom) attained by CPCCA, MacroPCA, and cellPCA as a function of ϵ^{obs} for data contaminated with cellwise outliers generated with $\gamma_{\text{cell}} = 3$, casewise outliers generated with $\gamma_{\text{case}} = 3$, and both with $\gamma_{\text{cell}} = 3$. The covariance model was A09 with $n = 100$ and $p = 20$.

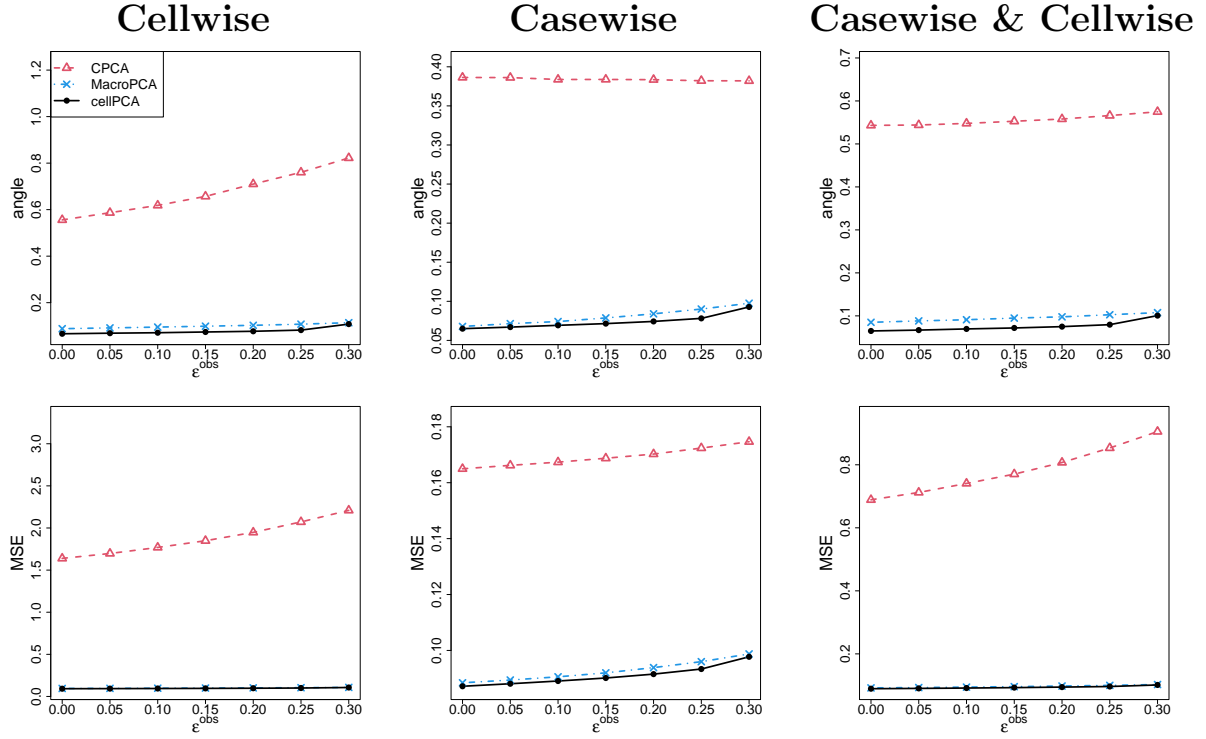


Figure 30: Median angle (top) and MSE (bottom) attained by CPCCA, MacroPCA, and cellPCA as a function of ϵ^{obs} for data contaminated with cellwise outliers generated with $\gamma_{\text{cell}} = 5$, casewise outliers generated with $\gamma_{\text{case}} = 5$, and both with $\gamma_{\text{cell}} = 5$. The covariance model was A09 with $n = 100$ and $p = 20$.

We now assess the performance of the out-of-sample prediction method described in Section 4.4. The *training data* are generated as in Section 6 by covariance model A09 with $n = 100$ and $p = 20$ without NAs, in the presence of cellwise outliers, casewise outliers, or both. The *test set* follows the same covariance model with again $n = 100$ and is either clean, contaminated with cellwise outliers, or simultaneously affected by cellwise outliers and missing values. Note that the test set does not contain casewise outliers because it is impossible to predict those, as they can be chosen arbitrarily. Analogously to (39) we compute the out-of-sample MSE given by

$$\text{MSE} = \frac{1}{n} \sum_{i=1}^n \sum_{j=1}^p \left(\widehat{x}_{ij}^* - x_{ij}^{*0} \right)^2 \quad (\text{A.23})$$

where \widehat{x}_{ij}^* is the prediction of x_{ij}^* and x_{ij}^{*0} is the original value of that cell before any contamination took place.

Figure 31 shows the median out-of-sample MSE of MacroPCA and cellPCA over 1000 replications. It has 9 panels. The three columns correspond to how the training data was generated, and the three rows reflect how the test set was generated. We clearly see that cellPCA has outperformed MacroPCA in all 9 situations.

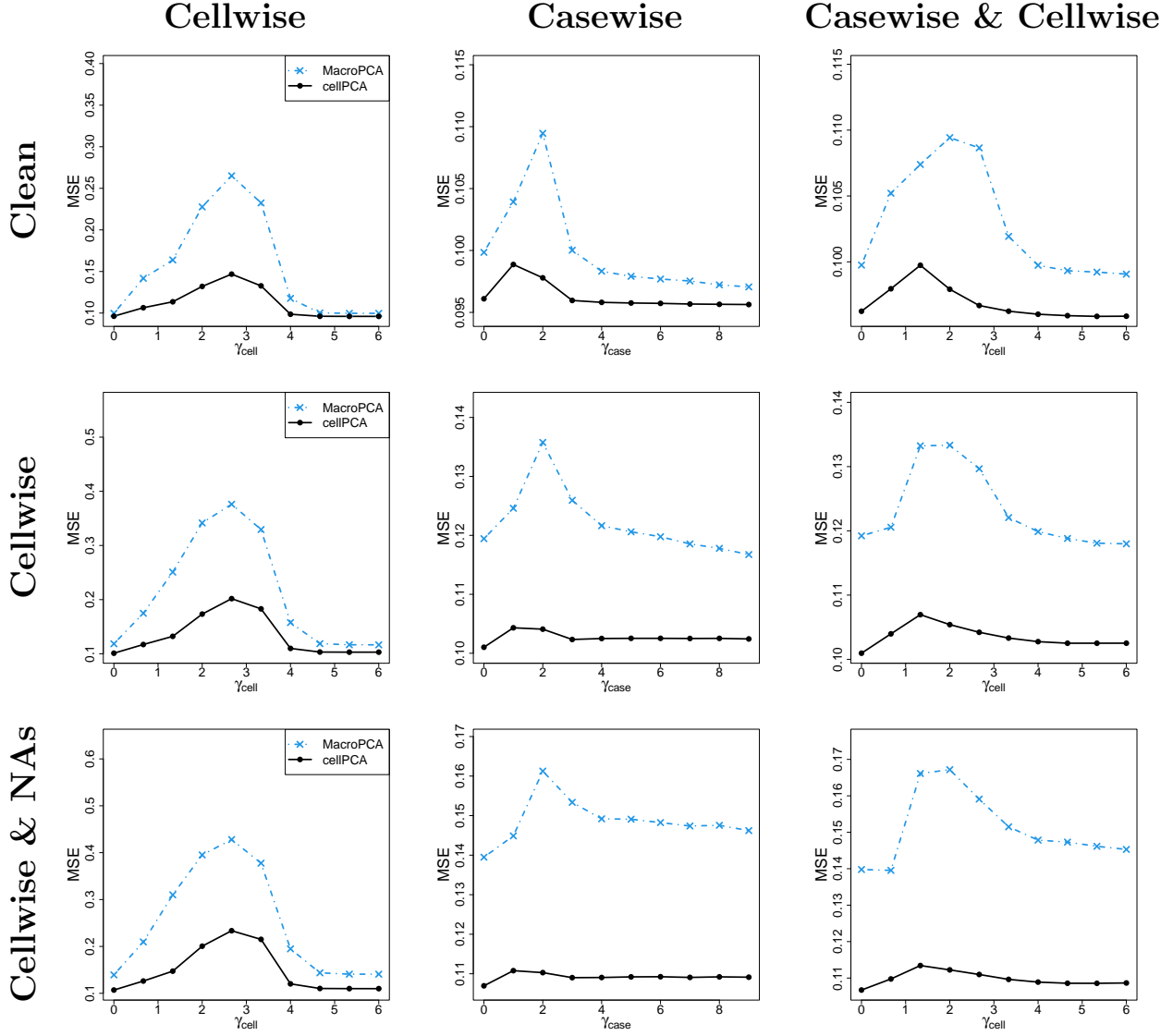


Figure 31: Median MSE of the out-of-sample prediction \hat{x} obtained by MacroPCA and cellPCA where the training data are generated by the covariance model A09 with $n = 100$ and $p = 20$ with cellwise outliers, casewise outliers, or both. The test set is either clean (top row), contaminated with cellwise outliers (middle row), or simultaneously affected by cellwise outliers and missing values (bottom row).

To investigate the effectiveness of the imputation method described in Section 4.2, we compare cellPCA and MacroPCA based on the out-of-sample imputation MSE, which is given by

$$\text{MSE} = \frac{1}{n} \sum_{i=1}^n \sum_{j=1}^p ((x_{ij}^*)^{\text{imp}} - x_{ij}^{*0})^2 \quad (\text{A.24})$$

where $(x_{ij}^*)^{\text{imp}}$ is the imputation of x_{ij}^* and x_{ij}^{*0} is the original value of that cell before any contamination took place. The data were generated as in Figure 31.

The resulting Figure 32 has rows and columns corresponding to those of Figure 31. Also here we see that cellPCA has substantially outperformed MacroPCA.

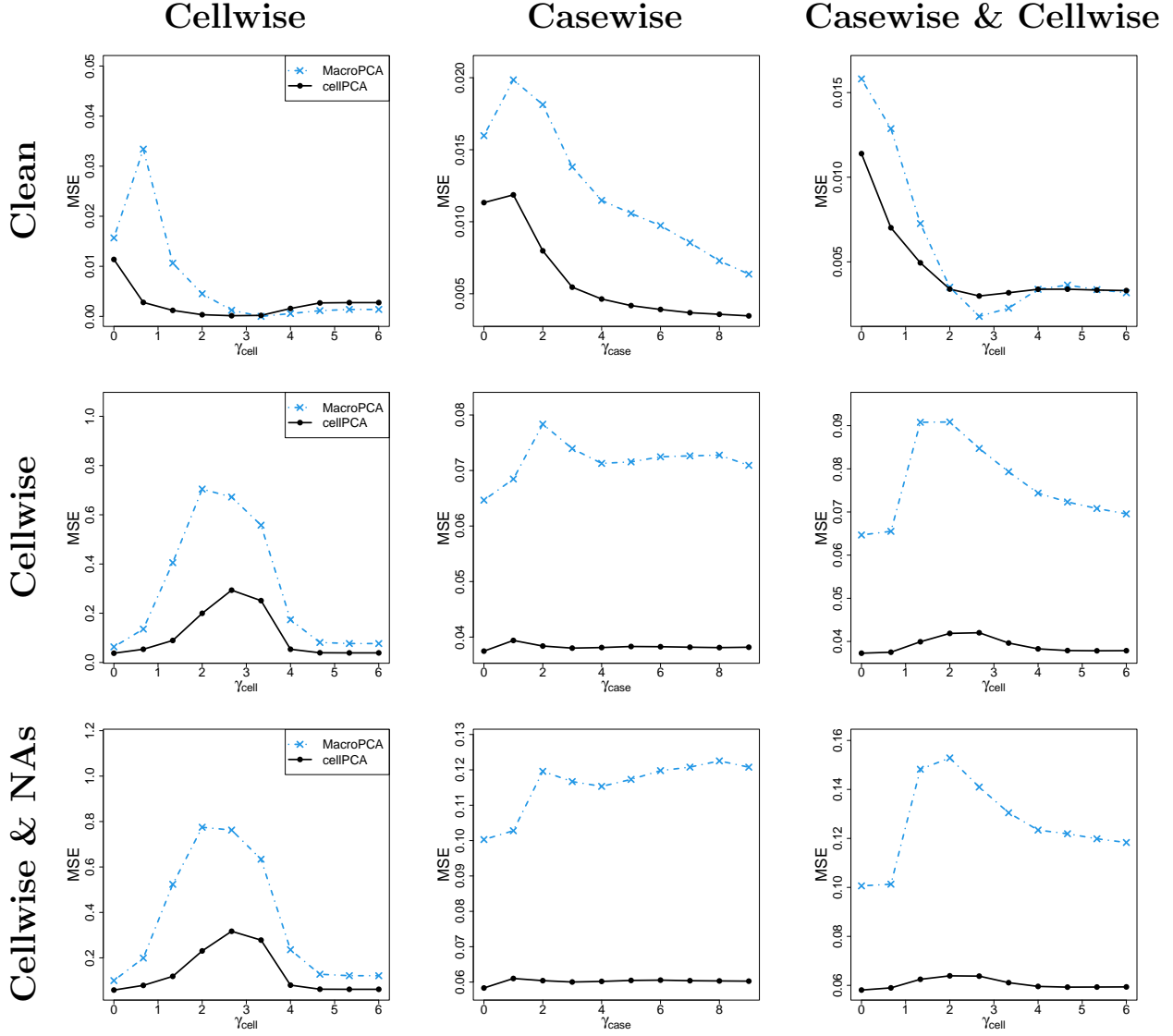


Figure 32: Median MSE of the imputation $(\mathbf{x}^*)^{\text{imp}}$ obtained by MacroPCA and cellPCA where the training data are generated by the covariance model A09 with $n = 100$ and $p = 20$ with cellwise outliers, casewise outliers, or both. The test set is either clean (top row), contaminated with cellwise outliers (middle row), or simultaneously affected by cellwise outliers and missing values (bottom row).

To evaluate the performance of the rank selection method discussed in Section 4.1, we run both MacroPCA and cellPCA and apply the Kneedle algorithm (Satopaa et al., 2011) to both. The data were generated from the covariance model A09 with $n = 100$ and $p = 20$, without NAs, in the presence of cellwise outliers, casewise outliers, or both. In each setting we ran 100 replications. From the way the A09 covariance was constructed, it is clear that the natural number of components is $k = 2$.

Figure 33 displays the average of the selected ranks \hat{k} obtained by MacroPCA and cellPCA, over the 100 replications. We see that MacroPCA already did quite well, with only small deviations from 2 when there is contamination. CellPCA did not even deviate at all.

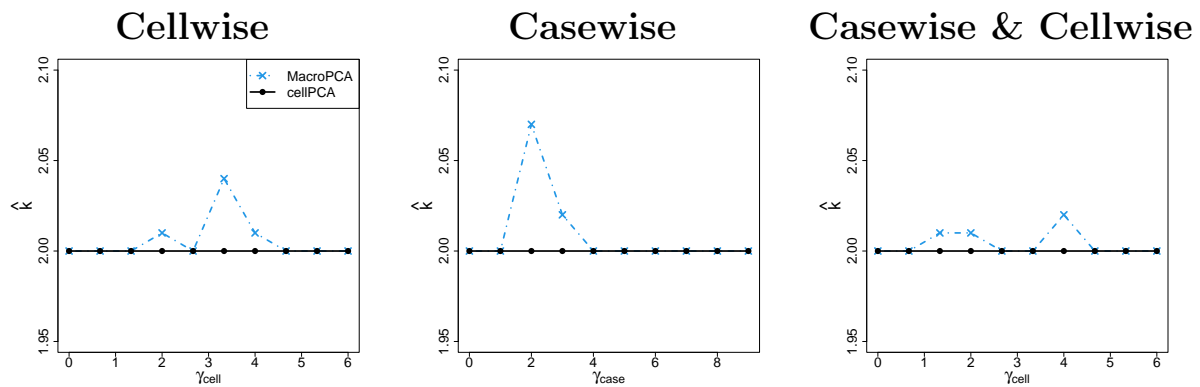


Figure 33: Average selected rank \hat{k} obtained by MacroPCA and cellPCA, over 100 replications. The data were generated by covariance model A09 with $n = 100$ and $p = 20$, without NAs, in the presence of cellwise outliers, casewise outliers, or both. The ranks were selected by applying the Kneedle algorithm to the scree plots.

M More on the Solfatara Data

Figure 34 shows frame 203 of the Solfatara data, taken in the Fall. The interpretation is similar to that in Section 7.2 for frame 14 taken in the Spring, only the shape of the condensation cloud is a bit different.

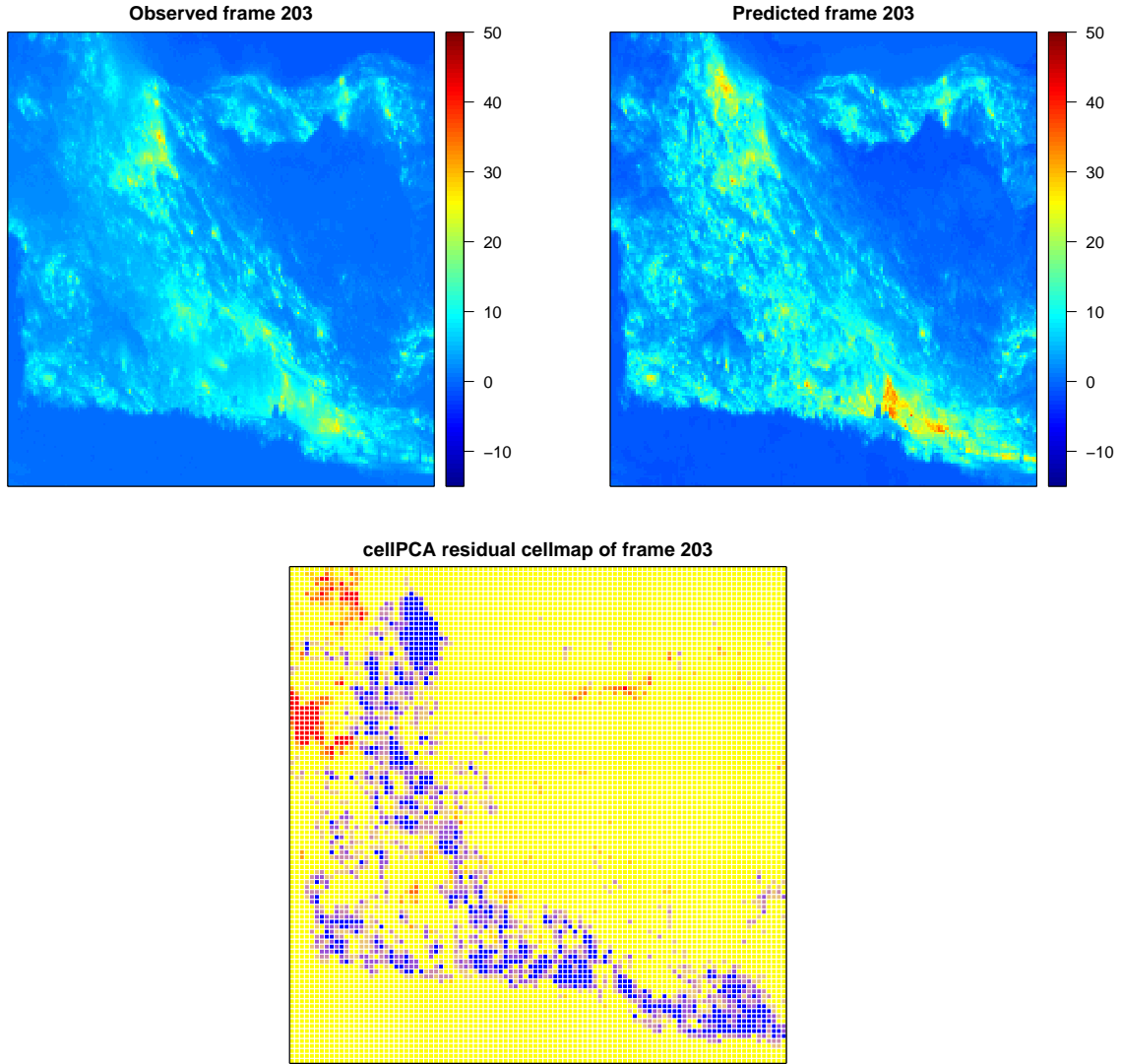


Figure 34: Solfatara data: observed frame 203, its prediction, and its residual cellmap.

Additional References

Casella, G. and R. L. Berger (2002). *Statistical Inference*, Volume 2. Duxbury Pacific Grove, CA.

Magnus, J. R. and H. Neudecker (2019). *Matrix Differential Calculus with Applications in Statistics and Econometrics, Third Edition*. Wiley.

Rio Branco de Oliveira, O. (2012). The implicit and the inverse function theorems: easy proofs, arXiv preprint 1212.2066.